

Theoretical Study of the Interaction of Amphiphilic Block Co-Polymers with Biological Interfaces and Small Molecules

By

Susruta Samanta

A thesis submitted in partial fulfillment

of the requirements for the degree of

Doctor of Philosophy

in **Chemistry**

Approved Thesis Committee:

Prof. Danilo Roccatano

Thesis supervisor, Jacobs University Bremen

Prof. Mathias Winterhalter

Internal reviewer, Jacobs University Bremen

Prof. Giuseppe Milano

External reviewer, University of Salerno, Italy

Date of defense: 18th December, 2012

School of Engineering and Science, Jacobs University Bremen

Funding

This research was carried out with the financial support from the **Deutsche Forschungsgemeinschaft (DFG)** for the project titled “*The study of detailed mechanism of polymers/biological membrane interactions using computer simulation.*” (RO 3571/3-1). Financial support from MoLife Research Center, Jacobs University Bremen is duly acknowledged.

Statutory Declaration

I, **SUSRUTA SAMANTA**, hereby declare that I have written this PhD thesis independently, unless where clearly stated otherwise. I have used only the sources, the data and the support that I have clearly mentioned. This PhD thesis has not been submitted for conferral of degree elsewhere.

Bremen, 18th January, 2013

Signature _____

Abstract

Synthetic polymers are versatile materials with an extraordinary range of technological applications playing essential and ubiquitous roles in everyday life. Presently, the applications of polymers are not limited to traditional areas of technology but extend to novel uses in the areas of nanotechnology connected to medicine and pharmacology. Polyethylene oxide (PEO) and polypropylene oxide (PPO) homo-polymers as well as the block co-polymers based on them (Pluronics or Poloxamers) are among the most versatile polymers used in these fields. These polymers have the advantages of being non-toxic, easily available, economic and customizable to meet specific purposes. Despite many experimental and theoretical studies on them, the actual mechanisms of their interactions with bio-systems and drug molecules are still unknown.

The research work reported in this PhD thesis is aimed to understand the behavior of these polymers in solution and their interactions with biological interfaces and drug molecules using molecular dynamics simulations. Recently proposed models for the ether based polymers and their monomers were successfully tested in a wide range of non-aqueous solvents to establish their versatility. The thermodynamics and kinetics of the polymers and the monomers were first studied at simple water/*n*-heptane interface. Eventually the research was extended to study their properties at lipid bilayer interfaces. The percolation behavior of the ether based polymers and their monomers were studied using standard molecular dynamics, steered molecular dynamics and umbrella sampling simulations. It has been shown that the percolation of PPO chains through lipid bilayer is favored compared to their PEO counterparts. PEO chains do not have any preference for the interior of the bilayer and but the PPO chains prefer to stay inside the bilayer. PPO chains with length comparable to the width of the bilayer tend to span across the bilayer. Pluronics also show similar effect with PPO parts spanned along the width of the bilayer and the PEO blocks in the polar headgroup region and water in both sides of the bilayer. The potential of mean force barriers of bilayer percolation were found to be smaller for PPO chains of all

lengths than their PEO counterparts.

The last part of the project aimed to investigate the mechanism of interaction of Pluronics with hydrophobic drug molecules. Curcumin, a natural drug from the Indian spice turmeric, has recently attracted interest as potential multivalent drug for the treatment of different diseases comprising cancer and Alzheimer's disease. For its hydrophobic nature, it has low solubility in water and therefore efforts are directed to find suitable polymeric carrier. For all these reason, Curcumin was chosen as model of hydrophobic drug for my study. A suitable force field model for this drug was optimized and used to study its interaction with Pluronics. The results of these MD simulation studies evidenced the mechanism of drug-polymer aggregate formation in which Curcumin is embedded into a hydrophobic PPO core surrounded by a hydrophilic PEO shell.

The findings of this thesis are useful in the better understanding of the interactions of block co-polymers with bio-membranes at atomic level. Moreover, they provide a better insight on the dynamics and thermodynamics of the drug encapsulation and delivery across cell membranes.

Acknowledgements

Working on the PhD has been a wonderful and overwhelming experience. I am indebted to many people for making the time working on my PhD an unforgettable experience

First of all, I would like to thank to my supervisor, Prof. Danilo Roccatano. To work with you has been a real pleasure to me. You have been a steady influence throughout my Ph.D. career. You have oriented and supported me with promptness and care, and have always been patient and encouraging at times of new ideas and difficulties. Your door was always open for discussions. Your ability to select and approach research problems, your academic ethics, and your hard work have set an example for me. I admire your ability to balance research interests and personal pursuits. I am deeply grateful to you.

Deepest gratitude is also due to the members of the supervisory committee, Prof. Mathias Winterhalter and Prof. Giuseppe Milano. Thank you for assessing my thesis and for the discussions that led to new ideas.

Special thanks also to all my group members - Khadga Karki, Samira Hezaveh, Rajni Verma, and Edita Sarukhanyan for sharing knowledge, invaluable assistance, and useful discussions throughout the course of my work. I thank my system 'Aragorn' for being a 'real Strider'. You literally lived by your words - "If by my life or death I can protect you, I will". When the hard disk crashed, you saved the data.

I thank the Acting Provost and Deans of School of Engineering and Science. I would also like to thank Dr. Achim Gelessus and CLAMV for taking care of the computational needs. I thank all the members of Jacobs University, Bremen.

I thank and acknowledge the financial support from Deutsche Forschungsgemeinschaft, and MoLife Research Center, Jacobs University, Bremen.

I am forever indebted to my parents for their understanding, endless patience and encouragement when it was most required. I thank my aunt, Dr. Gopa Samanta for being a source of inspiration. I thank my other family members, whose wishes always keep me going.

I thank Paromita for sharing the ups and downs of these years, her support, and care.

I would like to thank Prof. Amlan Kr. Das, who was always helpful and encouraging. Without your support, this day would not be possible.

I would like to thank Wolfgang & Gabi for making my stay in Bremen memorable. You have always made me feel at home away from home. I really appreciate your good wishes and kind gestures.

I am grateful to my friends Nirupam and Santanu. Without those wonderful weekends with you, the past three years would be extremely boring. You people really helped me to stay focused. Also, I thank my friends - Amit, Manas, Dinesh, Rishi, Sudhan-anna, Swagata and Shibabrata for always being there for me.

I thank my friends from Jacobs-Indians: Abhishek, Mahesh, Niraj, Indrajit, Dj, Sagar, Naveen, Rohan, Prasad, Binit, Sunil, Tripti, Rakesh, Rajesh, Sandeep, Shubham, Mahendran, Srikanth, Arumugam, Raghu, and Ashok-da. But for the cricket matches and get-togethers, life in Bremen would have been a shade duller. I would also like to thank my friends from HCU-Bongs, SMIT, RKMRC, and Katwa.

I thank everybody else who helped me till this moment. You know who you are.

Susruta Samanta

Bremen, Germany, 18th January, 2013

Table of Contents

INTRODUCTION	1
PREFACE.....	2
POLYETHYLENE OXIDE (PEO) AND POLYPROPYLENE OXIDE (PPO)	3
PLURONICS OR POLOXAMERS.....	4
MOLECULAR DYNAMICS SIMULATIONS.....	6
ALGORITHM.....	6
INTERACTION POTENTIALS.....	7
TEMPERATURE AND PRESSURE CONTROL.....	9
STEERED MOLECULAR DYNAMICS SIMULATIONS.....	10
UMBRELLA SAMPLING METHOD.....	11
AIM AND OUTLINE OF THE THESIS.....	14
REFERENCES.....	15
 CHAPTER 1.....	 19
ABSTRACT.....	20
INTRODUCTION.....	21
METHODS.....	23
FORCE-FIELD PARAMETERS.....	23
MOLECULAR DYNAMICS SIMULATIONS SETUP.....	23
DME AND DMP IN NON-AQUEOUS SOLVENTS.....	25
RESULTS AND DISCUSSIONS.....	26
DME IN NON-AQUEOUS SOLVENTS.....	26
DMP IN NON-AQUEOUS SOLVENTS.....	30
CONCLUSIONS.....	34
REFERENCES.....	35
 CHAPTER 2.....	 39
ABSTRACT.....	40
INTRODUCTION.....	41
METHODS.....	43
FORCE-FIELD PARAMETERS.....	43
MOLECULAR DYNAMICS SIMULATIONS SETUP.....	43
PEO, PPO AND PLURONIC P85 IN NON-AQUEOUS SOLVENTS.....	43
RESULTS AND DISCUSSIONS.....	45
PEO IN NON-AQUEOUS SOLVENTS.....	45
PPO IN NON-AQUEOUS SOLVENTS.....	54

PLURONIC P85 IN NON-AQUEOUS SOLVENTS.....	58
CONCLUSIONS.....	59
REFERENCES.....	60
CHAPTER 3.....	65
ABSTRACT.....	66
INTRODUCTION.....	67
METHODS.....	69
FORCE FIELD.....	69
SIMULATION SETUP:.....	70
CALCULATION OF THE FREE ENERGY OF SOLVATION AND PARTITION COEFFICIENT.....	71
SMD SIMULATIONS.....	72
UMBRELLA SAMPLING SIMULATIONS.....	73
UNCONSTRAINED SIMULATIONS AT THE INTERFACE.....	73
RESULTS AND DISCUSSIONS.....	75
FREE ENERGY AND PARTITION COEFFICIENT.....	75
PERCOLATION OF DME AND DMP THROUGH <i>N</i> -HEPTANE.....	75
SIMULATION OF DME AND DMP AT THE WATER/ <i>N</i> -HEPTANE INTERFACE:.....	78
PERCOLATION OF DME AND DMP THROUGH DMPC:.....	79
DME AND DMP AT THE WATER/DMPC INTERFACE:.....	85
SIMULATIONS WITH MULTIPLE DME AND DMP MOLECULES AT THE WATER/DMPC INTERFACE:.....	89
CONCLUSIONS.....	90
REFERENCES.....	92
CHAPTER 4.....	95
ABSTRACT.....	96
INTRODUCTION.....	97
METHODS.....	98
FORCE-FIELD.....	98
SIMULATION SETUP.....	98
RESULTS AND DISCUSSION.....	102
POLYMERS AT WATER/ <i>N</i> -HEPTANE INTERFACE.....	102
PEO AND PPO CHAINS AT WATER/DMPC BILAYER INTERFACE.....	104
PEO AT THE INTERFACE AND INSIDE THE BILAYER.....	106
PPO AT THE INTERFACE AND INSIDE THE BILAYER.....	106
PLURONICS AT WATER/DMPC BILAYER INTERFACE AND INSIDE DMPC BILAYER.....	107
PERCOLATIONS OF POLYMERS IN LIPID BILAYER.....	111
CONCLUSIONS.....	113
REFERENCES.....	115

CHAPTER 5.....	117
ABSTRACT.....	118
INTRODUCTION.....	119
METHODS.....	121
FORCE FIELD.....	121
SIMULATION SETUP:.....	122
RESULTS AND DISCUSSIONS.....	124
SIMULATION OF CURCUMIN IN WATER, METHANOL AND 1-OCTANOL.....	124
SIMULATION OF CURCUMIN IN DME/DMP MIXTURE IN WATER.....	129
SIMULATION OF CURCUMIN IN THE PRESENCE SINGLE PLURONIC (P85) CHAIN.	131
SIMULATION OF CURCUMIN IN THE PRESENCE MULTIPLE PLURONICS (P85) CHAINS.	133
CONCLUSIONS.....	136
REFERENCES.	137
SUMMARY AND OUTLOOK	141
SUMMARY.....	142
OUTLOOK.....	145
APPENDIX.....	I
APPENDIX I.....	I
APPENDIX II.....	IV
APPENDIX III.....	IX
LIST OF ABBREVIATIONS.....	XV
LIST OF TABLES.	XVI
LIST OF FIGURES.....	XVII





Introduction

Preface.

The development of synthetic polymers as drug carriers is one of the most active areas in biomedical research. Approximately half of the recently discovered molecules that have therapeutic potential are hydrophobic.^[1] To fully utilize the full potential of these molecules as drugs, it is important to fabricate an easily available and biocompatible carrier for them for better solubilization and controlled release. During last several years, amphiphilic, non-ionic block co-polymers have emerged as a potential candidate for this purpose.^[2, 3] In particular, tri block-copolymers Pluronics based on polyethylene oxide (PEO) and polypropylene oxide (PPO) are one of the most widely studied polymer among them.^[2-7] Pluronics being inexpensive, non-toxic, easily available and easily customizable to meet specific purposes, have become one of the promising substitute for lipopolymers for drug delivery.^[8] These polymers have low cytotoxicity which makes them undetectable by living cells or systems.^[5] Encapsulation of drugs in Pluronics matrix has found to enhance residence time and decrease the chances of proteolytic decomposition.^[2, 4, 6, 7, 9-11] Pluronics have also been found to be effective against drug resistant tumor cells.^[12] When combined with antitumor drugs, the chemotherapeutic material has a tendency to accumulate in tumor cells and affects the immune system to far less extent.^[13] In several studies, Pluronics have found to be a promoter for drug penetration across biological membranes.^[14-16]

Despite the large number of applications, little is known on the atomic details of their interaction with different biological interfaces and also with drug molecules.

My PhD thesis reports theoretical study on the interaction of ether-based polymers with DMPC lipid bilayer and with the drug Curcumin using molecular dynamics simulation techniques. In particular, I have investigated linear and triblock copolymers based on polyethylene oxide (PEO) and polypropylene oxide (PPO). Detailed description of the polymers involved in the project is given in the next section.

Polyethylene oxide (PEO) and polypropylene oxide (PPO).

PEO or polyethylene oxide is a non-ionic homopolymer produced by polymerization of ethylene oxide. Its chemical formula is $\text{CH}_3\text{-O-}[\text{CH}_2\text{-CH}_2\text{-O}]_n\text{-CH}_3$ (n is the number of polymer monomers). The smallest oligomer ($n=1$) corresponds to the 1, 2-dimethoxyethane (DME). PEO is an amphiphilic polymer and has many important applications. Unlike other polyethers (general formula $[(\text{CH}_2)_x\text{-O}]_m$) it is soluble both in common organic solvents and water. This behavior seems to be a result of the balance between the hydrophobic forces applied by the ethylene units, $-\text{CH}_2\text{-CH}_2-$, and the hydrophilic interaction of the units containing oxygen. The consequence of these two competitive forces makes PEO soluble in water in all proportion at temperature lower than the boiling point of water.^[17] PEO at low concentration enhances membrane fluidity and at higher concentration, causes membrane fusion.^[18, 19]

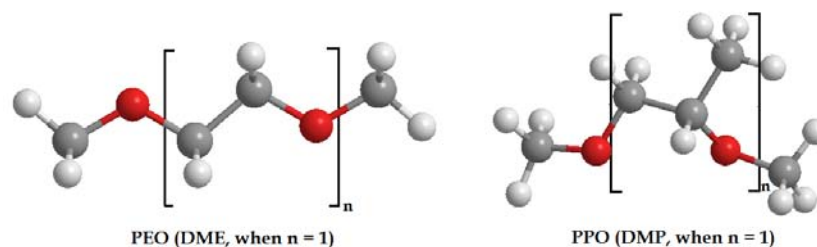


Figure 1: Chemical structure of polyethylene oxide/PEO (left) and polypropylene oxide/PPO (right) polymers.

PPO or polypropylene oxide is a hydrophobic polymer with amorphous structure.^[20] Its chemical formula is $\text{CH}_3\text{-O-}[\text{CH}_2\text{-C}(\text{CH}_3)\text{H-O}]_n\text{-CH}_3$. Due to the presence of a chiral carbon atom, PPO polymers can have three different configurations, i.e., Isotactic (all chiral atoms in the chain methyl groups have the same *R* or *S* configuration), Syndiotactic (chiral atoms with alternate *R* and *S* configurations) and Atactic (chiral carbon atoms with a random sequence of *R* and *S* configurations).

The smallest oligomer ($n=1$) of PPO corresponds to the compound 1,2-

dimethoxypropane (DMP). Only PPO oligomers with comparatively short chain length (molecular weight < 400 Da) are soluble in water.^[21] Its solubility decreases rapidly with increasing chain length. A limited number of experimental studies of aqueous solutions are available on the DMP and the PPO polymers in both water and organic solvents.

Pluronics or Poloxamers.

Pluronics are non-ionic triblock copolymers composed of a central hydrophobic chain of PPO flanked by two hydrophilic chains of PEO. Pluronics is readily soluble in aqueous solutions, polar and non-polar organic solvents.^[11] The chemical structure of Pluronics is shown in Fig. 2.

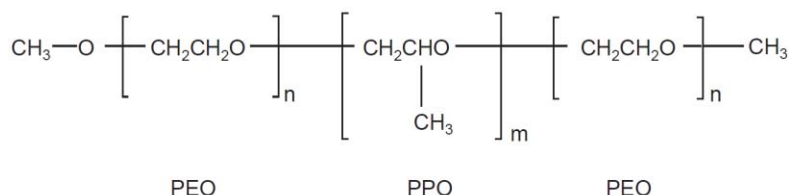


Figure 2: Chemical structure of PEO and PPO based triblock co-polymer Pluronics.

Because customizable length of polymer blocks, many different Pluronics exist those have slightly different properties. For the trade name 'Pluronics', coding of these copolymers start with a letter to define its physical form at room temperature (L for liquid, P for paste, F = flake (solid)) followed by two or three digits. The first digit (two digits in a three-digit number) in the numerical designation, multiplied by 300, indicates the approximate molecular weight of the hydrophobic part; and the last digit $\times 10$ gives the percentage PEO content. For example, L61 is a liquid Pluronics with a molecular mass of PPO block of 1,800 g/mol & 10% PEO content and P85 is a paste Pluronics with 50% PEO content & it has 2400 g/mol PPO in it. When the trade name 'Poloxamer' is used, the convention is slightly different. In that case, the first digit (two digits in a three-digit number) multiplied by 100, indicates the approximate molecular weight of the PPO part.^[22]

In the following Table 1, we present few commonly used Pluronics.

Table 1: Description of the Pluronics molecules used in this study.

Name	Composition	Molecular Weight	HLB ^a
L61	PEO ₂ -PPO ₃₀ -PEO ₂	1962	1.2
L64	PEO ₁₃ -PPO ₃₀ -PEO ₁₃	2930	14
P85	PEO ₂₅ -PPO ₄₀ -PEO ₂₅	4566	17
F127	PEO ₉₉ -PPO ₆₇ -PEO ₉₉	12644	24

^aHLB: hydrophilic-lipophilic balance. For PEO_n-PPO_m-PEO_n type polymers
 $HLB = [-36m/(2n+m) + 33]$. Lower HLB indicates higher hydrophobicity of the polymer.

Pluronics are usually soluble in water because of their hydrophilic PEO parts. Their properties in aqueous solutions depend on temperature and concentration. The presence of a more hydrophobic PPO unit permits the formation of micelles with an inner core formed by PPO and the outer shell by PEO blocks.^[23] Micelle formation occurs in certain conditions of temperature, salt concentration, pH, polymer concentration. It mainly occurs above Critical Micelle Concentrations (CMC) and above Critical Micelle Temperatures (CMT).^[4] For some Pluronics, CMC and CMT are in physiological ranges which make them become suitable compounds for application in drug delivery or gene therapy.

Molecular Dynamics Simulations.

Algorithm.

In MD simulation method, atomic trajectories are calculated from Newton's equations of motion:

$$\mathbf{m}_i \frac{d^2 \mathbf{r}_i(t)}{dt^2} = \mathbf{F}_i(\mathbf{r}_1 \dots \mathbf{r}_N) \quad (1.1)$$

Here \mathbf{r}_i are the position vectors of the particles with mass m_i , and \mathbf{F}_i is the force depending on the positions of all N particles in the system. The required force is obtained from the derivative of the interaction potential V between the particles:

$$\mathbf{F}_i = -\frac{\partial}{\partial \mathbf{r}_i} V(\mathbf{r}_1 \dots \mathbf{r}_N) \quad (1.2)$$

The interaction potential contains all necessary information to describe the system properly. Newton's classical equations of motion for N particles system interacting through a potential V do not have analytic solutions and, therefore, one needs to solve this problem numerically using finite difference methods. There are different algorithms to approximately integrate these differential equations and hence calculate positions, velocities in time. One of these algorithms, commonly used in MD simulations is the so-called Leap-Frog^[24] algorithm, which is a variant of the Verlet algorithm^[25, 26]. It is based on the following integration scheme,

$$\mathbf{v}_i(t + \frac{1}{2}\delta t) = \mathbf{v}_i(t - \frac{1}{2}\delta t) + \frac{\mathbf{F}_i}{m_i}(\delta t) \quad (1.3)$$

$$\mathbf{r}_i(t + \delta t) = \mathbf{r}_i(t) + \delta t \mathbf{v}_i(t + \frac{1}{2}\delta t) \quad (1.4)$$

where \mathbf{F}_i is the force acting on the particle i with mass m_i . This algorithm is used in the implementation in the Gromacs software, for all the simulations in this thesis.

Interaction Potentials.

In order to calculate the interactions between the particles, we need to describe them in form of analytical potentials or force field.

The atomic interactions are mainly divided into two parts as bonded and non-bonded ones that can be written as a summation of potentials derived from physical forces.^[27]

$$V(\mathbf{r}_1, \mathbf{r}_2 \dots \mathbf{r}_N) = E_{total} = E_{bonded} + E_{non-bonded} \quad (1.5)$$

where they are further defined as,

$$E_{bonded} = E_{bond} + E_{angle} + E_{dihedral} \quad (1.6)$$

$$E_{non-bonded} = E_{van-der-Waals} + E_{electrostatic} \quad (1.7)$$

Bonded interactions. Bond vibrations are two body interactions and are modelled as harmonic potential functions. The bond vibrations are given by,

$$E_{bond} = \sum_{bonds} \frac{1}{2} K_b (b - b_0)^2 \quad (1.8)$$

where K_b is the constant for bond force, b is the bond length, and b_0 is the bond length at the minimum energy.

The bond-angle vibrations are three body interactions which describe the deviation from ideal bond angle geometry and defined again defined using harmonic expression as,

$$E_{angle} = \sum_{angle} \frac{1}{2} K_\theta (\theta - \theta_0)^2 \quad (1.9)$$

where K_θ is the constant for angle force, θ is the angle, θ_0 is the angle at the minimum energy.

The torsional motions are described by dihedral angles between four atoms (i,j,k,l) and is assumed to be periodic and expressed as sum of cosine functions,

$$E_{dihedral} = \sum_{dihedral} K_f (1 + \cos(n\phi - \phi_s)) \quad (1.10)$$

where K_f is the rotation constant for the dihedral angle energy, ϕ is the dihedral angle formed by the two planes defined by the triplets of atoms (i-j-k) and (j-k-l), n is the periodicity of the rotational barrier and ϕ_s is the phase factor. Another functional form used to describe proper dihedral interactions which was used in this thesis, is the Ryckaert-Bellemans(RB)^[28] function defined as,

$$E_{dihedral} = \sum_{n=0}^4 C_n [\cos(\phi - \phi_s)]^n \quad (1.11)$$

where $\phi_s = \phi - \pi$.

Non-bonded interactions. The molecular non-bonded interactions as in equation 1.5 are consisting of van der Waals (VDW) and electrostatic interactions. The VDW interactions are presented by Lennard-Jones (LJ) potential function and it expresses the interaction energy between two atoms. The LJ potential is a short range potential defined as,

$$E_{van-der-Waals} = \sum_i \sum_{j>i} 4\epsilon_{ij} \left(\frac{\sigma_{ij}^{12}}{r_{ij}^{12}} - \frac{\sigma_{ij}^6}{r_{ij}^6} \right) \quad (1.12)$$

where r is the distance between particles, ϵ_{ij} is the well depth and σ_{ij} is the distance at which the inter potential is zero. This potential contains an attractive part and a repulsive part. Attractive forces are due to dipole-dipole interactions and the repulsive part is due to Pauli-exclusion principle and inter-nuclear repulsion.

The electrostatic interactions are defined as simple columbic potential function,

$$E_{electrostatic} = \sum_i \sum_{j>i} \left(\frac{q_i q_j}{4 \pi \epsilon_0 r_{ij}} \right) \quad (1.13)$$

where r is the distance between particles, q_i and q_j are the partial charges on the atoms i and j , respectively, and ϵ is the electric constant.

Temperature and Pressure control.

The temperature of the system can be calculated using the average kinetic energy of the N particles with N_f degrees of freedom,

$$\frac{1}{2}k_b N_f T = \sum_{i=1}^N \frac{1}{2} m_i v_i^2 \quad (1.14)$$

where v_i is the velocity of particle i with mass m_i .

The pressure expression of the system is based on virial theorem.^[29] Thus the pressure is expressed as summation of ideal part ($PV=Nk_bT$) and the summed product of forces (F_i) acting on particles and distances (r_i) between the centres of mass of the molecules,

$$P = \frac{Nk_bT}{V} + \frac{1}{3V} \langle \sum_{i=1}^N \mathbf{F}_i \cdot \mathbf{r}_i \rangle \quad (1.15)$$

In order to control the temperature of the system and the pressure one can use weak temperature and pressure coupling to an external bath i.e. Berendsen method.^[30] In this approach, at each integration step, the atomic velocities, v , are scaled to λv , to

change the temperature of the system $T(t - \frac{1}{2}\delta t)$ to the reference temperature, T_0 . λ is a constant and defined as,

$$\lambda = \left[1 + \frac{\delta t}{\tau_T} \left(\frac{T_0}{T(t - \frac{1}{2}\delta t)} - 1 \right) \right]^{\frac{1}{2}} \quad (1.16)$$

where τ_T is the coupling parameter and T_0 is the thermostat fixed temperature.

For the simulations reported in this thesis, the ‘velocity rescaling’ or ‘V-rescale’

thermostat was used. It is a Berendsen thermostat with an additional term to ensure correct kinetic energy distribution. V-rescale thermostat has all the advantages of Berendsen thermostat and produces correct canonical ensemble. When K is the kinetic energy, N_f is the number of degrees of freedom and dW is a Wiener process, the correction term is defined as

$$dK = (K_0 - K) \frac{dt}{\tau_T} + 2 \sqrt{\frac{KK_0}{N_f}} \frac{dW}{\sqrt{\tau_T}} \quad (1.17)$$

The coupling to the reference pressure, P_0 is performed by scaling of coordinates r to ηr as,

$$\eta = \left[1 + \frac{\gamma \delta t}{\tau_P} (P(t) - P_0) \right]^{\frac{1}{2}} \quad (1.18)$$

where $P(t)$ is the system pressure at time t and γ is the compressibility of the system. τ_P is again the coupling parameter or strength of coupling.

Steered Molecular Dynamics Simulations.

Percolation of molecules through lipid bilayer is a very slow process with time scale going beyond the standard computational affordable MD simulation length. In fact, Even for small molecules, the process may take from several hundreds of nanoseconds^[31] to microseconds. Hence, steered molecular dynamics (SMD) simulation method was used to speed up the diffusion of molecules at the interfaces. In SMD simulation a time-dependent external harmonic force is applied and the relative distance between two groups change continuously. This is not a equilibrium process and hence, very slow pulling regime is used to ensure operation in near-equilibrium conditions.^[32] A schematic diagram of SMD simulation is shown the Fig. 3. In this example, the bottom layer of DMPC is set as the reference and the DME/DMP molecule is set as the pull group. The center of mass of the pull group is pulled towards the reference with a spring having spring constant k and velocity of the end of the spring is v . Considering the

pulling is done in one direction, the force working on the pull group can be expressed as

$$F = k (x_0 - x + vt) \quad (1.19)$$

Where x_0 is the initial position of the restraint point. The potential of mean force (PMF) is obtained by integrating the force over the whole trajectory along the reaction pathway. However, being non-equilibrium method, the calculations of the equilibrium properties (e.g., PMF) require multiple number of pulling trajectories to obtain a reliable sampling.^[32, 33]

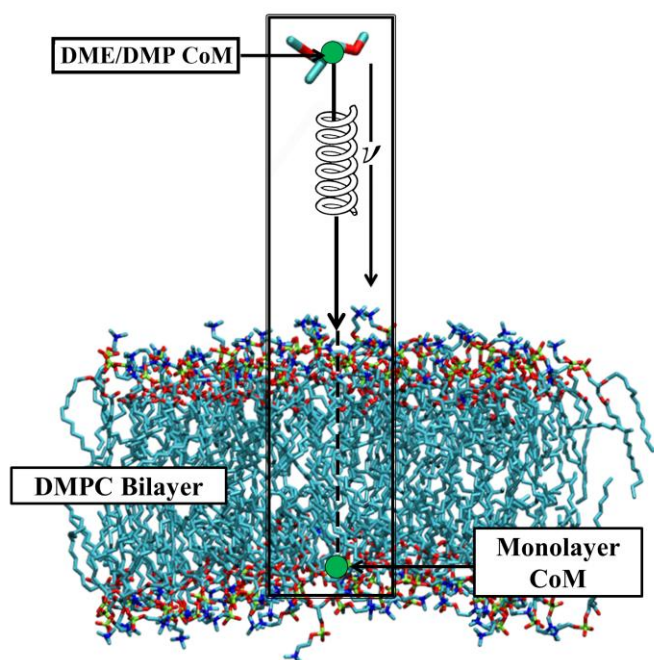


Figure 3: Schematic diagram of the setup used for SMD simulations. The center of mass (CoM) of the DME and DMP molecules was pulled along the z-direction at a constant velocity of v towards the center of mass of the head groups of the bottom layer of DMPC using a force constant of k .

Umbrella Sampling Method.

The PMF can be calculated using the umbrella sampling method.^[34-37] In this method, a set of N separate molecular dynamics simulations, in which a harmonic potential (umbrella potential),

$$w_i(\xi) = 0.5 K_i (\xi - \xi_i)^2 \quad (1.20)$$

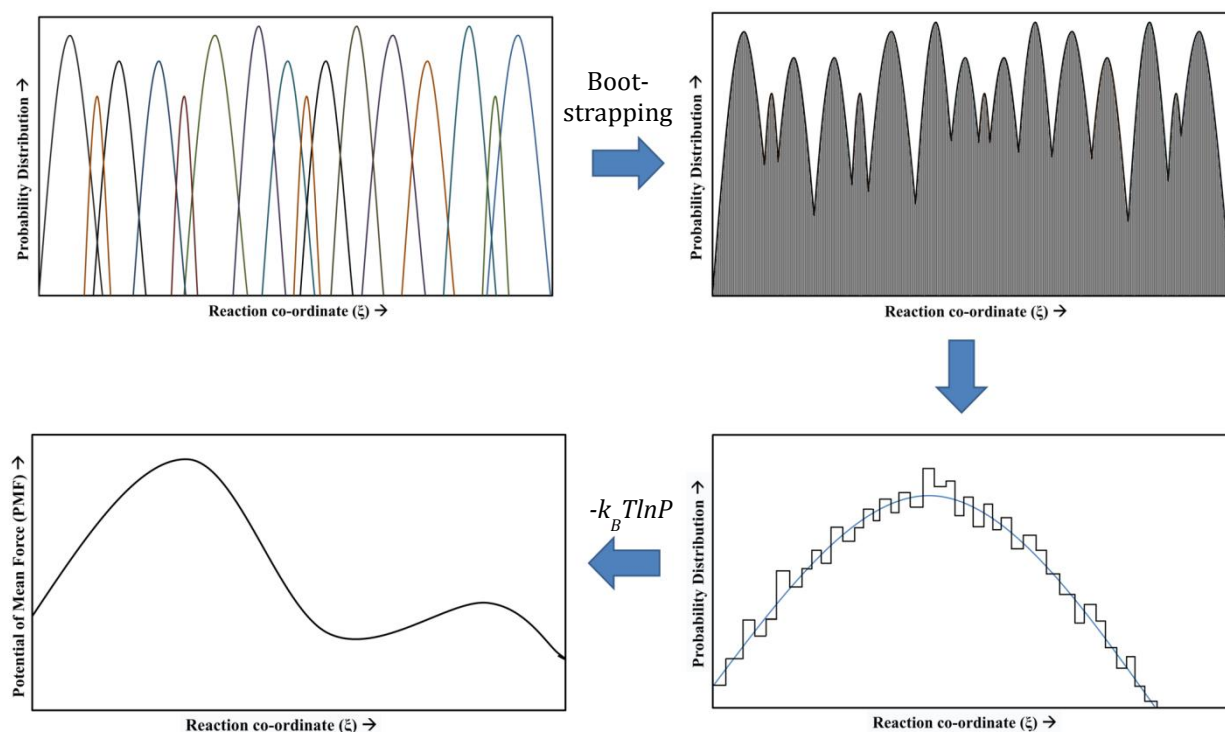


Figure 4: A schematic diagram showing the workflow of umbrella sampling method: i) The probability distribution obtained from each simulation is shown against reaction coordinate ii) The histogram is then bootstrapped iii) A large number of observations are obtained iv) The PMF profile is then obtained by evaluating PMF at each point

is applied between the centre of mass of the target molecule and the bottom bilayer, are performed. This restrains the molecule at a distance ξ_i with a force constant of K_i . In each simulation the value of ξ_i is changed from a maximum value corresponding to the molecule in the water phase to a minimum at which the molecule is in the middle of the lipid bilayer. From each simulation a histogram is calculated, representing the probability distribution (P_i) along the reaction coordinate biased by the umbrella potential. The most widely used technique to compute PMF from histograms by removing the bias added by umbrella potential is the weighted histogram analysis method (WHAM).^[38] WHAM computes PMF based on several numbers of trajectories along the reaction coordinate. Each trajectory is bootstrapped to produce a new set of histograms ($P_{i,b}$). This leads to all positions ξ_i considered to be a large set of

observations with distance $\xi_{i,b}$. The PMF for each $\xi_{i,b}$ is represented by

$$PMF = -k_B T \ln(P_{i,b}) \quad (1.21)$$

where k_B is the Boltzmann constant and T is the temperature. In the Fig. 4, a schematic diagram of the umbrella sampling workflow is shown. We used *g_wham* program of the GROMACS version 4.0.7 package to compute PMFs from the umbrella sampling simulations. This procedure implemented in this program takes into account the periodicity of the system and it has proven to yield more realistic PMF estimates in the case of longer sampling.^[35]

Aim and outline of the thesis.

The aim of this thesis can be summarized in three points:

- a) To optimize a new set of forcefield parameters for the ether based polymers compatible with existent force field for the simulation of biological systems (membrane and proteins).
- b) To understand the adsorption and percolation processes of these polymers through lipid bilayer interface.
- c) To study the interaction of triblock copolymer Pluronics with the drug molecules Curcumin.

Aforementioned points have been addressed in this thesis in five chapters.

Chapter 1 describes the structural, dynamic and thermodynamic properties of DME and DMP, in three non-aqueous solvents, i.e., methanol, carbon tetrachloride and *n*-heptane. In **Chapter 2** the conformational and dynamic properties of the polymers of DME and DMP, i.e., PEO and PPO in four non-aqueous solvents are reported. The forcefield parameters of the molecules were optimized for better performance in various environments. The results were compared with available experimental data and they were found to be satisfactory.

Chapter 3 describes the permeation of DME and DMP through water/*n*-heptane interface and DMPC lipid membrane. Since the actual process of permeation is too slow to be studied directly with normal MD simulation, steered molecular dynamics simulation was used to accelerate the process. The potential of mean force profile for that process for both DME and DMP were mapped using umbrella sampling method. Properties of the ether molecules in the interface were studied with unconstrained MD simulations at the interface.

Chapter 4 contains the results of the study of polymers (PEO, PPO and Pluronics)

at the water/*n*-heptane interface and at the water/DMPC interface. Percolation barriers for the smaller polymers were calculated using umbrella sampling method. Percolation of the longer polymers was studied using steered molecular dynamics simulations. Unconstrained simulations were used to obtain a better understanding of the interaction of the polymers with DMPC lipid membranes.

In **Chapter 5**, the force field parameterization for the natural drug Curcumin drug and the study of its interaction with Pluronics have been reported. Properties of the drug have been systematically studied in simple solutions, in DME/DMP/water mixture, in the presence of single and multiple Pluronic P85 chains. The study evidences the atomic detail of coating of the drug by the Pluronic chains.

Supporting data for the chapters are put in the **Appendix**. Finally, the major findings and possible future directions are summarized in the **Summary and Outlook** section.

REFERENCES.

- [1] C. A. Lipinski, *Journal of Pharmacological and Toxicological Methods* **2000**, *44*, 235.
- [2] R. Haag, F. Kratz, *Angewandte Chemie International Edition* **2006**, *45*, 1198.
- [3] I. R. Schmolka, in *Polymers for Controlled Drug Delivery* (Ed.: P. J. Tarcha), CRC Press, Boston, **1991**.
- [4] S. Fusco, A. Borzacchiello, P. A. Netti, *Journal of Bioactive and Compatible Polymers* **2006**, *21*, 149.
- [5] Y. Kodera, A. Matsushima, M. Hiroto, H. Nishimura, A. Ishii, T. Ueno, Y. Inada, *Progress in Polymer Science* **1998**, *23*, 1233.
- [6] C. D. H. Alarcon, S. Pennadam, C. Alexander, *Chemical Society Reviews* **2005**, *34*, 276.
- [7] P. Alexandridis, *Current Opinion in Colloid and Interface Science* **1996**, *1*, 490.

- [8] K. T. Oh, T. K. Bronich, A. V. Kabanov, *Journal of Controlled Release* **2004**, 94, 411.
- [9] N. S. Melik-Nubarov, O. O. Pomaz, T. Y. Dorodnych, G. A. Badun, A. L. Ksenofontov, O. B. Schemchukova, S. A. Arzhakov, *FEBS Letters* **1999**, 446, 194.
- [10] A. Sahu, N. Kasoju, P. Goswami, U. Bora, *Journal of Biomaterials Applications* **2011**, 25, 619.
- [11] R. K. Chowdhary, I. Sharif, N. Chansarkar, D. Dolphin, L. Ratkay, S. Delaney, H. Meadows, *Journal of Pharmacy and Pharmaceutical Sciences* **2003**, 6, 198.
- [12] A. V. Kabanov, E. V. Batrakova, V. Y. Alakhov, *Journal of Controlled Release* **2002**, 82, 189.
- [13] E. V. Batrakova, T. Y. Dorodnych, E. Y. Klinskii, E. N. Kliushnenkova, O. B. Shemchukova, O. N. Goncharova, S. A. Arjakov, V. Y. Alakhov, A. V. Kabanov, *British Journal of Cancer* **1996**, 74, 1545.
- [14] A. V. Kabanov, V. I. Slepnev, L. E. Kuznetsova, E. V. Batrakova, V. Alakhov, N. S. Melik-Nubarov, P. G. Sveshnikov, V. A. Kabanov, *Biochemistry International* **1992**, 26, 1035.
- [15] V. I. Slepnev, L. E. Kuznetsova, A. N. Gubin, E. V. Batrakova, V. Alakhov, A. V. Kabanov, *Biochemistry International* **1992**, 26, 587.
- [16] A. V. Kabanov, V. P. Chekhonin, V. Y. Alakhov, E. V. Batrakova, A. S. Lebedev, N. S. Melik-Nubarov, S. A. Arzhakov, A. V. Levashov, G. V. Morozov, E. S. Severin, V. A. Kabanov, *FEBS Letters* **1989**, 258, 343.
- [17] C. Branca, A. Faraone, S. Magazu, G. Maisano, P. Migliardo, V. Villari, *Journal of Molecular Liquids* **2000**, 87, 21.
- [18] R. I. MacDonald, *Biochemistry* **1985**, 24, 4058.
- [19] H. Ohno, N. Shimidzu, E. Tsuchida, S. Sasakawa, K. Honda, *Biochimica et Biophysica Acta (BBA) - Biomembranes* **1981**, 649, 221.
- [20] X. Xin, G. Y. Xu, Z. Q. Zhang, Y. J. Chen, F. Wang, *European Polymer Journal* **2007**, 43, 3106.
- [21] G. N. Malcolm, J. S. Rowlinson, *Transactions of the Faraday Society* **1957**, 53, 921.
- [22] R. Kayed, Vol. 814953 (Ed.: U. S. P. a. T. Office), USA, **2010**.

- [23] R. Ganguly, V. K. Aswal, *Journal of Physical Chemistry B* **2008**, 112, 7726.
- [24] R. W. Hockney, J. W. Eastwood, *Computer Simulation Using Particles*, CRC Press, **1988**.
- [25] L. Verlet, *Physical Review* **1967**, 159, 98.
- [26] L. Verlet, *Physical Review* **1968**, 165, 201.
- [27] D. van der Spoel, E. Lindahl, B. Hess, C. Kutzner, A. R. van Buuren, E. Apol, P. J. Meulenhoff, D. P. Tieleman, A. L. T. M. Sijbers, K. A. Feenstra, R. van Drunen, H. J. C. Berendsen, *Gromacs User Manual version 4.0*, **2005**.
- [28] J. P. Ryckaert, A. Bellemans, *Faraday Discussions of the Chemical Society* **1978**, 66, 95.
- [29] M. P. Allen, D. J. Tildesley, *Computer Simulation of Liquids*, Clarendon Press; Oxford University Press, Oxford [Oxfordshire], New York, **1987**.
- [30] H. J. C. Berendsen, J. P. M. Postma, W. F. Vangunsteren, A. Dinola, J. R. Haak, *Journal of Chemical Physics* **1984**, 81, 3684.
- [31] S. Hezaveh, S. Samanta, A. De Nicola, G. Milano, D. Roccatano, *Journal of Physical Chemistry B* **2012**, in press.
- [32] S. Park, F. Khalili-Araghi, E. Tajkhorshid, K. Schulten, *Journal of Chemical Physics* **2003**, 119, 3559.
- [33] S. Park, K. Schulten, *Journal of Chemical Physics* **2004**, 120, 5946.
- [34] C. Jarzynski, *Physical Review Letters* **1997**, 78, 2690.
- [35] J. S. Hub, B. L. de Groot, D. van der Spoel, *Journal of Chemical Theory and Computation* **2010**, 6, 3713.
- [36] M. Souaille, B. Roux, *Computer Physics Communications* **2001**, 135, 40.
- [37] B. Roux, *Computer Physics Communications* **1995**, 91, 275.
- [38] S. Kumar, D. Bouzida, R. H. Swendsen, P. A. Kollman, J. M. Rosenberg, *Journal of Computational Chemistry* **1992**, 13, 1011.

Chapter 1

Structure and Dynamics of 1,2-Dimethoxyethane and 1,2-Dimethoxypropane, in
Non-aqueous Solutions

Structure and Dynamics of 1,2-Dimethoxyethane and 1,2-Dimethoxypropane in Nonaqueous Solutions

ABSTRACT.

In this chapter, a comparative modelling study of 1,2-dimethoxyethane (DME) and 1,2-dimethoxypropane (DMP) at 298 K and 318 K in the infinite dilution condition in methanol, carbon tetrachloride, and *n*-heptane is reported. Both DME and DMP are united-atom models compatible with GROMOS/OPLS force fields. The structural, dynamic and thermodynamic properties of DME and DMP were found to be consistent with experimental results and expected trends. The free energy of solvation of DME in non-aqueous solvents follows the trend methanol < carbon tetrachloride < *n*-heptane, and that is consistent with the dielectric constant values of the solvents. The presence of an extra methyl group on chiral carbon makes DMP less soluble than DME in polar solvents but more soluble in non-polar solvents such as *n*-heptane.

INTRODUCTION.

1,2-dimethylethene oxide (DME) and 1,2-dimethoxypropane (DMP) are commonly used organic solvents.^[1-6] The presence of hydrophilic and hydrophobic moieties in the DME structure ($\text{CH}_3\text{-O-CH}_2\text{-CH}_2\text{-O-CH}_3$) results in a high solubility both in water (in all proportion and at different temperatures)^[7] and in common organic solvents of different polarity. The properties of DME have been investigated in the liquid phase, in aqueous solution, and in organic solvents using different experimental techniques. Dynamic properties and diffusive behavior of the molecule in solution have been studied using Raman spectroscopy, light scattering (Brillouin and photon correlation spectroscopy),^[8-11] and nuclear magnetic resonance (NMR) spectroscopy.^[12] Thermodynamic measurements^[13-15] in the pure liquid and in water solution have been used to obtain information on the intra- and inter-molecular interactions.^[16] Though study of DME and DMP in non-aqueous solvents much less than those of pure liquid and aqueous solution, thermodynamic data of DME in methanol, carbon tetrachloride (CCl_4), and *n*-heptane as well as in other solvents are also available.^[17-22]

DME (Fig. 1.1) is the smallest oligomer (one monomer) of the polyethylene oxide (PEO) polymer. For this reason, it was used as the reference model to parameterize force field for this polymer. Several theoretical studies on DME have been conducted using both quantum mechanical and MD simulations.^[23-36] From these studies, different force field models, parameterized against experimental properties of the pure liquid and of water solutions, have been proposed.

In the case of DMP, the smallest oligomer of the polypropylene oxide (PPO), the presence of an additional methyl group in the structure ($\text{CH}_3\text{-O-C}^*\text{H}(\text{CH}_3)\text{-CH}_2\text{-O-CH}_3$) renders the molecule more hydrophobic than DME and adds a chiral center. Different physical and thermodynamic properties are also available for the liquid DMP. In addition, the conformational population of the molecule in water and in different

organic solvents has been characterized using NMR spectroscopy.^[37] As for DME, it can be used as reference model to parameterize force fields for polymer PPO. To the best of our knowledge, very few theoretical studies on DMP are present in the literature and the only atomistic force field for MD simulations so far available is the all-atoms model proposed by Smith et al.^[30, 38]

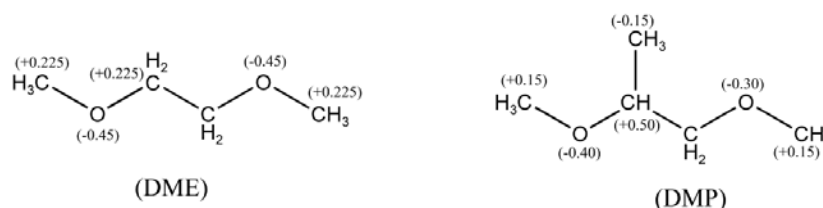


Figure 1.1: Molecular structures of DME and DMP with their partial charge on the heavy-atoms.

In addition, for both DME and DMP, none of the reported theoretical models have been also parameterized or tested against physico-chemical properties in both aqueous and non-aqueous solvents. Extending the parameterization of both solvents to non-aqueous conditions, besides unrevealing details of their properties in these conditions at atomistic level, can provide a more reliable model for studying their interaction and the corresponding polymers with biological, or in general, at organic interfaces. In this paper, we will propose new united atom models for both DME and DMP compatible with both GROMOS and OPLS united atom (OPLS-UA) force fields. In our study, the physical and thermodynamic properties of the new models have been tested at infinite dilution in methanol, carbon tetrachloride, and *n*-heptane using MD simulations. In the next chapter, the model of DME and DMP will be used to extend this study to the corresponding polymers (PEO and PPO) in the same milieu conditions. The aim of this study is to provide reliable models of these polymers that can be used to study their properties in non-aqueous milieu as biological membranes or in general, organic interfaces.

The chapter is organized as follows. The details of the force field parameterization are given in the ‘Methods’ section. In ‘Result and Discussions’,

calculated thermodynamic, dynamic, and structural properties of DME and DMP molecules in different solvents are reported. Finally, in 'Conclusions' overall properties of the models are discussed and summarized.

METHODS.

Force-field parameters.

DME. The initial Lennard-Jones (LJ) parameters have been derived from our previous study of a PEO model.^[39] The LJ interaction parameters of the ether oxygen atoms with methanol oxygen atoms have been modified for better reproduction of the structural and dynamic properties. The bonded parameters, in particular, dihedral angle parameters were taken from Anderson and Wilson.^[40] The initial quantum mechanically derived partial charges were taken from the same paper^[40] and subsequently adjusted using a trial-and-error approach to reproduce correct experimental density and diffusion coefficient for pure DME.^[41, 42]

DMP. Lennard-Jones parameters were taken the same as for the DME and PEO. The initial partial charges, taken from Smith et al.,^[38] were adjusted during the optimization procedure to reproduce the correct density and enthalpy of evaporation of the pure liquid. The bonded interaction parameters were also adapted from Smith et al.^[38] with the exception of the middle dihedral (O-C-C*-O) that it was modified to obtain the correct experimental dihedral distributions for our model. All DMP simulations have been performed using the *R*-isomer unless differently indicated.

Solvents. OPLS united atoms solvent models were used for methanol,^[43] carbon tetrachloride,^[44] and *n*-heptane.^[45]

Molecular dynamics simulations setup.

All MD simulations were performed using GROMACS (version 4.0.7) software package.^[46] In the simulations, all-bonds were constraint using the LINCS algorithm.^[47] The integration

time step was set to 2 fs. The temperature was maintained to the reference values using the Berendsen thermostat^[48] with coupling time constant $\tau_T = 0.1$ ps. The pressure was kept maintained at 1 bar using Berendsen barostat with coupling constant $\tau_p = 0.5$ ps. The isothermal compressibility values used for the pressure coupling algorithm were 1.2×10^{-4} , 1.06×10^{-4} , and $1.4 \times 10^{-4} \text{ bar}^{-1}$ for methanol, carbon tetrachloride, and *n*-heptane, respectively.^[49, 50] The long range interactions were applied using the particle mesh Ewald^[51] with a real space cut-off of 0.9 nm, a Fourier mesh spacing of 0.12 nm, and a fourth-order interpolation. The Lennard-Jones interactions were calculated using a cutoff of 1.4 nm. All the errors on the calculated properties have been evaluated using the block averaging method.^[52]

The diffusion coefficients from simulations (D_{PBC}) were calculated using the Einstein formula. The mean square displacement was calculated with respect to the coordinates of the molecular center of mass. The D_{PBC} was then corrected for the finite size effect using the approach proposed by Hasimoto^[53] and applied by Dunweg et al.^[54], Yeh et al.,^[55] and recently by Pranami et al.^[54-56] In the corrected diffusion coefficient (D) is given by

$$D = D_{PBC} + \frac{\xi k_B T}{6 \pi \eta L}$$

where L is the length of the cubic box, T is the simulation temperature, ξ is a constant with value 2.837297,^[53-55] k_B is the Boltzmann constant, and η is the viscosity of the medium.

Shear viscosities were calculated using non-equilibrium method.^[57] In this method the viscosity of the liquid is estimated from non-equilibrium systems where an external shear-stress acceleration field is applied to the system. The external acceleration field induces a velocity gradient of the same shape. The velocity gradient was calculated as described in the work of Hess.^[57] Under these conditions, for a Newtonian fluid, the dynamic viscosity (η) can be easily derived from the resulting velocity.^[57] For these simulations, a rectangular box of volume $4 \times 4 \times 14 \text{ nm}^3$ was used. The viscosity was calculated for different shear-stress acceleration rates and then extrapolated to obtain the

zero shear rate viscosity.

DME and DMP in non-aqueous solvents.

Each simulation was conducted using a 3 nm/side cubic box containing one DME or DMP molecule at its center and 380, 306, and 208 molecules of methanol, carbon tetrachloride, and *n*-heptane, respectively. Simulations were performed at 318 and 298 K in NPT conditions for 20 ns.

Gibbs free energy of solvation, ΔG , has been calculated for DME and DMP in all solvents at 298 K using the thermodynamic integration (TI) method with soft-core potential.^[58] The integration was performed on 17 λ points: 0, 0.01, 0.05, 0.1, 0.2, 0.3, 0.4, 0.5, 0.55, 0.6, 0.65, 0.7, 0.8, 0.9, 0.95, 0.98, 1. The λ points were chosen in order to get a smooth variation of the $dH/d\lambda$ curve. The soft-core parameters alpha and sigma were assigned the values of 1.51 and 0.30, respectively, as suggested by Villa and Mark.^[59] For each lambda, the system was first equilibrated for at least 150 ps allowed by a production run of at least 500 ps.

The spatial density distribution of the solvent molecules around the oligomers was calculated using *g_spatial* program of the GROMACS package. A cubic grid with 0.1 nm grid spacing was used for all the calculations. The solvent molecules were centered around the solute in each trajectory frame using a translational-rotational fit to the first configuration of the MD trajectory and removing the periodic boundary conditions. Finally, the atomic positions of the selected atoms of solvent molecules were mapped on a cubic grid centered on the geometric center of the reference solute and averaged with respect to the number of frames analyzed. The averaged volumetric density data obtained was analyzed using the program VMD.^[60]

RESULTS AND DISCUSSIONS.

DME in non-aqueous solvents.

Gibbs free energy of solvation (ΔG_{sol}) of one DME molecule in methanol, carbon tetrachloride, *n*-heptane, was also calculated at 298 K and results are shown in Table 1.1. Although experimental data are not available for a direct comparison, the expected trend of a gradual increase of ΔG_{sol} with the decrease of the dielectric constant is observed. Furthermore, with the exception of *n*-heptane and CCl_4 , the values are lower than the ΔG_{sol} in the pure liquid indicating a good solubility in these solvents.

Table 1.1: Free energy of solvation values of DME and DMP in solvents at 298 K.

Solvent	ΔG_{DME} (kJ/mol)	ΔG_{DMP} (kJ/mol)
Methanol	-25.3 ± 0.2	-18.4 ± 0.5
CCl_4	-12.2 ± 0.5	-12.9 ± 0.7
<i>n</i>-heptane	-11.1 ± 0.5	-12.7 ± 0.5
Water^[41, 42]	-22.1 ± 0.8	-16.0 ± 1.1

The calculated self-diffusion coefficients of DME molecules (D_{DME}) and the solvents (D_{sol}) at 318 and 298 K are reported in Table 1.2. Since direct experimental data of the self-diffusion coefficients are not available, the D values of the pure solvents at different temperatures were also calculated and compared with their corresponding experimental data.^[61-65] The comparison provides a ratio between the experimental and calculated data of 1.0, 0.7, 0.8 (at 318 K) and 0.8, 0.5, 0.7 (at 298 K) for methanol, CCl_4 , and *n*-heptane, respectively. The ratio is consistent with the published D values for the solvent models at both temperatures.^[64, 66, 67] The self-diffusion coefficients for the solvents were corrected to account the box size effects for the long range interactions as mentioned in the Methods section. The correction factor accounts for 21%, 15%, 18% (at 318 K) and 15%, 13%, 16% (at 298 K) for methanol, CCl_4 , and *n*-heptane, respectively. The deviations at 298 K are

consistent with the estimation of $\sim 12\%$ deviation of the D_{PBC} for similar system size reported by Yeh and Hammer.^[55]

Table 1.2: Diffusion coefficient values of DME and the solvents at 318 K and 298 K.

Solvent	318 K			298 K		
	D_{sol}	<i>Expt. D_{sol}</i> ($D_{\text{sol bulk}}$)	D_{DME}	D_{sol}	<i>Expt. D_{sol}</i> ($D_{\text{sol bulk}}$)	D_{DME}
Methanol	3.3	3.35 (4.0)	1.1	2.0	2.34 (3.0)	0.8
CCl₄	3.3	1.82 (3.1)	2.1	2.6	1.28 (2.7)	2.0
<i>n</i>-heptane	4.6	3.34 (4.7)	3.9	4.2	3.34 (4.3)	3.3
Water^[41, 42]	4.1	3.44 (4.0)	2.2	2.8	2.25 (2.8)	0.9

In the case of the systems with DME in infinite dilution conditions, the D_{sol} lies very close to that of the pure solvent value in all the cases. The D_{DME} follows a similar trend observed for the surrounding solvents. The D_{DME} value is higher in non-polar *n*-heptane and lower for the polar solvent methanol (and water). This can be explained by the free energy of solvation that shows better solvation of DME in polar solvents, and this can be accounted for restricted mobility of the solute molecule in polar solvents resulting in lower diffusion coefficient values. Relatively lower value for D_{DME} in CCl₄ can be related to the high molar mass of the solvent molecules.

In Fig. 1.2, the $O_{\text{DME}}-O_{\text{W}}$, $O_{\text{DME}}-O_{\text{MeOH}}$, $O_{\text{DME}}-\text{C}_{\text{CCl}_4}$, and $O_{\text{DME}}-\text{C}(4)_{\text{hep}}$ RDFs are reported. A sharp peak at 0.29 nm characterizes the RDF for the simulation in methanol. The better organization of the methanol molecules around the DME oxygen explains the calculated lower solvation free energy in methanol than in water. The RDF of DME in the carbon tetrachloride shows two main features at 0.80 and 1.32 nm. The RDF in *n*-heptane shows very similar peak positions but the peaks are more flat and smooth. The same peak positions are observed at 298 K as well. Coordination numbers of the first two shells in

different solvents are reported in Table A1.2 in Appendix I.

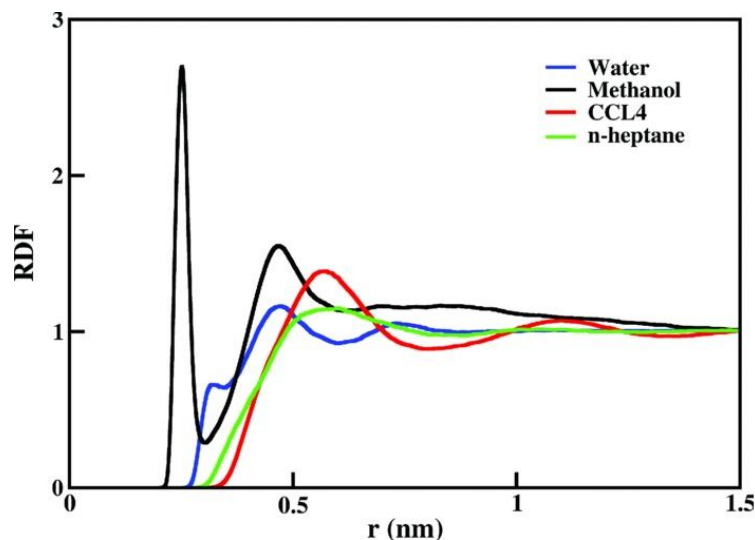


Figure 1.2: RDF plots of $O_{DME}-O_{MeOH}$, $O_{DME}-C(4)_{hep}$, and $O_{DME}-CCl_4$ and in comparison with $O_{DME}-O_W$ ^[41, 42] at 318 K for one DME molecule in different solvents.

In Fig. 1.3, the spatial density distributions of the solvent atoms in the first solvation shell of DME (upper row) at 318 K are reported. The central molecule is a representative structure of DME. For methanol, the density distributions of the hydrogen and oxygen atoms are localized in the region between the two oxygen atoms of the DME and DMP. This indicates that solvent molecules are involved in hydrogen bonding interactions with both of these two atoms. The density distribution for DME is higher and more localized than that for DMP as a consequence of the more hydrophilic nature of the molecule. In fact, the methyl group on DMP chiral carbon prevents the formation of strong hydrogen bond with the solvent molecules. In addition, the presence of localized hydrogen bond interactions determines the observed non-uniform density distributions. On the contrary, for the non-polar solvents, we have more uniform distributions as a consequence of the absence of strong localized interactions. From Fig. 1.3, it is also evident that the solvent chirality of the DMP has no major effect on the spatial distribution of the solvent atoms around DME. In both cases we observe an inner cloud of carbon on one side of the DME molecule and a

cloud of oxygen on the other side.

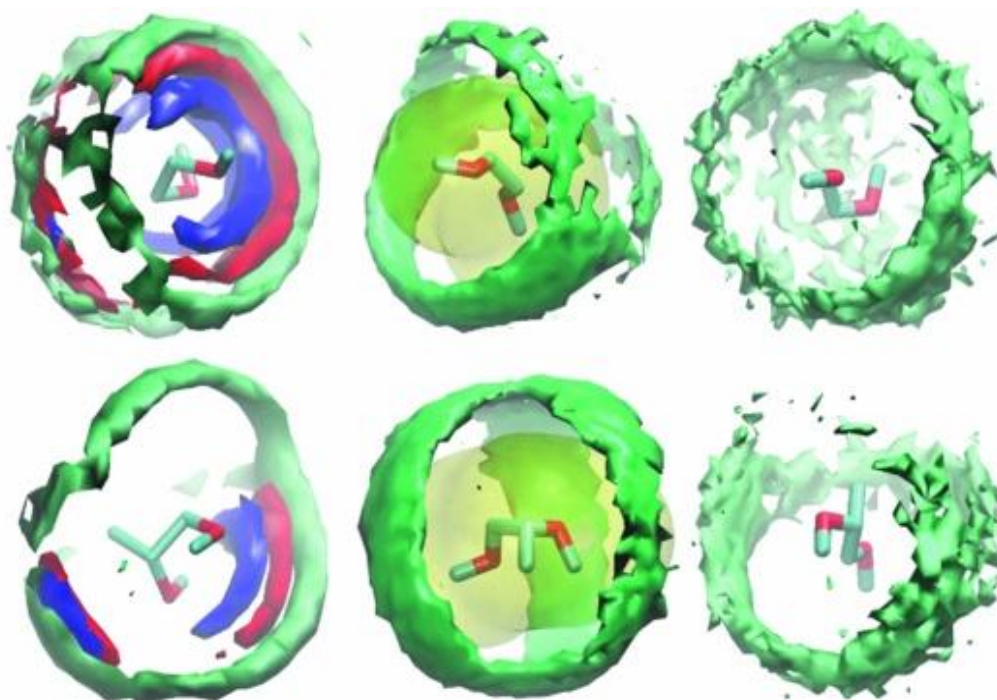


Figure 1.3: Spatial density distributions of the solvent atoms in the first solvation shell of DME (upper row) and DMP (lower row) at 318 K. From the left to right, methanol, CCl_4 , and *n*-heptane density distribution are reported, respectively. The hydrogen atoms are in blue, oxygen in red, carbon in green, and chlorine in yellow. The density surfaces have isovalues of 0.004, 0.0016, and 0.0008 for methanol, carbon tetrachloride, and *n*-heptane, respectively.

In Table 1.3, the percentages of conformational population of the three most abundant conformers of DME (TGT, TGG', and TGG) are reported. The data indicate that the overall contribution of TGT configuration tends to increase with the polarity of the solvent. The populations in CCl_4 are similar to those in *n*-heptane and they are also consistent with the experimental NMR measurements in the same solvent and in benzene.^[68, 69] The experimental and theoretical data also show that the populations do not have substantial changes going from liquid phase to non-polar solvents.^[68, 69] At 298 K, a decrease in the population of conformers in polar solvents and a small increase in the non-polar one was observed.

Table 1.3: Dihedral distributions (in percentage) of DME in the solvents at 318 K and 298 K.

Solvent	318 K			298 K		
	<i>TGT</i>	<i>TGG'</i>	<i>TGG</i>	<i>TGT</i>	<i>TGG'</i>	<i>TGG</i>
Methanol	45	23	25	34	21	17
CCl₄	36	16	14	38	13	19
<i>n</i>-heptane	35	15	12	26	14	16
Water^[41, 42]	54	12	18	49	20	18

In Fig. 1.4, the distributions of the DME dipole moment calculated from the simulations are reported. The distribution from polar solvent, methanol, (also water) shows a strong peak around 3.2 D, while for carbon tetrachloride and *n*-heptane the distribution is almost flat in the range from 1.0 to 3.2 D with a small peak at 3.2 D. For methanol, the maximum of the distribution corresponds to the dipole moment of the most populated conformations TGT and TGG (Table 1.3). Values at both 298 and 318 K of the average dipole moment of different conformers do not show significant differences (Table A1.1 in Appendix I).

DMP in non-aqueous solvents.

The values for ΔG_{sol} of DMP in methanol, carbon tetrachloride, and *n*-heptane are reported in Table 1.1 As for the DME, the gradual increase of the value from water to *n*-heptane is consistent with the lowering of dielectric constant. In the case of DMP in *n*-heptane and carbon tetrachloride, the ΔG_{sol} values are smaller than those of DME in the same solvent. The presence of the methyl group allows more favorable interactions with these more hydrophobic solvents than DME. The higher ΔG_{sol} values for DMP also indicate lower solubility in polar solvents than DME.

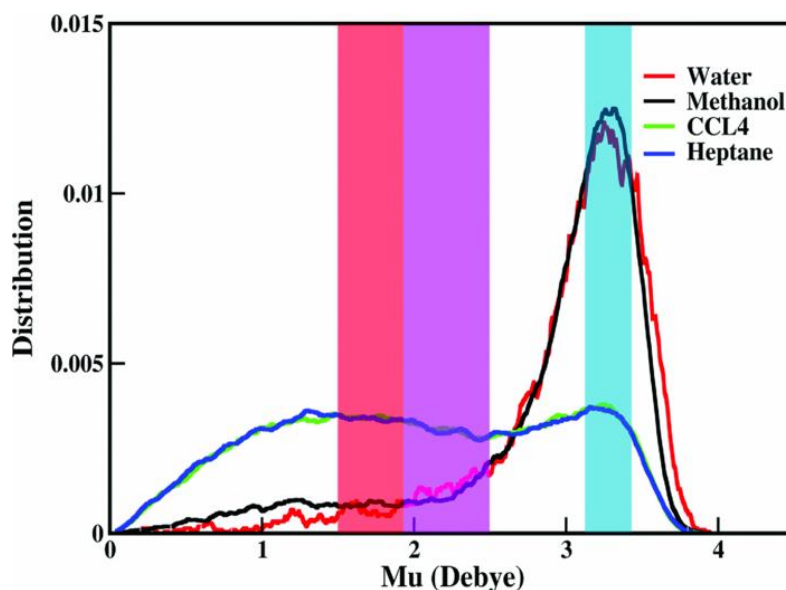


Figure 1.4: Dipole moment distribution of DME in methanol, carbon tetrachloride, and *n*-heptane in comparison to water at 318 K. The colored bands are showing the distribution of the dipoles for the three most populated conformation (red: TGG', purple: TGT, blue: TGG).

The calculated diffusion coefficients of solvents and DMP are reported in Table 1.4. The trends are more or less similar to that of DME. This indicates that the presence of an extra methyl group does not have a significant effect on the dynamic properties of DMP at infinitely diluted conditions. The self-diffusion values at 298 K are also reported in the same table. We observe a similar trend for the diffusion coefficient of solvent molecules.

Table 1.4: Diffusion coefficient values of DMP and the solvents at 318 K and 298 K.

Solvent	318 K			298 K		
	D_{sol}	<i>Expt. D_{sol}</i> ($D_{sol\ bulk}$)	D_{DMP}	D_{sol}	<i>Expt. D_{sol}</i> ($D_{sol\ bulk}$)	D_{DMP}
Methanol	3.4	3.35 (4.0)	2.2	2.0	2.34 (3.0)	2.0
CCl ₄	3.0	1.82 (3.1)	2.4	2.7	1.28 (2.7)	2.7
<i>n</i> -heptane	4.8	3.34 (4.7)	4.2	4.2	3.34 (4.3)	2.8
Water ^[41, 42]	3.8	3.44 (4.0)	1.5	2.7	2.25 (2.8)	1.1

Fig. 1.5 presents the radial distribution function of $O_{DMP}-O_{MeOH}$, $O_{DMP}-C_{CCl_4}$, and $O_{DMP}-C(4)_{hep}$ at 318 K. The positions of the RDF features resemble those of the DME RDFs, but the peaks are shorter and smoother because of the hindrance produced by the methyl group on the chiral carbon. At 298 K, the RDF shows a similar trend. The solvation number of the first two shells in different solvents is reported in Table A1.3 in Appendix I. As we expect, the solvation numbers in methanol are higher in the case of DME than DMP. On the contrary, in case of CCl_4 , the higher value of DMP than DME shows better interaction of the former with this solvent. Finally, no relevant differences in the number of solvation molecules are observed for the simulation in *n*-heptane.

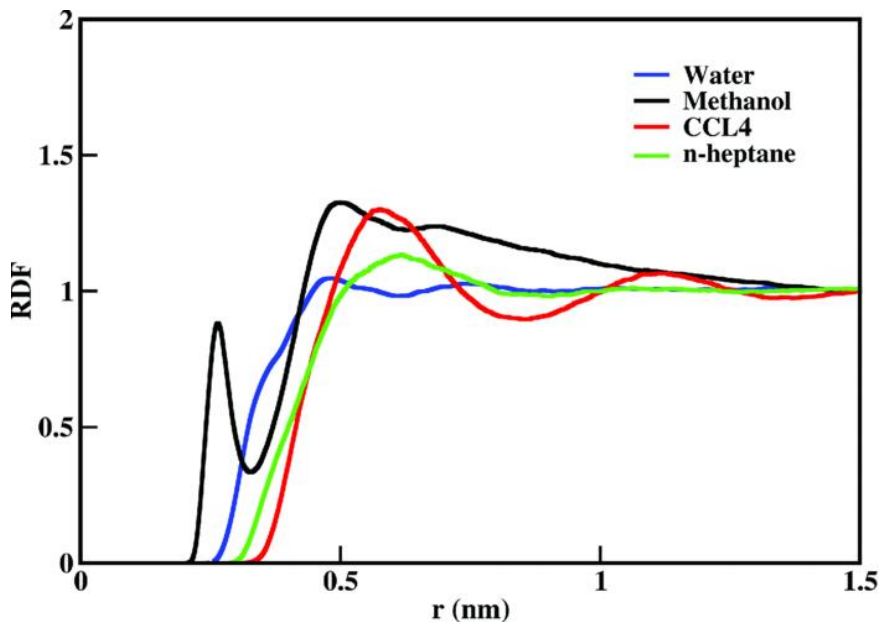


Figure 1.5: RDF plots of $O_{DMP}-O_{MeOH}$, $O_{DMP}-C(4)_{hep}$, and $O_{DMP}-C_{CCl_4}$ in comparison with $O_{DMP}-O_W$ ^[41, 42] at 318 K for one DMP molecule in different solvents.

The conformation population of the middle dihedral (OC^*CO) was analyzed and the results were compared with the experimental ones in gas phase.^[37] The results, shown in Table 1.5, indicate that for non-polar carbon tetrachloride and *n*-heptane, the dihedral distribution is very similar to the experimental one in gas phase. However, in polar solvents the population of gauche conformers increases considerably, and at 298 K, we observe an

increase in the population of trans form and a decrease in gauche form as expected by the higher conformational energy of gauche than the trans conformers.

Table 1.5: Percentage of conformational population of DMP in the solvents at 318 K and 298 K.

Solvent	318 K			298 K		
	<i>G</i>	<i>T</i>	<i>G'</i>	<i>G</i>	<i>T</i>	<i>G'</i>
Methanol	65	20	15	68	17	15
CCl₄	40	39	21	47	31	22
<i>n</i>-heptane	44	38	18	50	27	22
Water^[41, 42]	70	16	14	79	12	9
Gas phase^[37]	41	39	20	-	-	-

In Fig. 1.6, distributions of DMP dipole moments at 318 K in different solvents are reported. In polar solvents, as methanol (and water^[41, 42]), there are strong peaks around 3.0 D. On the contrary, for CCl₄ and *n*-heptane, the distribution is very similar and more uniform and similar to the DME ones. As for DME, we have considered the three dihedrals COC*C, OC*CO, and C*COC and calculated the average dipole moment for their four most abundant conformations TGT, TG'T, GGT, and GTT. In Fig. 1.6, the range of dipole values for these conformations is reported as colored bands.

The distributions from polar solvents show a strong peak around 3.0 D which is populated by GGT and GTT conformations. The same peak is also present in CCl₄ and *n*-heptane, but is less intense. In addition, in the apolar solvents the distribution is rather constant for different conformations. The values of dipole moment for the most abundant conformers at 298 and 318 K are reported in Table A1.1 in Appendix I.

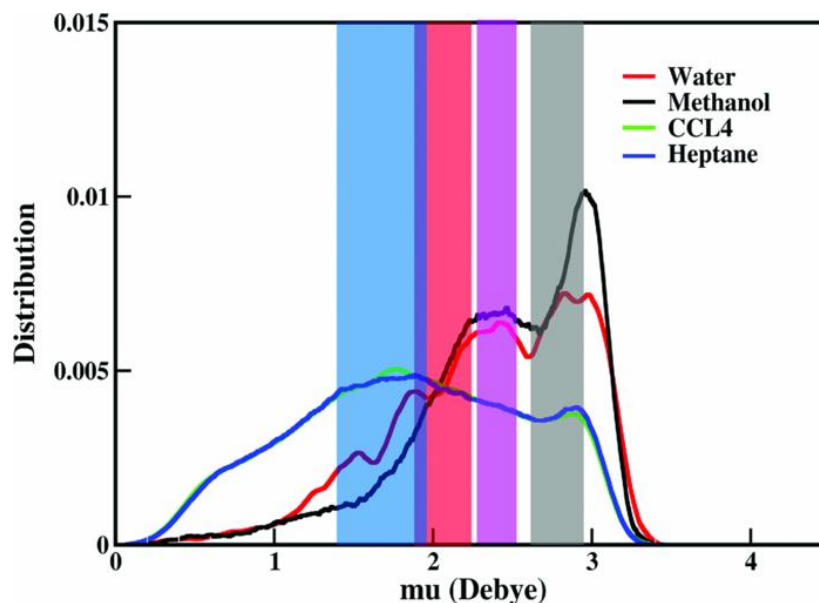


Figure 1.6: Dipole moment distribution of DMP in methanol, carbon tetrachloride, and *n*-heptane in comparison to water^[41, 42] at 318 K. Stripes (Blue: TGT, red: TG'T, purple: GTT and gray: GGT) are showing the average position of the dipoles for most abundant conformations of DMP.

CONCLUSIONS.

Recently we proposed two new united atom force field models for DME and DMP compatible with GROMOS and OPLS-UA force fields and they performed satisfactorily in water.^[41, 42] In this work we have tested the properties of them in methanol, carbon tetrachloride, and *n*-heptane solutions. The aim of this study was to provide models of both molecules compatible with hydrophilic and hydrophobic environments and transferable to the corresponding PEO and PPO polymers. The compatibility to different milieu conditions is important for the study of their interaction with biological interfaces.

The new DME force field shows substantial improvement over other available force fields on several aspects. First of all, we tested the all-round performance of the model using non-aqueous solvents. To the best of our knowledge these are the first DME and DMP models to be parameterized against these conditions. In our study, we considered three

organic solvents (methanol, carbon tetrachloride, and *n*-heptane) having large difference in polarity to study solvent effects on DME and DMP. The results of our simulations show that the ΔG_{sol} of DME shows a decreasing trend going from methanol, carbon tetrachloride, and *n*-heptane, which is in agreement with the dielectric constant of the solvents. Contrary to the DME, the presence of an extra methyl group makes DMP less soluble than DME in water but more soluble in non-polar solvents as *n*-heptane. However, the ΔG_{sol} of DMP shows less discrimination for methanol, carbon tetrachloride and *n*-heptane.

In conclusion, the new force fields consistently reproduce the behavior of both oligomers in non-aqueous solvents with their expected physical and thermodynamic properties.

REFERENCES.

- [1] C. A. Vincent, *Solid State Ionics* **2000**, 134, 159.
- [2] C. Vinas, R. Benakki, F. Teixidor, J. Casabo, *Inorganic Chemistry* **1995**, 34, 3844.
- [3] M. E. Mason, G. R. Waller, *Analytical Chemistry* **1964**, 36, 583.
- [4] D. S. Erley, *Analytical Chemistry* **1957**, 29, 1564.
- [5] F. E. Critchfield, E. T. Bishop, *Analytical Chemistry* **1961**, 33, 1034.
- [6] R. Shaw, W. H. Elliott, *Journal of Lipid Research* **1978**, 19, 783.
- [7] C. Branca, A. Faraone, S. Magazu, G. Maisano, P. Migliardo, V. Villari, *Journal of Molecular Liquids* **2000**, 87, 21.
- [8] H. Matsuura, K. Fukuhara, *Journal of Molecular Structure* **1985**, 126, 251.
- [9] S. A. Wahab, H. Matsuura, *Chemistry Letters* **2001**, 30, 198.
- [10] M. Georgiev, T. Popova, Z. S. Nickolov, N. Goutev, G. Georgiev, H. Matsuura, *Central European Journal of Chemistry* **2004**, 2, 617.
- [11] N. Goutev, K. Ohno, H. Matsuura, *Journal of Physical Chemistry A* **2000**, 104, 9226.
- [12] K. Inomata, A. Abe, *Journal of Physical Chemistry* **1992**, 96, 7934.

-
- [13] G. Douheret, J. C. R. Reis, M. I. Davis, I. J. Fjellanger, H. Hoiland, *Physical Chemistry Chemical Physics* **2004**, 6, 784.
- [14] A. Henni, P. Tontiwachwuthikul, A. Chakma, *Canadian Journal of Chemical Engineering* **2005**, 83, 358.
- [15] R. L. McGee, W. J. Wallace, R. D. Rataiczak, *Journal of Chemical and Engineering Data* **1983**, 28, 305.
- [16] E. E. Fenn, D. E. Moilanen, N. E. Levinger, M. D. Fayer, *Journal of the American Chemical Society* **2009**, 131, 5530.
- [17] S. Kinugasa, H. Nakahara, J. I. Kawahara, Y. Koga, H. Takaya, *Journal of Polymer Science Part B-Polymer Physics* **1996**, 34, 583.
- [18] J. H. Sung, D. C. Lee, H. J. Park, *Polymer* **2007**, 48, 4205.
- [19] P. Zhou, W. Brown, *Macromolecules* **1990**, 23, 1131.
- [20] M. Duval, *Macromolecules* **2000**, 33, 7862.
- [21] V. Crupi, G. Maisano, D. Majolino, R. Ponterio, V. Villari, E. Caponetti, *Journal of Molecular Structure* **1996**, 383, 171.
- [22] J. Luettmmer-Strathmann, *International Journal of Thermophysics* **2005**, 26, 1693.
- [23] M. La Rosa, A. Uhlherr, C. H. Schiesser, K. Moody, R. Bohun, C. J. Drummond, *Langmuir* **2004**, 20, 1375.
- [24] F. R. Trouw, O. Borodin, J. C. Cook, J. R. D. Copley, G. D. Smith, *Journal of Physical Chemistry B* **2003**, 107, 10446.
- [25] O. Borodin, D. Bedrov, G. D. Smith, *Macromolecules* **2001**, 34, 5687.
- [26] O. Borodin, D. Bedrov, G. D. Smith, *Journal of Physical Chemistry B* **2002**, 106, 5194.
- [27] B. K. Annis, O. Borodin, G. D. Smith, C. J. Benmore, A. K. Soper, J. D. Londono, *Journal of Chemical Physics* **2001**, 115, 10998.
- [28] G. D. Smith, R. L. Jaffe, D. Y. Yoon, *Journal of the American Chemical Society* **1995**, 117, 530.
- [29] G. D. Smith, D. Bedrov, O. Borodin, *Physical Review Letters* **2000**, 85, 5583.
- [30] G. D. Smith, D. Bedrov, *Journal of Physical Chemistry A* **2001**, 105, 1283.
- [31] G. D. Smith, D. Bedrov, *Macromolecules* **2002**, 35, 5712.
- [32] G. D. Smith, O. N. Starovoytov, O. Borodin, D. Bedrov, *Journal of Chemical Theory and*

Computation **2011**, 7, 1902.

- [33] E. E. Dormidontova, *Macromolecules* **2004**, 37, 7747.
- [34] D. Bedrov, O. Borodin, G. D. Smith, *Journal of Physical Chemistry B* **1998**, 102, 9565.
- [35] J. M. Stubbs, J. J. Potoff, J. I. Siepmann, *Journal of Physical Chemistry B* **2004**, 108, 17596.
- [36] I. Vorobyov, V. M. Anisimov, S. Greene, R. M. Venable, A. Moser, R. W. Pastor, A. D. MacKerell, *Journal of Chemical Theory and Computation* **2007**, 3, 1120.
- [37] Y. Sasanuma, *Journal of Physical Chemistry* **1994**, 98, 13486.
- [38] G. D. Smith, O. Borodin, D. Bedrov, *Journal of Physical Chemistry A* **1998**, 102, 10318.
- [39] S. Pal, G. Milano, D. Roccatano, *Journal of Physical Chemistry B* **2006**, 110, 26170.
- [40] P. M. Anderson, M. R. Wilson, *Molecular Physics* **2005**, 103, 89.
- [41] S. Hezaveh, Jacobs University Bremen (Bremen), **2012**.
- [42] S. Hezaveh, S. Samanta, G. Milano, D. Roccatano, *Journal of Chemical Physics* **2011**, 135, 164501.
- [43] W. L. Jorgensen, D. S. Maxwell, J. TiradoRives, *Journal of the American Chemical Society* **1996**, 118, 11225.
- [44] W. L. Jorgensen, J. M. Briggs, M. L. Contreras, *Journal of Physical Chemistry* **1990**, 94, 1683.
- [45] W. L. Jorgensen, J. D. Madura, C. J. Swenson, *Journal of the American Chemical Society* **1984**, 106, 6638.
- [46] B. Hess, C. Kutzner, D. van der Spoel, E. Lindahl, *Journal of Chemical Theory and Computation* **2008**, 4, 435.
- [47] B. Hess, H. Bekker, H. J. C. Berendsen, J. G. E. M. Fraaije, *Journal of Computational Chemistry* **1997**, 18, 1463.
- [48] H. J. C. Berendsen, J. P. M. Postma, W. F. Vangunsteren, A. Dinola, J. R. Haak, *Journal of Chemical Physics* **1984**, 81, 3684.
- [49] American Institute of Physics., D. E. Gray, *American Institute of Physics handbook*, 3d ed., McGraw-Hill, New York,, **1972**.
- [50] *CRC Handbook of Chemistry and Physics*, CRC Press, Cleveland, Ohio, **1977**.
- [51] T. Darden, D. York, L. Pedersen, *Journal of Chemical Physics* **1993**, 98, 10089.

- [52] H. Flyvbjerg, H. G. Petersen, *Journal of Chemical Physics* **1989**, 91, 461.
- [53] H. Hasimoto, *Journal of Fluid Mechanics* **1959**, 5, 317.
- [54] B. Dunweg, K. Kremer, *Journal of Chemical Physics* **1993**, 99, 6983.
- [55] G. Hummer, I. C. Yeh, *Journal of Physical Chemistry B* **2004**, 108, 15873.
- [56] G. Pranami, M. H. Lamm, R. D. Vigil, *Physical Review E* **2010**, 82, 51402.
- [57] B. Hess, *Journal of Chemical Physics* **2002**, 116, 209.
- [58] A. E. Mark, in *Encyclopedia of Computational Chemistry*, Vol. 2 (Ed.: P. v. R. Schleyer), John Wiley & Sons, **1998**, p. 1211.
- [59] A. Villa, A. E. Mark, *Journal of Computational Chemistry* **2002**, 23, 548.
- [60] W. Humphrey, A. Dalke, K. Schulten, *Journal of Molecular Graphics* **1996**, 14, 33.
- [61] K. Krynicki, C. D. Green, D. W. Sawyer, *Faraday Discussions* **1978**, 199.
- [62] M. A. McCool, L. A. Woolf, *Journal of the Chemical Society-Faraday Transactions I* **1972**, 68, 1971.
- [63] J. W. Moore, R. M. Wellek, *Journal of Chemical and Engineering Data* **1974**, 19, 136.
- [64] M. Haughney, M. Ferrario, I. R. McDonald, *Journal of Physical Chemistry* **1987**, 91, 4934.
- [65] R. L. Hurle, L. A. Woolf, *Australian Journal of Chemistry* **1980**, 33, 1947.
- [66] H. J. C. Berendsen, J. P. M. Postma, W. F. van Gunsteren, J. Hermans, (Ed.: B. Pullman), Reidel: Dordrecht, **1981**, p. 331.
- [67] H. J. C. Berendsen, J. R. Grigera, T. P. Straatsma, *Journal of Physical Chemistry* **1987**, 91, 6269.
- [68] R. Begum, T. Sagawa, S. Masatoki, H. Matsuura, *Journal of Molecular Structure* **1998**, 442, 243.
- [69] O. W. Howarth, M. Michael, R. N. Ibbett, *Polymer* **1997**, 38, 355.

Chapter 2

Solvent Effects on Conformation and Dynamics of Polyethylene Oxide and Polypropylene Oxide Chains in common organic solvents

Solvent Effects on Conformation and Dynamics of Polyethylene Oxide and Polypropylene Oxide Chains in common organic solvents

ABSTRACT.

In this chapter, the conformational and dynamic properties of polyethylene oxide (PEO) and polypropylene oxide (PPO) polymer chains at 298 K have been studied at infinite dilution condition in methanol, chloroform, carbon tetrachloride and *n*-heptane using molecular dynamics simulations. The conformational properties of PEO and PPO show an increasing gauche preference for the O-C-C-O dihedral in the following order methanol>chloroform>carbon tetrachloride=*n*-heptane. On the contrary, the preference for trans conformation has a maximum in carbon tetrachloride and *n*-heptane followed in the order by chloroform and methanol. The PEO conformational preferences are in qualitative agreement with results of NMR studies. PEO chains formed different type of hydrogen bonds with polar solvent molecules. In particular, the occurrence of bifurcated hydrogen bonding in chloroform was also observed. Radii of gyration of PEO chains of length larger than *n*=9 monomers showed a good agreement with light scattering data in methanol. For the shorter chains the observed deviations are probably due to the enhanced hydrophobic effects caused by the terminal methyl group. The fitting of the end-to-end distance with the semi-flexible chain model at 298 K provided a persistence length for PEO as 0.387 nm in methanol.

INTRODUCTION.

Polyethylene oxide (PEO) and polypropylene oxide (PPO) homo-polymers are important polyethers with a broad range of application in polymer chemistry, biotechnology and particularly, in medicine. Polyethylene oxide is an amphiphilic non-toxic^[1] homopolymer with $\text{CH}_3\text{-O-}[\text{CH}_2\text{-CH}_2\text{-O}]_n\text{-CH}_3$ chemical formula, in which n is the number of monomers. PEO is completely soluble in water and in other organic solvents, such as methanol, acetonitrile, dioxane, chloroform, and benzene.^[2] This behavior is the result of a balance between the hydrophobic forces caused due to the presence of ethylene units and hydrophilic interactions determined by oxygen atoms. The consequence of these two complementary interactions leads to the solubility of PEO in water for a broad range of concentrations and temperatures.^[3] These peculiar properties are exploited in electrochemistry as polymer electrolyte membranes and gels for battery^[4-6], fuel cells^[7, 8] ion chromatography,^[9] and crystallography as macromolecule crystallization agent.^[10] The amphiphilic behavior of PEO in water solution has attracted a large interest, and thus, a large number of experimental studies have been published.^[11-18] On the contrary, structural and dynamics study of this polymer in other solvents are not well covered and, to the best of our knowledge, only a limited number of studies of this polymer in methanol, ethanol and chloroform are reported in literature.^[19-21]

Several computational studies, at atomistic level, have also been conducted on the PEO polymers to complement the available experimental data and hence understand their molecular properties at atomic level.^[21-32] However, the scarce availability of experimental data of PEO in other solvents has also limited the number of computational studies in non-aqueous milieu.^[33, 34]

Polypropylene oxide (PPO) polymer differs from PEO by the presence of an extra methyl group, $(\text{X-O-}[\text{C}^*\text{H-CH}_2\text{-O}]_n\text{-Y})$ bound to the chiral carbon atom (C^*) in each unit, which makes this polymer more hydrophobic than PEO. Therefore, PPO can be stereoregular or stereoirregular (isotactic, syndiotactic and atactic) accordingly to the

alternation of the chiral center configurations in each repeating unit. Some experimental studies of PPO in solutions like chloroform, carbon tetrachloride and benzene are available. These studies report the thermodynamic properties of this polymer and details on the conformation adopted by the chains.^[35-38] Different quantum mechanical calculations^[39] of PPO chains have been reported. However, few atomistic molecular dynamics simulations studies are available on this polymer ^[40-42] and none of them in non-aqueous solutions.

Pluronics are linear ABA-type triblock copolymers with the middle (B) block of PPO and outer (A) blocks of PEO. They have broad range of applications in biotechnology (e.g. detergent, lubrication, emulsification),^[43] biomedical sciences (e.g. drug delivery and biocompatible material)^[44] and gene therapy.^[45] The broad range of use for these polymers is a consequence of their properties in solution and at interfaces, in particular, the possibility to modulate solubility and other solution thermodynamic properties by changing the block composition. Therefore, they can be customized for specific applications by an appropriate choice of relative proportions of PPO and PEO units.^[35] Despite the vast amount of experimental information, their structural and dynamic properties in different solvents have been poorly studied from a theoretical perspective.

In the previous chapter, we have proposed a new united atom GROMOS/OPLS-UA compatible force field model optimized for the smaller ($n=1$) PEO and PPO oligomers, 1,2-dimethoxyethane (DME) and 1,2-dimethoxypropane (DMP).^[33] We studied their structure and dynamic properties in methanol (MeOH), carbon tetrachloride (CCl₄) and *n*-heptane. In this work, we extend the study by considering polymers of different chain lengths ($n=2, 3, 4, 5, 6, 7, 9, 18, 27, 36, 43$) in the same solvent conditions and in addition, in chloroform (CHCl₃). This work aims to understand the effect of solvents on the conformation and dynamics of these polymers in solutions. Further, the study of these polymers in different milieu conditions is also important for understanding their

interactions with organic and biological interfaces.

METHODS.

Force-field parameters.

PEO and PPO. The force field parameters for PEO and PPO polymers were taken from the DME and DMP model reported in our previous paper.^[33] The force field parameters are compatible with GROMOS/OPLS-UA. We adopted this force field for compatibility with a commonly used model of biological membrane.^[46]

Solvents. OPLS united atoms solvent models were used for methanol,^[47] carbon tetrachloride,^[48] and *n*-heptane.^[49] For chloroform, the model by Dietz and Heinzinger was used.^[50]

Molecular dynamics simulations setup.

All MD simulations were performed using GROMACS (version 4.0.7) software package.^[51] In the simulations, all-bonds were constrained using the LINCS algorithm.^[52] The integration time step was set to 2 fs. The temperature was maintained to the reference values using the Berendsen thermostat^[53] with coupling time constant $\tau_T=0.1$ ps. The pressure was kept constant to 1 bar using Berendsen barostat^[53] with coupling constant $\tau_p=0.5$ ps. The isothermal compressibility values used for the barostat algorithm were 1.2×10^{-4} , 1.0×10^{-4} , 1.06×10^{-4} and 1.4×10^{-4} bar⁻¹ for methanol, chloroform, carbon tetrachloride and *n*-heptane, respectively. The long range interactions were applied using the Particle Mesh Ewald (PME)^[54] with a real space cut-off of 0.9 nm, a Fourier mesh spacing of 0.12 nm and fourth-order interpolation. The Lennard-Jones interactions were calculated using a cut-off of 1.4 nm. All the errors on the calculated properties have been evaluated using the block averaging method.^[55]

PEO, PPO and Pluronic P85 in non-aqueous solvents.

Single chains of polymers with different lengths of 2, 3, 4, 5, 6, 7, 9, 18, 27, 36, and 43 for

PEO and PPO were simulated for 50 ns in all solvents in *NPT* ensemble at $T=298$ K. The detailed compositions of the simulated systems are reported in Table A1.4 in Appendix I. A Single chain of Pluronic P85 (PEO₂₆-PPO₄₀-PPO₂₆) was also simulated in a box of ~ 8 nm/side containing 5862, 2695, 2371 and 1608 molecules of methanol, chloroform, carbon tetrachloride and *n*-heptane, respectively. The simulations were run for 100 ns at 293 and 298 K in *NPT* ensemble.

End-to-end distance relaxation time. The end-to-end distance (h) relaxation time (τ) was calculated by computing the autocorrelation function, $C(t)$ of the end-to-end vector L as,

$$C(t) = \frac{\langle L(0).L(t) \rangle}{\langle L^2 \rangle}$$

and then by fitting $C(t)$ with the Kohlrausch-Williams-Watts stretched exponential function,^[56]

$$C(t) = \exp \left[- (t / \alpha)^\beta \right]$$

where α and β are the two fitting parameters. The relaxation time is then equal to the time integral of the stretched exponential, which is given,

$$C(t) = \frac{\alpha}{\beta} \Gamma \left(\frac{1}{\beta} \right)$$

with Γ as the Euler function.

Persistence length calculation. The contour and persistence length of the polymer chains were calculated by comparing end-to-end distributions calculated from the trajectories to worm-like chain (WLC) ^[57, 58] model given by,

$$P(R) = \frac{4\pi NR^2}{l_c^2 A^{\frac{9}{2}}} \exp\left(-\frac{3l_c}{4l_p A}\right)$$

where N is the normalization factor, l_c is contour length or the length of fully extended polymer, l_p is the persistence length and A is equal to,

$$A = 1 - \frac{R^2}{l_c^2}$$

RESULTS AND DISCUSSIONS.

PEO in non-aqueous solvents.

The rotation about the O-C-C-O and C-O-C-C dihedrals in PEO determines the overall polymer conformation and interaction with its environment.^[59] Therefore, we have analyzed the population distributions of the two dihedrals for all the PEO chains in different solvents.

In Fig. 2.1 the dihedral distributions of the two dihedrals in different solvents are shown and in Table 2.1 the fraction values of trans (T) and gauche (G) conformers are reported. Since no significant variations were observed among the distributions of the different polymer chains, only the distributions for the PEO18 polymer are reported. The distributions in Fig. 2.1 show a clear preference for gauche (a) and trans (b) conformation for the O-C-C-O and C-O-C-C dihedrals, respectively. The distributions have very similar shape in all solvents with two peaks centered on the gauche conformation (around -60° , 60°). However, the gauche population decreases going from methanol to *n*-heptane. These results are consistent with the NMR results indicating that polar solvents tend to enhance the stability of gauche conformations.^[60] The same authors also investigated the trans and gauche fractions of O-C-C-O dihedral of PEO3 (triglyme) in water, methanol and chloroform.^[60] They reported a population of 89% and 89% gauche conformers in methanol and chloroform, respectively.^[61] On the other

hand, they have shown that trans fraction in this dihedral are in the order of 11% in chloroform and methanol. These results qualitatively agree with the relative in the populations obtained from our simulations of gauche conformations in the solvents.

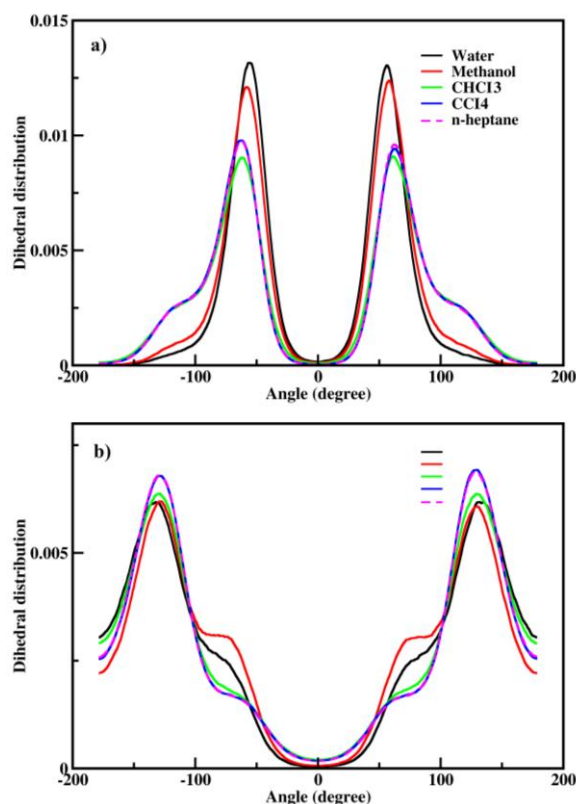


Figure 2.1: Dihedral distribution of O-C-C-O bond (up) and C-O-C-C bond (down) for PEO in different solvents. CCl₄ and *n*-heptane have the same distribution. Water was put for reference.^[62, 63]

From the C-O-C-C bond dihedral distributions in Fig. 2.1, the two peaks are observed which are centered for all the distributions on the trans conformation (around -130°, 130°). It is again consistent with NMR data of triglyme and IR spectroscopy for PEO.^[59] Our results show that this dihedral has a large population of trans conformers but smaller fraction of gauche ones in all solvents. However, methanol has a lower population of trans conformers compared to chloroform, carbon tetrachloride and *n*-heptane. Methanol shows the highest gauche population that decreases going from chloroform to carbon tetrachloride and *n*-heptane, respectively.

Table 2.1: Dihedral distribution of O-C-C-O bond (above) and C-O-C-C bond (below) for PEO in different solvents. Carbon tetrachloride and *n*-heptane are having the same distribution.

O-C-C-O	Methanol	CHCl ₃	CCl ₄	<i>n</i> -heptane
T	0.07	0.14	0.15	0.15
G	0.93	0.86	0.85	0.85
C-O-C-C				
T	0.61	0.67	0.68	0.68
G	0.38	0.33	0.32	0.32

Based on IR spectroscopy data of PEO ($n=1$ to 4) in methanol and chloroform the conformational behavior of the O-C-C-O dihedral suggests the presence of several types of hydrogen bonds between the polymer chain and water. They revealed that both the hydrogen bonding and the structural matching between the PEO chain and the solvent are important in the conformational stabilization of the chain in these solvents.^[17, 64, 65] Therefore we have analyzed hydrogen bonds formation between the polymer oxygen atoms and polar protic solvents molecules by calculating the number and types of hydrogen bonds. The numbers of hydrogen bonds calculated for PEO₂ in methanol and chloroform resulted in 1-2 per PEO molecule. Hydrogen bond distances decreases from chloroform (0.34 nm) > methanol (0.25 nm). These results show that methanol forms stronger hydrogen bonding with PEO. More affinity of PEO to methanol was previously shown from low free energy of DME in methanol.^[33]

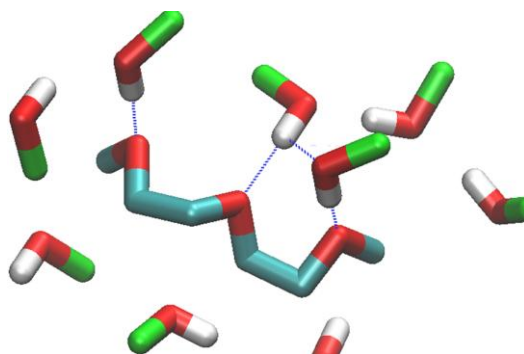


Figure 2.2: Hydrogen bonds (blue lines) between PEO₂ and methanol molecules. Hydrogen-bonded bridge by one or more than one methanol molecule between the ether oxygen atoms. For clarity, only some solvent molecules are shown. Oxygen, carbon and hydrogen are shown in red, blue and white, respectively and CH₃ in methanol is in green.

For methanol, an IR experimental study suggests that, in analogy with water, that methanol can form hydrogen bonds with the PEO chain by forming bridges of two or more linked methanol molecules between the ether oxygen atoms.^[65] This was also observed from our simulation and one example is shown in Fig. 2.2.

In the case of chloroform the analysis of the experimental results for DME suggested that chloroform can form strong bifurcated hydrogen bonds with the adjacent oxygen atoms of ethers.^[65] The analysis of the PEO2 and PEO7 in chloroform simulations evidenced the presence of two hydrogen bond types, the first type which is between the hydrogen of the solvent and one oxygen of the polymer and the second one is bifurcated type in which a single hydrogen participates the hydrogen bonding with two oxygen atoms of the same chain (Fig. 2.3). While for the PEO2 chain only one bifurcated H-bond was observed at a time, for the PEO7 simultaneous bifurcated hydrogen bonds along the chain (Fig. 2.3b) can be observed. *Ab-initio* calculations^[17] show that the bifurcated hydrogen bond occurs at the distance of 0.209 and 0.230 nm between hydrogen and the two adjacent oxygen. The average values from our results were 0.215 and 0.227 nm in excellent agreement with the *ab-initio* calculations.

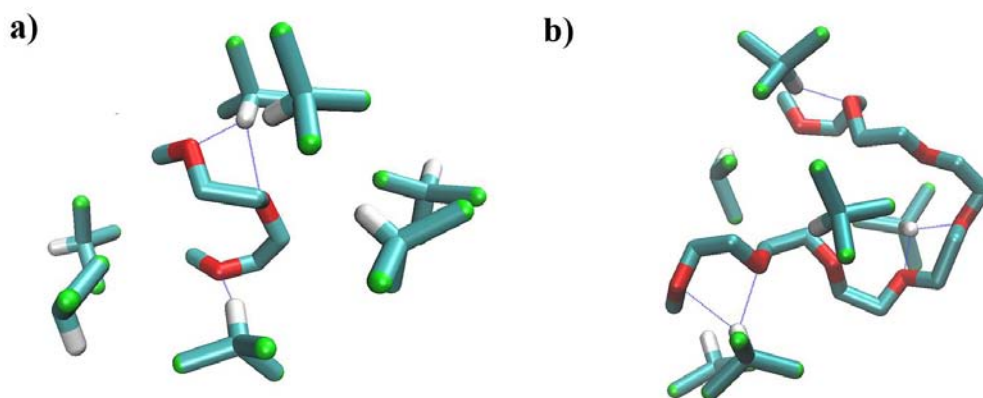


Figure 2.3: Hydrogen bonds (blue lines) between PEO2 (a) and PEO7 (b) and chloroform molecules. Normal and bifurcated hydrogen bonds formation is shown in blue lines. For long chains as PEO7, simultaneous bifurcated bonds were observed. For clarity, only some solvent molecules are shown. Oxygen, carbon, hydrogen and chlorine are shown in red, blue, white and green, respectively.

Calculated radius of gyration (R_g) and average end-to-end distances ($\langle h \rangle$) are shown in Fig. 2.4 and 2.5. In Fig. 2.4, the radii of gyration are plotted vs. molecular weight for all chains in all different solvents. The curves are fitted using the power law,^[18]

$$R_g = aM_w^\nu$$

where M_w is the molecular weight and ν is the Flory exponent.^[66] Our results were compared with the available extrapolated experimental data from power law of long chains.^[18] All the curves especially in methanol show two trends. One for short chains up to $n=9$ and another for the longer chains from $n=18-43$.

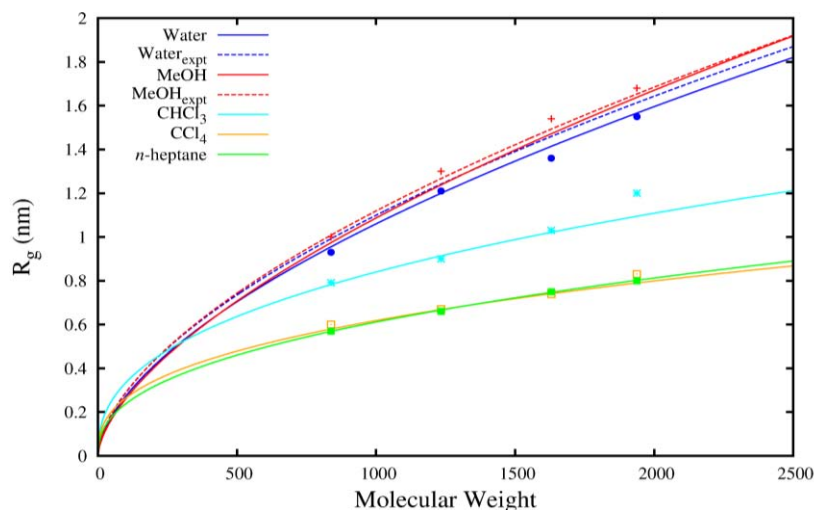


Figure 2.4: Radius of gyration for PE018-43 plotted against molecular weight for all solvents at 298 K. Water is shown for reference.^[62, 63]

For short chains the R_g values in methanol are smaller than experimental extrapolated values and deviating from power law derived from longer chains simulations. A possible explanation of this effect is the presence of methyl end-groups that decrease the hydration. The effect is more dominant in short chains than longer ones causing these deviations. The effect of end-groups was studied both experimentally and theoretically in PEO chains.^[25, 67-69] Based on these studies, it was shown that the solubility is strongly affected by methyl end-groups. The reduced solvation probably favors more compact polymer conformation and decreasing the value of R_g as we

observed in our simulations.

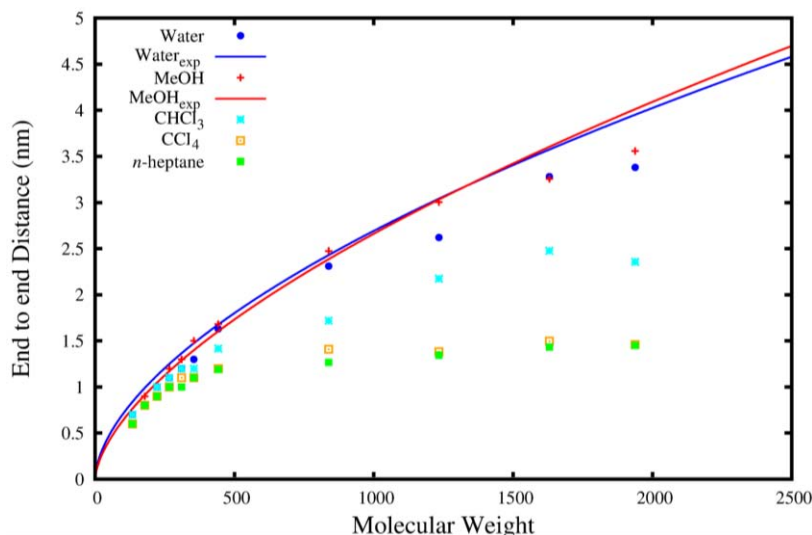


Figure 2.5: End-to-end distance of PEO chains in all solvents. The points are from water and methanol simulation values. Water is shown for reference.^[62, 63]

For methanol, recent light scattering data were available for high molecular weights (10^5 - 10^6).^[20] In this case, they reported a power law as,

$$R_g = 0.019 \times M_w^{0.60}$$

and the expression of the fitted power law from our simulations is,

$$R_g = 0.015 \times M_w^{0.62}$$

In this case a good agreement between the experimental and calculated values is observed.

For other solvents, the power laws obtained by fitting the longer chains are following,

$$R_g = 0.018 \times M_w^{0.55} \text{ for chloroform,}$$

$$R_g = 0.048 \times M_w^{0.37} \text{ for carbon tetrachloride,}$$

$$R_g = 0.036 \times M_w^{0.41} \text{ for } n\text{-heptane,}$$

respectively. The lower values of the Flory exponent clearly indicate a more compact chain especially for carbon tetrachloride and *n*-heptane as they are not good solvents for the hydrophilic PEO chain. As shown in Fig. 2.4 and from the higher value of the Flory exponent, chloroform has an intermediate behavior between polar and non-polar solvents probably due to the peculiar hydrogen bonding between PEO and solvent molecules that favors more extended configuration of the polymer.

End-to-end distance values were compared with the experimental extrapolated ones derived from the radius of gyration values by applying the formula,^[70]

$$R_g = \frac{0.665}{\sqrt{6}} \langle h^2 \rangle^{0.5}$$

In Fig 2.5, differently from the radius of gyration, the end-to-end distance values in methanol show a slow convergence in compare to the one from extrapolated experimental curve. In fact, the agreement with experimental extrapolated value is smaller as the chain length gets larger than 27 monomers. Longer simulation time is required to improve these values. The distributions in carbon tetrachloride and *n*-heptane were very similar and only the *n*-heptane distributions are shown. In methanol and chloroform, the distributions are very close, however the height of the peaks decreases going from methanol to chloroform. The WLC model fitting to the distributions for PEO was previously used by Lee et al. at atomistic and coarse-grained level [29, 71]. We fitted the distributions to the WLC model (Fig. 2.6) and derived the persistence length and counter length of the chains. However, for the distributions in carbon tetrachloride and *n*-heptane, it was not possible to obtain even a reliable WLC fit because of the multimodal shape of the curves due to the larger variety of conformations in solution.

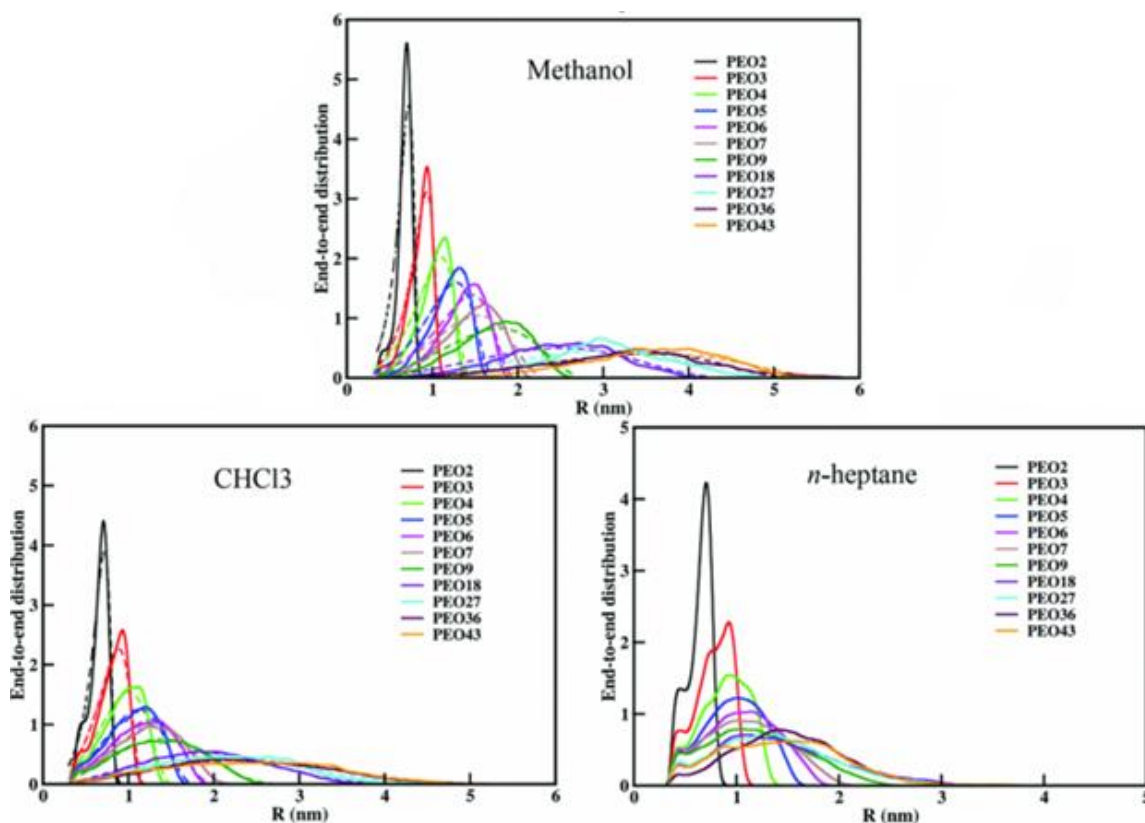


Figure 2.6: End-to-end distribution of PEO2-43 chains in all solvents. The lines are data from simulations and the dashed lines are those from fitting to the WLC model. For sake of clarity, since carbon tetrachloride and *n*-heptane distribution are very similar, only the one for *n*-heptane is shown.

From the fitting, the persistence lengths were calculated as 0.387 and 0.343 nm for methanol and chloroform, respectively. The comparison of persistence lengths shows that PEO is slightly stiffer in methanol than in chloroform; this is due to formation of stronger hydrogen bonds that prevent chains to become compact. On the other hand, based on Flory for simple chains like PEO the characteristic ratio C_∞ is related to the persistence length ^[72] as,

$$C_\infty = \frac{2l_p}{l_b} - 1$$

where l_p is persistence length and l_b (for PEO $l_b=0.15$ nm) is the bond length. Using the value of $C_\infty=4.1$ for PEO from Mark and Flory,^[73] a value of $l_p= 0.373$ nm at 296 K was

obtained.^[29] The value of C_∞ for PEO in methanol at 293 K is 4.0 ^[72] that corresponds, by applying the value of $l_p = 0.375$ nm, which is comparable to our simulation result at 298 K.

Table 2.2: The calculated end-to-end distance relaxation times (in ps) for the PEO chains.

n	Methanol	CHCl ₃	CCl ₄	<i>n</i> -heptane
2	4.6	1.8	5.0	2.7
3	8.4	4.3	9.5	4.8
4	16.6	5.6	17.1	7.8
5	21.0	9.3	25.0	11.4
6	30.8	14.4	37.6	19.4
7	38.4	17.1	47.0	25.7
9	53.2	25.3	60.1	41.8
18	269.8	108.8	222.7	139.4
27	422.8	135.1	248.2	147.2
36	482.5	176.8	380.3	157.7
43	607.3	224.4	441.0	180.5

The dynamics of the polymer in solution was analyzed by calculating the end-to-end relaxation times. In Table 2.2 the calculated fitted parameters for each chain length are reported. The relaxation times were scaled by the ratio between experimental and calculated solvent model viscosities that have a value of 1.19, 0.82, 1.80 and 1.33 for methanol, chloroform, carbon tetrachloride and *n*-heptane, respectively. The resulting relaxation time showed a solvent dependence with the value for methanol > carbon tetrachloride > chloroform > *n*-heptane, respectively. This is in consistent with higher solvation of PEO in methanol due to stronger hydrogen bonding. However due to the large viscosity difference between the two solvents, the value for carbon tetrachloride is higher than in chloroform. In fact, the viscosity of carbon tetrachloride is almost two times higher than that of chloroform.^[74] This can delay the relaxation time of chains in carbon tetrachloride even more than the effect of hydrogen bonding in chloroform.

PPO in non-aqueous solvents.

The population of the PPO conformers in the different solutions was analyzed by monitoring the O-C-C*-O dihedral. Since the population distributions of this dihedral do not show large variation for all the considered chain lengths in the different solvents, we report the results of the analysis for the chains of length $n=9$ as representative example. The results of the analysis are reported in Table 2.3.

Table 2.3: Dihedral angle population distribution (in percentage) of PPO with different chain tacticity.

O-C-C*-O	Methanol			CHCl ₃			CCl ₄			<i>n</i> -heptane		
	T	G	G'	T	G	G'	T	G	G'	T	G	G'
Atactic	8	47	45	14	49	37	17	43	40	17	44	39
Syndiotactic	20	44	36	27	43	30	30	38	32	30	36	34
Isotactic	3	54	43	5	51	44	8	54	38	8	52	40
C*-O-C-C*												
Atactic	38	32	30	34	36	30	42	31	27	41	31	28
Syndiotactic	40	29	31	40	34	26	43	29	28	41	29	30
Isotactic	34	17	49	31	7	62	43	15	42	39	17	44
C-C*-O-C												
Atactic	58	22	20	69	17	14	62	20	18	63	19	18
Syndiotactic	49	25	26	59	23	18	60	20	20	60	21	19
Isotactic	68	16	16	87	8	5	68	17	15	68	17	15

The conformation property of PPO with different tacticities shows a preponderant gauche preference for the O-C-C*-O dihedral with the following trend from methanol>chloroform>carbon tetrachloride=*n*-heptane. This attractive gauche effect was previously shown from NMR studies and also it was shown that both gauche and anti-gauche conformers become more stabilized by increasing the solvent polarity. [36, 37, 75] On the other hand, our results show that trans conformation has a maximum preference in *n*-heptane followed in a decreasing order by carbon tetrachloride, chloroform, and methanol.

For C*-C-O-C* and C-C*-O-C dihedrals a higher trans preference was observed especially for C-C*-O-C dihedral and in case of C*-C-O-C*, the gauche conformer is more

stabilized than C-C*-O-C. On average the gauche preference does not vary much for C*-O-C-C* in all solvents especially for atactic chains. In all mediums the O-C-C*-O and C*-O-C-C* dihedrals of syndiotactic chains were having the highest population of trans conformers while for isotactic ones were minimum. However for C-C*-O-C the isotactic chains had the highest population of trans which was maximum in polar solvents. The dihedral populations for atactic chains are always between those of syndiotactic and isotactic ones.

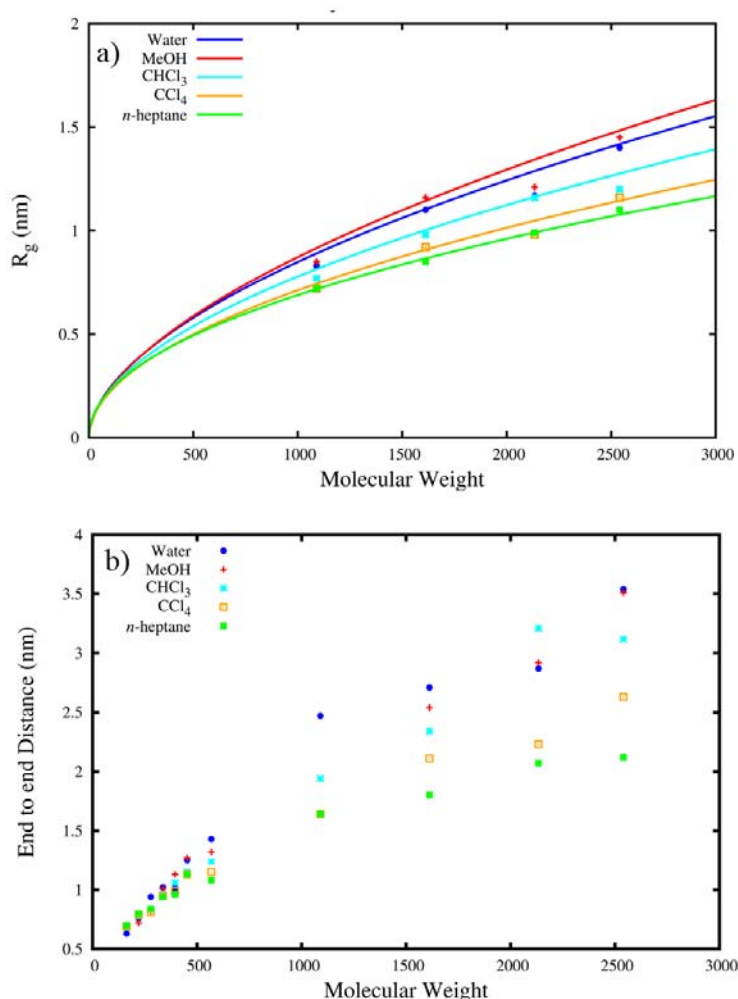


Figure 2.7: Radius of gyration (a) and end-to-end (b) distances of PPO in the different solvents plotted against molecular weight. Water is shown for reference.^[62, 63]

The average number of hydrogen bonds of polar solvent for the different PPO9 chains was also calculated. For methanol, and chloroform the number of hydrogen bonds per monomer varied from 0 to 1 with average values of 0.3 to 0.4 and 0.03, respectively. The results also indicated that the tacticity of the chain is not playing any important role in the solvation of the polymer in the considered polar solvents. For PPO, the number of hydrogen bonds per monomer in methanol is less than half of those for PEO and, in the case of chloroform, it is ten times lower. The reason of this difference is probably due to the side methyl groups that interfere with the formation of solvent hydrogen bonds.

Radii of gyration and end-to-end distances were calculated for each chain in all solvents and the results are shown in Fig. 2.7. As for PEO, a reliable fitting was possible only for longer polymer chains. In methanol, the fitting of the calculated R_g values for $n=18$ to 43 resulted in a power law as,

$$R_g = 0.017 \times M_w^{0.57}$$

This value of the exponent, ν are lower than those for PEO in the same conditions. The fitting of R_g from the simulations in other solvents resulted in the following power law relations:

$$R_g = 0.020 \times M_w^{0.53} \text{ for chloroform,}$$

$$R_g = 0.021 \times M_w^{0.51} \text{ for carbon tetrachloride,}$$

$$R_g = 0.025 \times M_w^{0.48} \text{ for } n\text{-heptane,}$$

respectively. Comparing the exponent obtained for PPO with those for PEO, it can be concluded that the long and more hydrophobic PPO chains are less compact in carbon tetrachloride and n -heptane than PEO, while it is more compact than PEO in methanol and chloroform. These results also show that the chain length affects the solubility of

PPO in the different solvents as a consequence of the polymer hydrophobicity change, being more hydrophobic as the chain length increase.

PP09 was used to examine the effect of tacticity on R_g of PPO chain, and the results are reported in Table 2.4. For each solvent, the maximum and minimum values of R_g are observed for syndiotactic and isotactic chains, respectively. For the three different atactic chains, containing a 50% random distribution of R/S chiral centers, no significant difference of the calculated R_g values was observed.

Table 2.4: Radius of gyration (in nm) and end-to-end average distances (in nm) for PP09 with different tacticities.

	R_g	$\langle h \rangle$
Methanol		
Atactic	0.57±0.005	1.52±0.02
Syndiotactic	0.60±0.004	1.68±0.01
Isotactic	0.47±0.004	1.43±0.01
CHCl₃		
Atactic	0.51±0.003	1.24±0.02
Syndiotactic	0.53±0.004	1.36±0.01
Isotactic	0.50±0.001	1.48±0.01
CCl₄		
Atactic	0.50±0.004	1.15±0.03
Syndiotactic	0.51±0.004	1.27±0.01
Isotactic	0.41±0.004	1.49±0.01
<i>n</i>-heptane		
Atactic	0.48±0.004	1.10±0.02
Syndiotactic	0.52±0.004	1.30±0.01
Isotactic	0.47±0.002	1.48±0.01

The end-to-end distance distributions of PPO chains in all solvents were also calculated. However, the fitting of the distributions with the WLC model was not possible due to the multimodal nature of all the distributions.

The relaxation times obtained from the fitting of the $C(t)$ curves for different PPO chain lengths are reported in Table 2.5.

Table 2.5: End-to-end relaxation times (in ps) for each PPO length.

<i>n</i>	Methanol	CHCl ₃	CCl ₄	<i>n</i> -heptane
2	20.2	3.8	8.7	5.1
3	71.2	21.8	64.3	55.3
4	95.1	30.2	120.0	90.7
5	118.2	32.8	141.9	101.1
6	146.8	41.0	166.8	116.8
7	170.1	56.6	198.9	130.3
9	190.3	75.7	256.9	159.6
18	240.0	115.7	475.3	307.6
27	342.8	198.8	725.0	419.8
36	530.1	271.8	814.1	604.8
43	650.3	395.6	1020.2	753.0

Values were scaled by the ratio between experimental and calculated solvent model viscosities using the same values as for PEO. It is evident that the relaxation values increase by increasing the length of polymer. However, in comparison to PEO, the relaxation times are longer; especially for longer chain lengths. For longer chains the relaxation times have the maximum value in carbon tetrachloride and the minimum one in chloroform.

Pluronic P85 in non-aqueous solvents.

From Table 2.6 at 293 K, as expected, the value of radius of gyration of Pluronic P85 was found to be maximum in methanol. However, the values in carbon tetrachloride and *n*-heptane are almost half of those in methanol and shows the chain is more compact due to the low solubility of the PEO blocks in these non-polar solvents. We also observe a decrease of the R_g for methanol and chloroform at 298 K. For non-polar solvents (carbon tetrachloride and *n*-heptane), the values at the higher temperature (298 K) are comparable to those at 293 K. In polar solvents the effect is associated with the decrease in the number of hydrogen bonds of the polymer with solvent molecules.^[76-80]

Table 2.6: Radius of gyration (in nm) for P85 at different temperature.

Temperature	Methanol	CHCl ₃	CCl ₄	<i>n</i> -heptane
293	2.40±0.5	1.30±0.01	1.03±0.01	0.98±0.01
298	1.52±0.4	1.16±0.01	1.04±0.01	0.98±0.05

CONCLUSIONS.

In this chapter, we have reported our study results on the effect of solvents (methanol, chloroform, carbon tetrachloride and *n*-heptane) on the conformation and dynamics of PEO and PPO chains at 298 K in dilute solutions. In addition, simulation of the Pluronic P85 was performed in the same solvents to check the transferability of the model to the corresponding block copolymers. The study of the polymer in different milieu conditions is important for understanding the interaction of their macromolecule with biological interfaces.

The dihedral distributions in methanol and chloroform were found in very good agreement with NMR data. We also showed the gauche preference for the C-C bond dihedrals in both PEO and PPO. The effect of the solvent on the gauche preference for PEO and PPO show the following trend from methanol>chloroform>carbon tetrachloride=*n*-heptane. On contrary, the trans conformation population increases in the order from carbon tetrachloride and *n*-heptane>chloroform >methanol. For PEO in the last two solvents, this trend is in agreement with the experimental NMR studies. The persistence length of 0.387 for PEO, calculated in methanol, is also in good agreement with the experimental value. In addition, the hydrogen bonding with polar solvent molecules was studied. In the case of PEO, different types of hydrogen bonding were observed. In particular, the simulations in chloroform showed the presence of bifurcated hydrogen bonds with the hydrogen of the chloroform molecules as predicted from experimental observations. In the case of PPO, the

absence of strong hydrogen bonding was observed.

The structure and dynamics of chains in the solvents were also studied by calculating the R_g , end-to-end distances and their relaxation time. For the R_g , the power law dependence with the chain lengths for PEO showed a good agreement with the experimental data in methanol. In case of non-polar solvents, polymer chains tend to become more compact than in polar solvent as expected by the less solubility. The good solvent behavior of the chloroform is an exception due to the hydrogen bonding between PEO chains and the solvent molecules. For PPO there are no experimental data available for comparison. However, the comparison with the PEO revealed that long PPO chains ($n=18$ to 43) are less compact in carbon tetrachloride and *n*-heptane, and more compact in water, methanol and chloroform than PEO which is due to its more hydrophobicity.

To conclude, in this study we have used a novel GROMOS/OPLS based force field to analyze different physico-chemical properties of PEO, PPO and the Pluronic P85 in different solvent conditions. The results of this work can be extended to study the interaction of these polymers with biological and nanotechnologically relevant interfaces (e.g. lipid bilayers, silica surfaces and carbon nanotubes) and for the parameterization of coarse-grained model of the same polymer for study aggregations phenomena at mesoscale level.

REFERENCES.

- [1] H. F. Smyth, C. S. Weil, M. D. Woodside, J. B. Knaak, L. J. Sullivan, Carpenete.Cp, *Toxicology and Applied Pharmacology* **1970**, 16, 442.
- [2] P. Zhou, W. Brown, *Macromolecules* **1990**, 23, 1131.
- [3] C. Branca, A. Faraone, S. Magazu, G. Maisano, P. Migliardo, V. Villari, *Journal of Molecular Liquids* **2000**, 87, 21.
- [4] J. H. Shin, W. A. Henderson, S. Passerini, *Journal of the Electrochemical Society* **2005**, 152, A978.
- [5] Y. K. Kang, K. Cheong, K. A. Noh, C. Lee, D. Y. Seung, *Journal of Power Sources* **2003**, 119, 432.

-
- [6] D. Baril, C. Michot, M. Armand, *Solid State Ionics* **1997**, 94, 35.
- [7] H. Bai, W. S. W. Ho, *Journal of Membrane Science* **2008**, 313, 75.
- [8] Y. Wu, C. Wu, F. Yu, T. Xu, Y. Fu, *Journal of Membrane Science* **2008**, 307, 28.
- [9] T. Takeuchi, B. Oktavia, L. W. Lim, *Analytical and Bioanalytical Chemistry* **2009**, 393, 1267.
- [10] A. Mcpherson, *Methods in Enzymology* **1985**, 114, 120.
- [11] K. Devanand, J. C. Selser, *Nature* **1990**, 343, 739.
- [12] K. Devanand, J. C. Selser, *Macromolecules* **1991**, 24, 5943.
- [13] B. Hammouda, D. L. Ho, *Journal of Polymer Science Part B-Polymer Physics* **2007**, 45, 2196.
- [14] A. L. Sturlaugson, M. D. Fayer, *Journal of Physical Chemistry B* **2011**, 115, 945.
- [15] A. L. Sturlaugson, K. S. Fruchey, S. R. Lynch, S. R. Aragoln, M. D. Fayer, *The Journal of Physical Chemistry B* **2010**, 114, 5350.
- [16] E. E. Fenn, D. E. Moilanen, N. E. Levinger, M. D. Fayer, *Journal of the American Chemical Society* **2009**, 131, 5530.
- [17] N. Goutev, H. Matsuura, *Journal of Physical Chemistry A* **2001**, 105, 4741.
- [18] S. Kawaguchi, G. Imai, J. Suzuki, A. Miyahara, T. Kitano, *Polymer* **1997**, 38, 2885.
- [19] D. L. Ho, B. Hammouda, S. R. Kline, W. R. Chen, *Journal of Polymer Science Part B-Polymer Physics* **2006**, 44, 557.
- [20] J. H. Sung, D. C. Lee, H. J. Park, *Polymer* **2007**, 48, 4205.
- [21] K. Tasaki, *Macromolecules* **1996**, 29, 8922.
- [22] D. Bedrov, O. Borodin, G. D. Smith, *Journal of Physical Chemistry B* **1998**, 102, 9565.
- [23] D. Bedrov, M. Pekny, G. D. Smith, *Journal of Physical Chemistry B* **1998**, 102, 996.
- [24] O. Borodin, D. Bedrov, G. D. Smith, *Journal of Physical Chemistry B* **2002**, 106, 5194.
- [25] E. E. Dormidontova, *Macromolecules* **2004**, 37, 7747.
- [26] G. D. Smith, D. Bedrov, O. Borodin, *Physical Review Letters* **2000**, 85, 5583.
- [27] K. Tasaki, *Journal of the American Chemical Society* **1996**, 118, 8459.

-
- [28] S. Pal, G. Milano, D. Roccatano, *Journal of Physical Chemistry B* **2006**, *110*, 26170.
- [29] H. Lee, R. M. Venable, A. D. MacKerell, R. W. Pastor, *Biophysical Journal* **2008**, *95*, 1590.
- [30] J. Fischer, D. Paschek, A. Geiger, G. Sadowski, *Journal of Physical Chemistry B* **2008**, *112*, 8849.
- [31] A. Bormuth, P. Henritzi, M. Vogel, *Macromolecules*, *43*, 8985.
- [32] M. Slabanja, G. Wahnström, *Chemical Physics Letters* **2001**, *342*, 593.
- [33] S. Hezaveh, S. Samanta, G. Milano, D. Roccatano, *Journal of Chemical Physics* **2011**, *135*, 164501.
- [34] S. Aparicio, R. Alcalde, J. L. Trenzado, M. N. Caro, M. Atilhan, *Journal of Physical Chemistry B* **2011**, *115*, 8864.
- [35] M. Carlsson, D. Hallen, P. Linse, *Journal of the Chemical Society-Faraday Transactions* **1995**, *91*, 2081.
- [36] T. Hirano, T. Tsuruta, P. H. Khanh, *Makromolekulare Chemie* **1972**, *153*, 331.
- [37] N. Oguni, S. Maeda, H. Tani, *Macromolecules* **1973**, *6*, 459.
- [38] A. Abe, T. Hirano, T. Tsuruta, *Macromolecules* **1979**, *12*, 1092.
- [39] Y. Sasanuma, *Macromolecules* **1995**, *28*, 8629.
- [40] G. D. Smith, O. Borodin, D. Bedrov, *The Journal of Physical Chemistry A* **1998**, *102*, 10318.
- [41] G. D. Smith, D. Bedrov, *Journal of Physical Chemistry A* **2001**, *105*, 1283.
- [42] P. Ahlstrom, O. Borodin, G. Wahnstrom, E. J. W. Wensink, P. Carlsson, G. D. Smith, *Journal of Chemical Physics* **2000**, *112*, 10669.
- [43] M. Granite, A. Radulescu, W. Pyckhout-Hintzen, Y. Cohen, *Langmuir* **2011**, *27*, 751.
- [44] X. Xin, G. Y. Xu, Z. Q. Zhang, Y. J. Chen, F. Wang, *European Polymer Journal* **2007**, *43*, 3106.
- [45] L. Wasungu, A. L. Marty, M. F. Bureau, A. Kichler, M. Bessodes, J. Teissie, D. Scherman, M. P. Rols, N. Mignet, *Journal of Controlled Release* **2011**, *149*, 117.
- [46] O. Berger, O. Edholm, F. Jahnig, *Biophysical Journal* **1997**, *72*, 2002.
- [47] W. L. Jorgensen, D. S. Maxwell, J. TiradoRives, *Journal of the American Chemical Society* **1996**, *118*, 11225.

-
- [48] W. L. Jorgensen, J. M. Briggs, M. L. Contreras, *Journal of Physical Chemistry* **1990**, *94*, 1683.
- [49] W. L. Jorgensen, J. D. Madura, C. J. Swenson, *Journal of the American Chemical Society* **1984**, *106*, 6638.
- [50] W. Dietz, K. Heinzinger, *Berichte der Bunsengesellschaft für physikalische Chemie* **1984**, *88*, 543.
- [51] B. Hess, C. Kutzner, D. van der Spoel, E. Lindahl, *Journal of Chemical Theory and Computation* **2008**, *4*, 435.
- [52] B. Hess, H. Bekker, H. J. C. Berendsen, J. G. E. M. Fraaije, *Journal of Computational Chemistry* **1997**, *18*, 1463.
- [53] H. J. C. Berendsen, J. P. M. Postma, W. F. Vangunsteren, A. Dinola, J. R. Haak, *Journal of Chemical Physics* **1984**, *81*, 3684.
- [54] T. Darden, D. York, L. Pedersen, *Journal of Chemical Physics* **1993**, *98*, 10089.
- [55] H. Flyvbjerg, H. G. Petersen, *Journal of Chemical Physics* **1989**, *91*, 461.
- [56] U. Buchenau, in *Springer Proceedings in Physics, Vol. 37* (Eds.: D. Richter, A. J. Dianoux, W. Petry, J. Teixeira), Springer-Verlag, Berlin, **1989**.
- [57] N. B. Becker, A. Rosa, R. Everaers, *European Physical Journal E* **2010**, *32*, 53.
- [58] D. Thirumalai, in *Theoretical and Mathematical Models in Polymer Research: Modern Methods in Polymer Research and Technology* (Ed.: A. I. U. Grosberg), Academic Press, San Diego, CA, Boston, **1998**, pp. 1.
- [59] J. J. Shephard, P. J. Bremer, A. J. McQuillan, *Journal of Physical Chemistry B* **2009**, *113*, 14229.
- [60] Y. Sasanuma, H. Ohta, I. Touma, H. Matoba, Y. Hayashi, A. Kaito, *Macromolecules* **2002**, *35*, 3748.
- [61] Y. Sasanuma, K. Sugita, *Polymer Journal* **2006**, *38*, 983.
- [62] S. Hezaveh, Jacobs University Bremen (Bremen), **2012**.
- [63] S. Hezaveh, S. Samanta, G. Milano, D. Roccatano, *Journal of Chemical Physics* **2012**, *136*, 124901.
- [64] R. Begum, H. Matsuura, *Journal of the Chemical Society-Faraday Transactions* **1997**, *93*, 3839.
- [65] S. A. Wahab, H. Matsuura, *Chemistry Letters* **2001**, *30*, 198.

- [66] M. Rubinstein, R. H. Colby, *Polymer Physics*, Oxford University Press., Oxford, U.K., **2003**.
- [67] H. Frielinghaus, W. B. Pedersen, P. S. Larsen, K. Almdal, K. Mortensen, *Macromolecules* **2001**, *34*, 1096.
- [68] M. Spitzer, E. Sabadini, W. Loh, *Journal of the Brazilian Chemical Society* **2002**, *13*, 7.
- [69] Z. N. Medved, M. B. Bulgakova, *Zh. Prikl. Khim.* **1980**, *53*, 1669.
- [70] C. Tanford, *Physical Chemistry of Macromolecules.*, John Wiley & Sons., New York, **1961**.
- [71] H. Lee, A. H. de Vries, S. J. Marrink, R. W. Pastor, *Journal of Physical Chemistry B* **2009**, *113*, 13186.
- [72] P. J. Flory, *Statistical Mechanics of Chain Molecules*, Wiley, New York, **1967**.
- [73] J. E. Mark, P. J. Flory, *Journal of the American Chemical Society* **1965**, *87*, 1415.
- [74] Y. Marcus, *The properties of solvents*, Wiley, Chichester; New York, **1998**.
- [75] Y. Sasanuma, *The Journal of Physical Chemistry* **1994**, *98*, 13486.
- [76] C. Branca, S. Magazu, G. Maisano, P. Migliardo, V. Villari, *Journal of Physics: Condensed Matter* **1998**, *10*, 10141.
- [77] S. L. Hager, T. B. Macrury, *Journal of Applied Polymer Science* **1980**, *25*, 1559.
- [78] S. Magazu, *Journal of Molecular Structure* **2000**, *523*, 47.
- [79] G. Maisano, D. Majolino, P. Migliardo, S. Venuto, F. Aliotta, S. Magazu, *Molecular Physics* **1993**, *78*, 421.
- [80] K. Sasahara, M. Sakurai, K. Nitta, *Colloid & Polymer Science* **1998**, *276*, 643.

Reprinted with permission from *J. Phys. Chem. B*, **2012**, 116 (17), pp 5141–5151

(DOI: 10.1021/jp211564x). Copyright (2012) American Chemical Society.

Chapter 3

Diffusion of 1,2-Dimethoxyethane and 1,2-Dimethoxypropane Through
Phosphatidylcholine Bilayers

Diffusion of 1,2-Dimethoxyethane and 1,2-Dimethoxypropane Through Phosphatidycholine Bilayers.

ABSTRACT.

In this chapter, a theoretical study of 1,2-dimethoxyethane (DME) and 1,2-dimethoxypropane (DMP) at water/*n*-heptane and 1,2-dimyristoyl-*sn*-glycero-3-phosphatidycholine (DMPC) lipid bilayer/water interfaces using the umbrella sampling method is reported. Recently proposed GROMOS96/OPLS compatible models for DME and DMP have been used for the simulation studies. The percolation free energy barrier of one DME and DMP molecule from water to *n*-heptane phase calculated using the umbrella sampling method turned out to be ~18.5 kJ/mol and ~6 kJ/mol, respectively. In the case of the DMPC lipid bilayer, overall free energy barriers of ~20 kJ/mol and ~12 kJ/mol were obtained for DME and DMP, respectively. The spontaneous diffusion of DME and DMP in the lipid bilayer has also been investigated using unconstrained molecular dynamics simulations at the water/DMPC interface and inside the lipid bilayer. As expected from the estimated percolation barriers, simulation results show that DME, contrary to DMP, spontaneously diffuse into the aqueous solution from the lipid interior. In addition, simulations with multiple DME or DMP molecules at the interface show spontaneous diffusion within 50 ns inside the DMPC layer only for DMP.

INTRODUCTION.

Ether-based molecules such as crown-ethers, polymers, and especially polyethylene oxide (PEO) and polypropylene oxide (PPO) based copolymers are of great interest for basic research and also for their applications in biotechnology and medicine.^[1-6] A significant amount of work has been published on the applications of block copolymers in the medical and pharmaceutical fields.^[7] In fact, block copolymers, being inexpensive, nontoxic and easily available; are promising substitutes for lipopolymers for drug delivery.^[8] As an example, encapsulation in polymer of peptide based drugs increases residence time and bioavailability by decreasing the chances of proteolytic decomposition.^[2, 3, 5, 6, 9, 10] Other interesting applications include, for example, the use of crown ether modified peptide to create artificial membranes or grafting of lipids and polymers to achieve specific bioactivities.^[11-14]

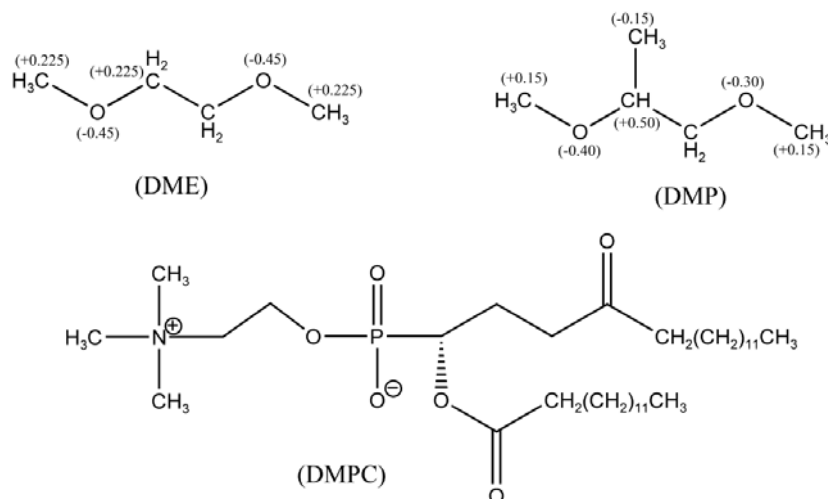


Figure 3.1: Molecular structures of DME, DMP and one chain of DMPC. Partial charge on the heavy-atoms of the DME and DMP molecules are shown in parenthesis.

For all these applications, it is of utmost importance to understand the atomistic details of the interaction of these molecules with biological membranes. Although a good number of experimental studies have already been done on the structural

characteristics and interactions of ethylene oxide/propylene oxide based polymers with biomembranes and lipid bilayers,^[10, 15-17] the details of permeation of these polymers systems across lipid membrane itself are not well known at the molecular level. Therefore, atomistic simulations of these polymers at the interface of lipid bilayers can shed light on these processes. The simplest models of these polymers are the DME and DMP molecules (Fig. 3.1). They can be considered as the smallest oligomers of the polyethylene oxide (PEO) and polypropylene oxide (PPO) polymers, the building blocks of common biocompatible block copolymers. Despite the widespread biomedical applications of these molecules, accurate molecular dynamics (MD) simulations studies to assess their thermodynamics and dynamics of the interaction with biological interfaces are limited.^[18-23] One of the reasons for so few studies is the timescale of this process which can go beyond the capacity of standard MD simulations. A more convenient way to simulate these processes is the use of potential driven and/or constrained MD simulations. The steered molecular dynamics (SMD) method ^[24, 25] (also known as ‘pulling simulation’) is commonly used to drive a process along a given pathway by applying an external constant force to the system. The additional force allows the system to easily overcome energy barriers speeding up the simulation of the process.^[18, 26, 27] The integration along the pathway of the variation of this external force provides the potential of mean force (PMF) of the process. SMD being a non-equilibrium method requires a large number of pulling simulations to provide a reliable PMF profile from which one can derive thermodynamic properties with good accuracy.^[25, 28, 29] An equivalent approach to the SMD is the umbrella sampling (US) method.^[30] In this case, the potential of mean force properties of system is obtained by conformational sampling along the reaction pathway (generated, for example, by a SMD simulation) to generate overlapped probability distributions. The resulting distributions are then combined with the weighted histogram analysis method (WHAM) to reconstruct the barrier.^[31] These two techniques have been used to study small molecules^[32-35] and polymer^[18, 36] permeation in lipid bilayers with good accuracy.

Nevertheless, to the best of our knowledge, a quantitatively accurate characterization of the lipid bilayer permeation barrier by DME and DMP molecules has not yet been performed. In the present work, we use the recently published force field models for DME and DMP molecules^[37] to study their interaction with *n*-heptane and DMPC lipid bilayer interfaces and characterize, using both SMD and US methods, the percolation barriers through them. The models of DME and DMP are further validated by calculating their partition coefficient between 1-octanol and water. The percolation of DME and DMP through water/*n*-heptane interface was investigated to understand their behavior in the presence of a simple hydrophobic interface, which is comparable to the aliphatic tail region of the lipid bilayer.

The chapter is organized as follows: The details of force fields and simulation procedures are given in the Methods Section. In the first part of the Results and Discussions, the results obtained from umbrella sampling simulations of percolation of both DME and DMP through *n*-heptane/water and DMPC/water interfaces are reported. In the second part, free simulations of DME and DMP at the DMPC interface are performed to investigate the occurrence of a spontaneous diffusion process. Finally, in the Conclusions section, a summary of the properties of DME and DMP at interfaces and the implications for the interaction of a polymer with a biological membrane are summarized.

METHODS.

Force Field.

For the DMPC bilayer, the united atom model of Berger et al.^[38] was used. This lipid model is a combination of GROMOS and OPLS parameters, optimized to reproduce the experimental physical properties of a lipid bilayer. For DME and DMP, the recent models by Hezaveh et al.^[37] were used. For the water model, the simple point charge (SPC)^[39] model was used, and for 1-octanol and *n*-heptane, the OPLS united atom (OPLS-UA)

model^[40, 41] was used.

Simulation Setup:

All the simulations were performed using the GROMACS (version 4.0.7)^[42] software package. The program VMD^[43] was used for the graphical representation of the molecular systems.

For the water/*n*-heptane interface system, 208 *n*-heptane molecules were sandwiched between ~3350 water molecules along the *z*-direction in a box of dimension 3.7×3.7×11.2 nm³. The lipid bilayer simulations were performed using a simulation box containing one DME or DMP molecule and a bilayer composed by 128 DMPC lipids chains, 64 for each layer. The box had dimension of 6.4×6.4×9.5 nm³, and it was filled with ~8000 water molecules for a total of ~30000 atoms. A schematic diagram of the position and density distribution of the DMPC bilayer along with the relevant components of the system is shown in Fig. 3.2.

The bilayer simulations were performed at 310 K, above the crystalline fluid/liquid phase transition temperature, using the V-rescale thermostat^[44] with a coupling constant of 0.1 ps. For comparison, the temperature of the water/*n*-heptane systems was set the same. The pressure was kept constant at 1 bar using the Berendsen barostat^[45] with a coupling constant of 0.5 ps. For lipid bilayer simulations, a semi-isotropic barostat was used to take in account the difference in compressibility of the system along the *x*, *y* and *z* directions. The bond lengths were constrained using LINCS^[46] algorithm. An integration time step of 2 fs was used for all the simulations. Electrostatic interactions were evaluated using particle mesh Ewald method^[47] with a cutoff of 1.0 nm, grid spacing of 0.12 nm and a fourth order spline interpolation. Lennard-Jones interactions were truncated at 1.0 nm.

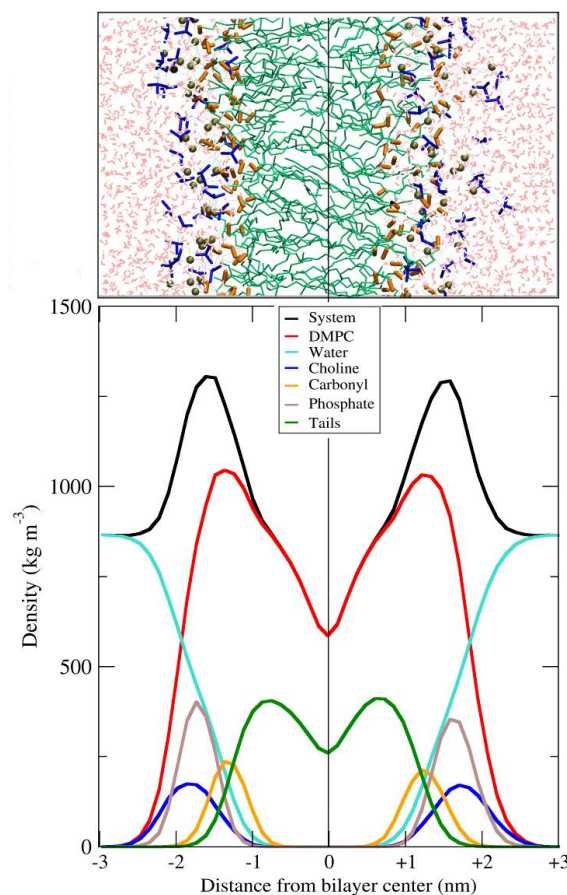


Figure 3.2: Schematic diagram of the density profile of the DMPC bilayer along z-axis. A snapshot of the simulated system is shown above. For better understanding of the position of the components, they have shown in different colors – water molecules in red, the choline groups in blue, the carboxylic groups in orange, the phosphate groups as tan spheres and the aliphatic chains are shown in green. The density profile of the whole system along with relevant components of the system is shown in the bottom half.

Calculation of the Free Energy of Solvation and Partition Coefficient.

Simulations were performed in 1-octanol as solvent for calculating the partition free energy of DME and DMP in water/1-octanol. One molecule of DME or DMP was centered in a ~ 4 nm/side cubic box including 124 1-octanol molecules. Gibbs free energy of solvation in 1-octanol (ΔG_{sol}) at 298 K was calculated for both molecules using the thermodynamic integration (TI) method.^[48] The Gibbs free energy of solvation in water (ΔG_{hyd}) and in vacuum (ΔG_{vac}) were taken from our recent publication.^[37] The TI

integration was performed on 17 λ points: 0, 0.01, 0.05, 0.1, 0.2, 0.3, 0.4, 0.5, 0.55, 0.6, 0.65, 0.7, 0.8, 0.9, 0.95, 0.98 and 1.00. The λ points were chosen in order to get a smooth variation of the $dH/d\lambda$ curve. The soft-core parameters α and σ were assigned the values of 1.51 and 0.30 respectively, as suggested by Villa and Mark.^[49] For each λ , the system was first equilibrated for 150 ps followed by a production run of 500 ps. The ΔG_{vac} was subtracted from the ΔG_{oct} value in 1-octanol to obtain the final ΔG_{sol} value. From ΔG_{sol} and ΔG_{hyd} at the temperature T , the corresponding partition coefficient is calculated according to the following formula^[41],

$$\log P_{1-octanol/water} = \frac{\Delta G_{hyd} - \Delta G_{sol}}{2.303RT} \quad (\text{Eqn. 1})$$

where R is the universal gas constant.

SMD Simulations.

SMD method was used to speed up the diffusion of DME/DMP through a) *n*-heptane layer and b) one of the monolayers of the DMPC bilayer. The SMD simulations were performed to obtain the frames for umbrella sampling simulations and also to test the convergence of the two methods. The SMD simulations were performed using a slow pulling regime to ensure operation in near-equilibrium conditions.^[29] The pulling parameters adopted by Pal et al.^[18] to study the percolation of a PEO chain through a DMPC lipid bilayer were used. For qualitative estimations, SMD takes less computational time and resources than the US methods. However, being non-equilibrium method, the calculations of the equilibrium properties require multiple number of pulling trajectories to obtain a reliable sampling.^[25, 29] From the initial tests (reported in Appendix II), it was clear that it is not possible to rely on relatively small number of SMD simulations for the calculation of quantitative free energy profile for a complex system like this. Therefore, the SMD simulations were mainly used to generate starting points for the US simulations.

Umbrella Sampling Simulations.

US method was used to calculate the free energy profiles for the percolation of the DME and DMP molecules through *n*-heptane and DMPC layer. This method has been recently used by MacCallum et al.^[32] to study the diffusion of small amino acid side chain model molecules through lipid bilayers. In the present work, we have adopted a similar procedure. A harmonic restraint with a force constant 3000 kJ/mol nm² was applied to the distance between the center of mass (CoM) of the DME/DMP molecule and the head groups of the bottom DMPC layer, in the direction normal to the bilayer. Fifty starting US configurations of both DME and DMP molecules were taken from the path of one of the SMD trajectories. The first configurations were taken at least 3 nm away from the bilayer center and the last one was taken in the bilayer center. The difference of distances between the CoM of the DME/DMP molecules and the reference group for two consecutive conformations was always less than 0.1 nm to ensure the correct calculation of the PMF profile. The same method was used for the water/*n*-heptane interface system. In this case, the *n*-heptane molecules were set to be the reference group and ~65 configurations taken from one SMD simulation were selected for umbrella sampling. Each frame was simulated for 5 ns. The distance was sampled at every 100 fs. The weighted histogram analysis method (WHAM)^[31] was used to calculate the PMF profile. The free energy profiles obtained from the calculations were rescaled to assign a zero reference value to the profiles in the bulk water. In the case of US, three different simulations of length 1, 5, and 7 ns were used to evaluate the convergence of the PMF of the DME molecule. For the system in consideration, the PMF profile did not change for simulation lengths larger than 5 ns, and therefore we have used this time scale for all the frames of US simulations of DME and DMP for both permeation through the DMPC layer and relatively simpler *n*-heptane/water interface.

Unconstrained Simulations at the Interface.

To understand the behavior of the ether molecules at interfaces, a set of 50 ns unconstrained simulations were run with DME and DMP molecules at the water/*n*-heptane

interface. The simulation boxes of dimensions $3.7 \times 3.7 \times 7.6 \text{ nm}^3$ were filled with 208 molecules of *n*-heptane and ~ 1700 molecules of water along with one molecule of DME/DMP. Simulations were done at 310 K in NPT conditions to be consistent with the umbrella sampling simulations.

The diffusive behavior of DME and DMP in different positions of the DMPC/water interface was analyzed by selecting six starting conformations from the umbrella sampling simulations for an unconstrained run of 50 ns at 310 K. The starting positions of DME and DMP with respect to the bilayer for the selected sets are shown in Fig. 3.3. Two additional 50 ns simulations were also run with nine molecules of DME and DMP at the interface region of the DMPC bilayer (1 nm away from the upper boundary of DMPC).

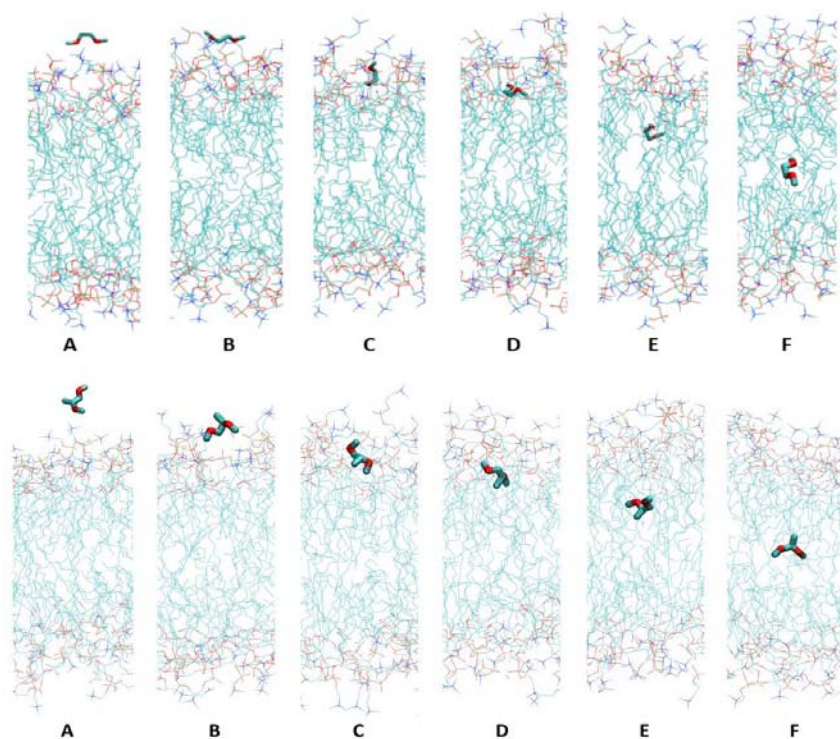


Figure 3.3: The selected six frames from the umbrella sampling simulations for detailed investigations.

These specific frames were used as the starting configuration for unconstrained simulations. Initial positions of DME with respect to the bilayer are shown in the top row and that for DMP are shown in the bottom row.

RESULTS AND DISCUSSIONS.

Free Energy and Partition Coefficient.

Gibbs free energy values for DME and DMP in 1-octanol was calculated to be 80.3 and 63.1 kJ/mol, respectively. Their ΔG values in vacuum were calculated to be 59.8 and 38.2 kJ/mol, respectively. Hence, Gibbs free energies of solvation in 1-octanol, calculated for both DME and DMP are -20.5 ± 1.3 and -24.9 ± 1.0 kJ/mol, respectively. The value for DME is in good agreement with the estimated value of -19.1 kJ/mol.^[50, 51] To the best of our knowledge, the same value for DMP is not available in the literature for a direct comparison. However, the water/1-octanol partition coefficient values ($\log P$) are available for both DME and DMP. Thus, by applying Eqn. 1 with the values of ΔG_{sol} calculated in this work and ΔG_{hyd} available from our previous work,^[37] values of $\log P_{DME} = -0.28$ and $\log P_{DMP} = 1.57$ were obtained. These values are close to the experimental values of -0.21 and 1.78, for DME and DMP, respectively.^[52, 53]

Percolation of DME and DMP through *n*-Heptane.

The middle part of the DMPC bilayer is made of aliphatic chains that can be mimicked by a layer of aliphatic liquid such as *n*-heptane.^[54] Therefore, as the first part of our study, the PMF barriers for the diffusion of the two molecules from water to the organic phase were calculated and then compared with those through the lipid bilayer.

In Fig. 3.4, the PMFs profiles calculated using umbrella sampling method are shown. The heights of the PMF energy barriers are significantly different for DME and DMP, although their profiles look qualitatively similar. For DME, the height for the energy barrier (from water to *n*-heptane) is equal to ~ 18.5 kJ/mol but it is only ~ 6.0 kJ/mol for DMP. In both profiles, a minimum at the *n*-heptane/water interface is observed. The origin of these minima is related to the nature of the interface. The *n*-heptane molecule being a hydrophobic solvent, exerts repulsive force towards water and hence molecular density drops significantly at interfaces, resulting in a reduction of

the PMF in these regions.

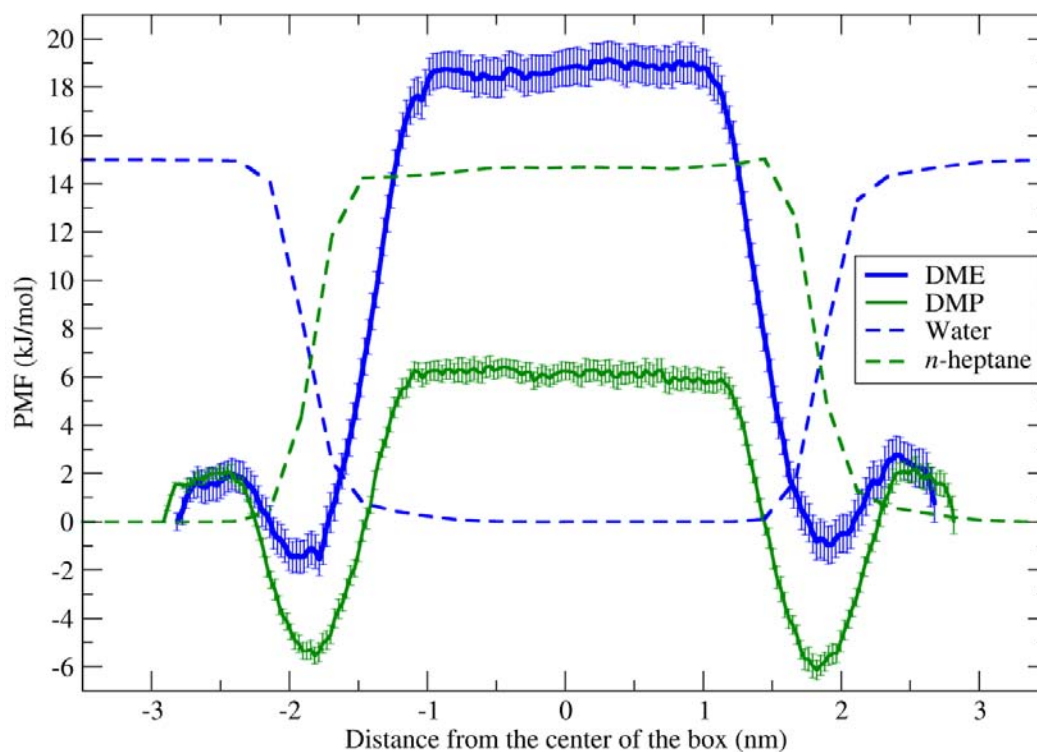


Figure 3.4: PMF profiles for percolation of DME (blue) and DMP (green) molecules from water to water layer through *n*-heptane layer. The relative positions of the solvents are shown in dashed line. The center of the box is the center of the *n*-heptane layer along *z*-direction.

Fig. 3.5 shows the non-bonded energy contribution of DME and DMP with other relevant components of the system, i.e., water and *n*-heptane. For this purpose, five sets of simulations from the umbrella sampling trajectories were considered for further analysis where the ether molecule reside in five different environments: in bulk water (1.85 nm away from the interface), in water near the interface (0.25 nm away from the interface), in the interface, in *n*-heptane near the interface (0.25 nm away from the interface) and in bulk *n*-heptane (1.85 nm away from the interface). When the solutes are in the water phase, Lennard-Jones contributions with water have average values of -61.15 (± 0.56) kJ/mol and -73.42 (± 0.26) kJ/mol, respectively for DME and DMP. In the *n*-heptane phase the values of Lennard-Jones interaction energies with *n*-heptane

increase to $-48.87 (\pm 0.65)$ kJ/mol and $-56.83 (\pm 0.68)$ kJ/mol, respectively for DME and DMP.

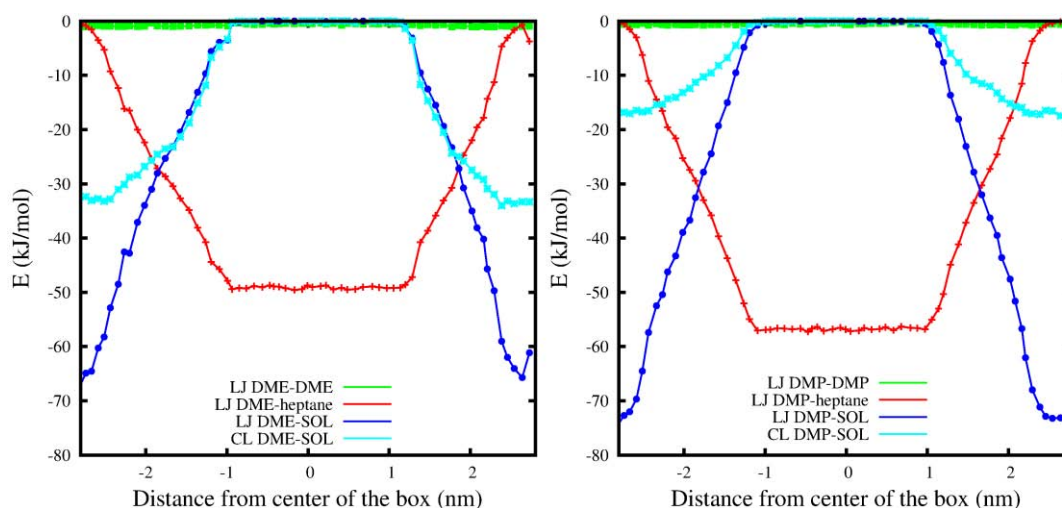


Figure 3.5: Non-bonded energy contribution in terms of Lennard-Jones (LJ) and Coulombic (CL) potential for percolation of DME (left) and DMP (right) through *n*-heptane. The center of the box is the center of the *n*-heptane layer along *z*-direction.

Similarly, the Coulombic energies reach minima of $-33.32 (\pm 0.57)$ kJ/mol and $-16.39 (\pm 0.43)$ kJ/mol for interaction with water for DME and DMP, respectively. As the OPLS model of *n*-heptane has null partial charges on the carbon atoms, Coulombic interactions of DME and DMP with *n*-heptane are not shown. Both of the scenarios support relatively greater affinity of DMP toward *n*-heptane than that for DME. This behavior is also evidenced in our previous study of the models.^[37] The presence of the extra methyl group makes DMP more hydrophobic than DME and hence more soluble in aliphatic solvents.^[37] Entering the *n*-heptane phase cause greater loss in hydrogen bonding for DME than DMP (average number of H-bonds 0.965 for DME and 0.478 for DMP), indicating a considerable reduction of the system stability. Also, the Coulombic energy contributions indicate relatively better solvation of DME in water. These factors contribute toward the upheaval of the energy barrier of percolation in the *n*-heptane phase from the water phase, resulting in a lower energy barrier for DMP than that for

DME during diffusion through the *n*-heptane phase.

Simulation of DME and DMP at the water/*n*-Heptane Interface:

Fig. 3.6 shows the density distribution of DME and DMP during a 50 ns unconstrained simulation of a single ether molecule at the water/*n*-heptane interface. From the figure, it is evident that DMP has relatively higher affinity to the interface than DME. Also, higher density of DME in the water phase indicates its higher affinity toward the water phase. Although experimental data for DME/DMP at these interfaces are not available for direct comparison, there are experimental studies with Pluronics in air/water or air/oil interfaces.^[55-58]

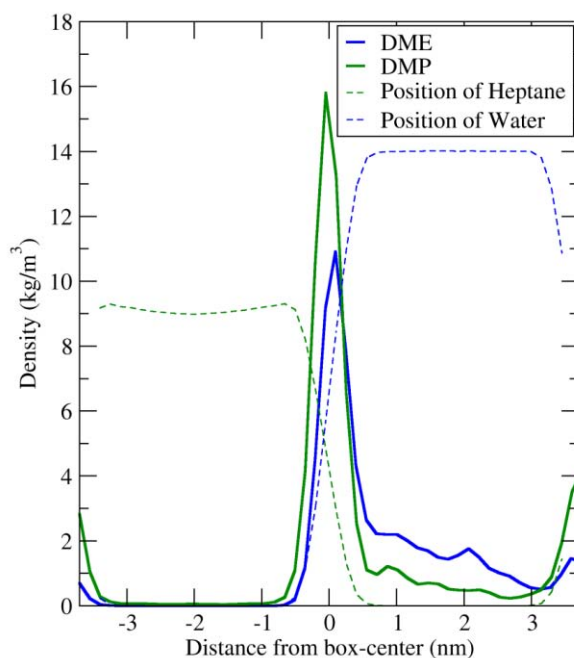


Figure 3.6: Average density distribution of DME and DMP during 50 ns unconstrained simulation at water/*n*-heptane interface. The positions of the solvents are shown as dashed line.

Since Pluronics are the block copolymers having DME and DMP as their smallest oligomers, their properties at interfaces can be qualitatively compared with these systems. Neutron scattering and other techniques confirm bottle-brush type of arrangement of Pluronics at the air/oil and air/water interfaces.^[55-58] It is seen that PPO

part of the polymer (of which DMP is the monomer model) accumulates at the interface region, and the PEO part (of which DME is the monomer model) flanks in the water region. Our unconstrained simulations show similar distribution of DME and DMP molecules in proximity of the *n*-heptane interface. In addition, the US simulations show the presence of a negative PMF value at the interface regions (Fig. 3.4) and the depth of the well is greater in case of DMP (-2 kJ/mol for DME and -5.5 kJ/mol for DMP). This supports better accumulation of DMP in the interface region than DME, as seen in the experiments.

Percolation of DME and DMP through DMPC:

A snapshot of the simulated system, along with partial density profiles, is shown in Fig. 3.2. In Fig. 3.7, the relative PMF profiles of DME and DMP are shown. For DME, the height for the energy barrier is equal to ~ 20 kJ/mol but it is only ~ 12 kJ/mol for DMP. The PMF curve of DME starts with a steep rise, and after a small dip, the curve continues to rise smoothly until it reaches a plateau near the center of the bilayer. The initial slope in the PMF profile is obviously due to the steric effect of the bulky trimethyl amine group, which imposes an energy barrier for the process. But as soon as the barrier is crossed, the molecule faces a relatively favorable molecular environment flanked by hydroxyl groups and ether like oxygen atoms. Also, the density profile (Fig. 3.2) indicates less steric hindrance in this part of the bilayer. As a result, a small dip in the PMF curve is observed. The subsequent encounter with the hydrophobic aliphatic tail region of the DMPC produces a rise in the PMF curve. After reaching the middle of the lipid bilayer the curve converge to a plateau. In the same figure, the PMF curve for DMP is reported.

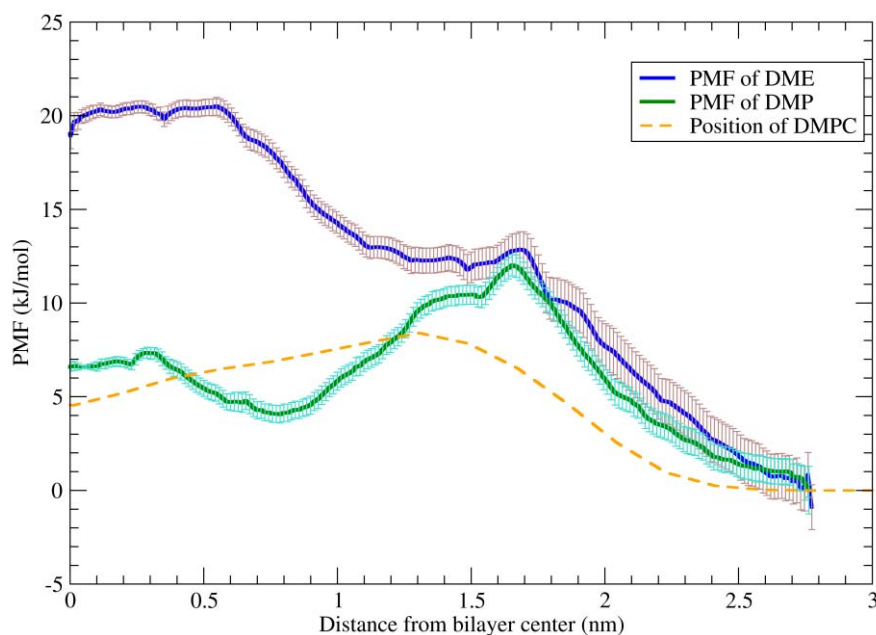


Figure 3.7: The comparison of PMF profiles of percolation of DME and DMP molecule using umbrella sampling. The position of the DMPC bilayer is shown in orange.

As for DME, we observe an initial rise in PMF due to the steric effect of the head groups of the DMPC upper layer, followed by a minimum due to the attraction from the next hydrophobic part of the lipid. DME having less affinity for the hydrophobic part of the lipid bilayer does not show such behavior. The relative height of the permeation barrier to the water phase is similar to that calculated of the *n*-heptane/water system. Comparing these PMF profiles with selected profiles from the work of MacCallum et al.,^[32] where they studied percolation of amino acid equivalent molecules (The side chains were truncated at β -carbon, and α -carbon was replaced by hydrogen. As a result, Leucine, Glutamine, and Asparagine reduces to isobutane, acetamide, and propanamide, respectively) through 1,2-dioleoyl-*sn*-glycero-3-phosphocholine (DOPC) bilayer, similar trend in the qualitative and quantitative nature of the PMF profiles is observed. Although the molecules they studied are not directly comparable to the DME/DMP systems, the PMF curves for hydrophobic branched molecules (e.g., isobutane) and hydrophilic polar molecules (e.g., acetamide and propanamide) are qualitatively similar

to that of DMP and DME, respectively.

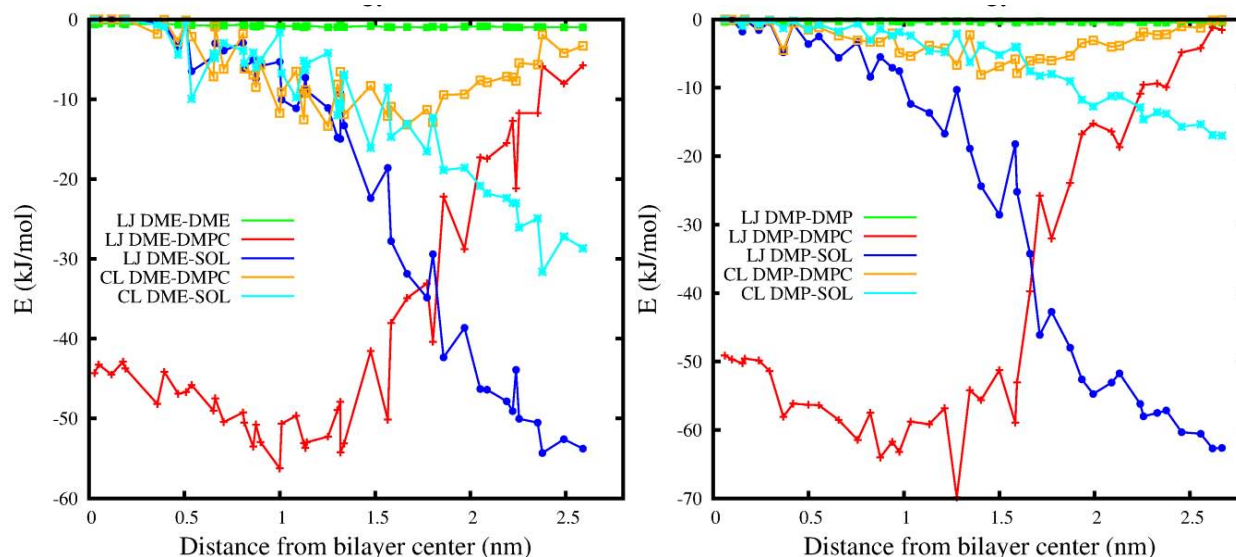


Figure 3.8: Nonbonded energy contributions calculated from all the frames of the umbrella sampling simulations: Lennard-Jones (LJ) and Coulombic (CL) energies for percolation of DME (left) and DMP (right) through DMPC.

In Fig. 3.8 average Lennard-Jones (LJ) and Coulombic energies calculated for each frame of the umbrella sampling simulation along the pathway are shown. For a more detailed investigation, two sets of six different simulations from the US simulations for DME and DMP were considered. These simulations in the two sets are taken from distinctively different environments along the US pathways. The LJ contributions for DMPC bilayer have a minimum value of $-69.86 (\pm 0.97)$ kJ/mol for DMP and the same for DME is $-56.24 (\pm 0.48)$ kJ/mol. This indicates better stabilization of DMP in the DMPC layer. Though the Lennard-Jones contribution slightly favors DMP over DME, the comparison of Coulombic potentials of both ethers and water indicates a more favorable affinity of DME to the water phase. These factors contribute to the higher energy barrier for the percolation of DME relative to that of DMP.

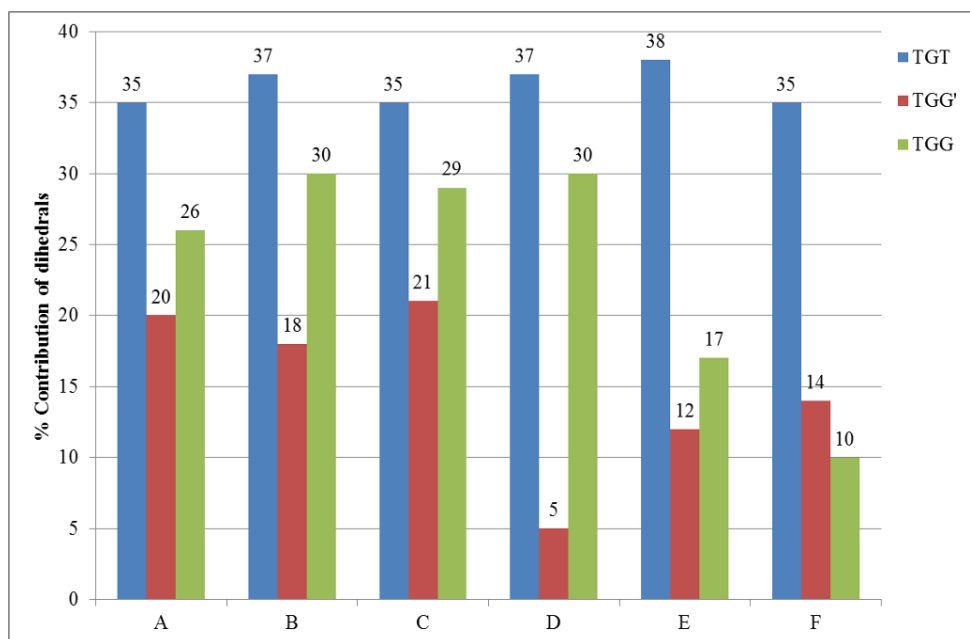


Figure 3.9: Comparison of population distribution of the three dihedrals of the DME molecule for the six selected sets of simulations. The percentage of most populated conformers, TGT, TGG' and TGG are shown as blue, red and green bars, respectively. A-F denotes the selected sets (as shown in Figure 3).

The conformational population of DME molecules in the six sets of simulations was investigated. In a previous study, we showed that TGG, TGG' and TGT (where T stands for trans and G for gauche) are the three most abundant conformers of DME in aqueous and various non-aqueous (methanol, carbon tetrachloride and *n*-heptane) solvents, and depending on the solvent, the percent populations of different conformers vary significantly.^[37] In Fig. 3.9, the histogram of the percentage values of these three conformers of DME for the six selected simulations is reported. The graph evidences a significant fluctuation in the population of the TGG (high dipole moment) and TGT (low dipole moment) conformers. The percentage of TGG conformers drops as DME enters the aliphatic region. Also, a drop in the percentage of the low dipole TGT conformers at the polar region of the bilayer is observed. These observations are also supported by our previous study of DME in different polar and nonpolar solvent systems.^[37] In simulation C corresponding to the DME molecule residing in the middle of the polar

region of the bilayer (Fig. 3.3), all the conformers have comparable contribution (Fig. 3.9). This indicates large conformational variability evidenced also by the high fluctuations of the end-to-end distance of the molecule during the umbrella sampling simulation run (Table 3.1).

Table 3.1: The distance from bottom heads of the bilayer and fluctuation in end-to-end distances (right) of DME for the six selected frames as shown in Figure 3.7.

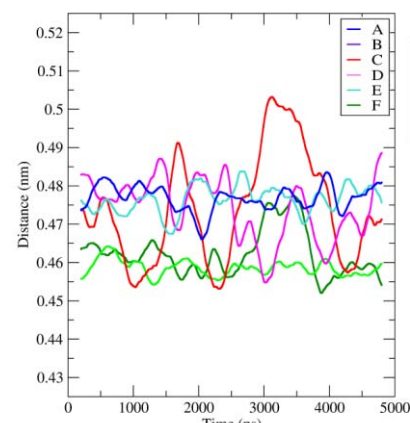
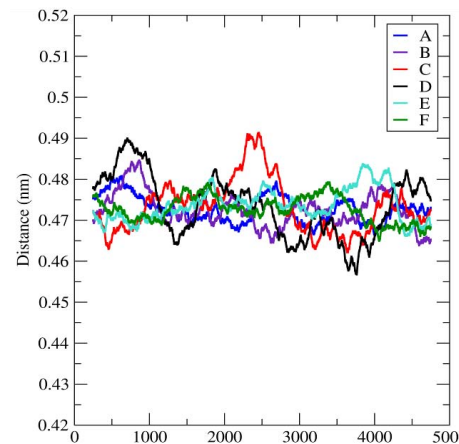
Frame#	Distance from bottom COM (nm)	Avg. end to end distance (nm)	
A	4.09	0.477	
B	3.83	0.476	
C	2.97	0.474	
D	2.74	0.473	
E	2.26	0.462	
F	1.65	0.458	

Table 3.2: The distance from bottom heads of the bilayer and fluctuation in end-to-end distances (right) of DMP for the six selected frames as shown in Figure 3.7.

Frame#	Distance from bottom COM (nm)	Avg. end to end distance (nm)	
A	4.41	0.473	
B	3.74	0.472	
C	3.24	0.473	
D	2.88	0.474	
E	2.30	0.474	
F	1.80	0.473	

This is also observed for the simulation D where the conformer fluctuates in between the high and low dipole conformation resulting in high fluctuation in the end-to-end distance. Interestingly, the end-to-end fluctuations for the DMP molecule are far less than the DME ones (Table 3.2). This indicates a different entropic contribution to the overall free energy of percolation of the two molecules. The reduced mobility of DMP molecule indicates minor disturbance in the ordered lipid tail region. In addition, it has been seen from the unconstrained simulations that the proximity of the polar region of the DMPC layer helps to stabilize the DMP molecule inside the bilayer. As a result, DMP tends to accumulate near the headgroup region once inside the bilayer (Fig. 3.12). These factors result in the formation of a dip in the PMF profile of DMP in this region.

Considering the hydrogen bonding capability of the two molecules throughout the pathway, DME tends to form more hydrogen bonds than DMP with an average number of 0.505 and 0.187 for DME and DMP, respectively (Fig. 3.10). However, once inside the bilayer, there is no chance of H-bonding in the aliphatic region of the bilayer. When compared to DMP, DME loses H-bonding to a larger extent which causes greater loss of stability, resulting in higher PMF values.

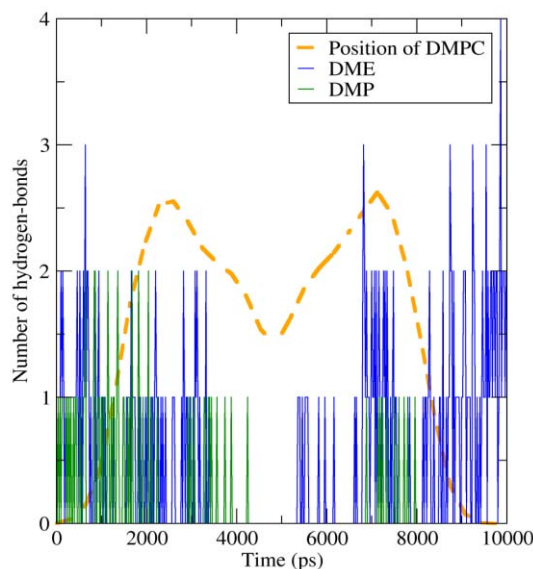


Figure 3.10: Plot for average number of hydrogen bonds for DME (blue) and DMP (green) throughout the path of percolation through DMPC bilayer. The position of DMPC bilayer is shown in orange dashed line.

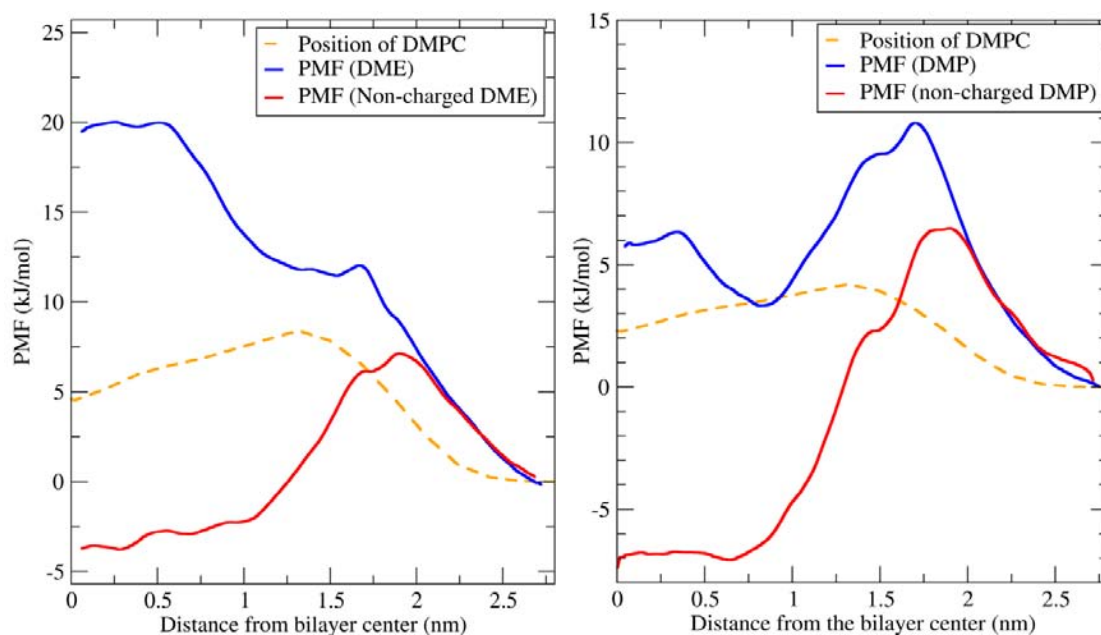


Figure 3.11: Comparison of the PMF profile for percolation of charged and non-charged DME (left) and DMP (right) in DMPC layer obtained by umbrella sampling method.

To better understand the role of the electrostatic interaction on the percolation barrier, a set of umbrella sampling simulations of DME and DMP with the partial charges on all atoms set to zero were also performed. In Fig. 3.11, the new calculated PMF profiles are compared with those of the charged models. For DME, the two PMF curves show large differences. On the contrary, that for DMP molecule is similar and comparable to the uncharged DME one. These results indicate that partial charges and, hence, the associated dipoles of the two molecules play an important role in the percolation process of these molecules through the DMPC layer.

DME and DMP at the water/DMPC Interface:

The estimated value of the barriers of permeation for DMP is ~6 kJ/mol is ~2.58 kT (k = Boltzmann constant, $T = 310\text{K}$), indicating a possible spontaneous insertion of DMP into the lipid bilayer. Therefore, unconstrained simulations for 50 ns were performed for both DME and DMP molecules for all six configurations shown in Fig. 3.3. Density

distributions of DME and DMP during the simulation along the Z-axis of the box for all the frames were calculated and they are shown in Fig. 3.12. The distribution indicates the affinity of DME toward the water phase. In all the simulations, the DME molecule moves away from the interior of the bilayer phase and accumulates close to the water interface, as evidenced by the large peaks at 5 nm. For the simulation started with the DME molecule in the center of the bilayer (frame F), the molecule resides in the polar headgroup region of the bilayer.

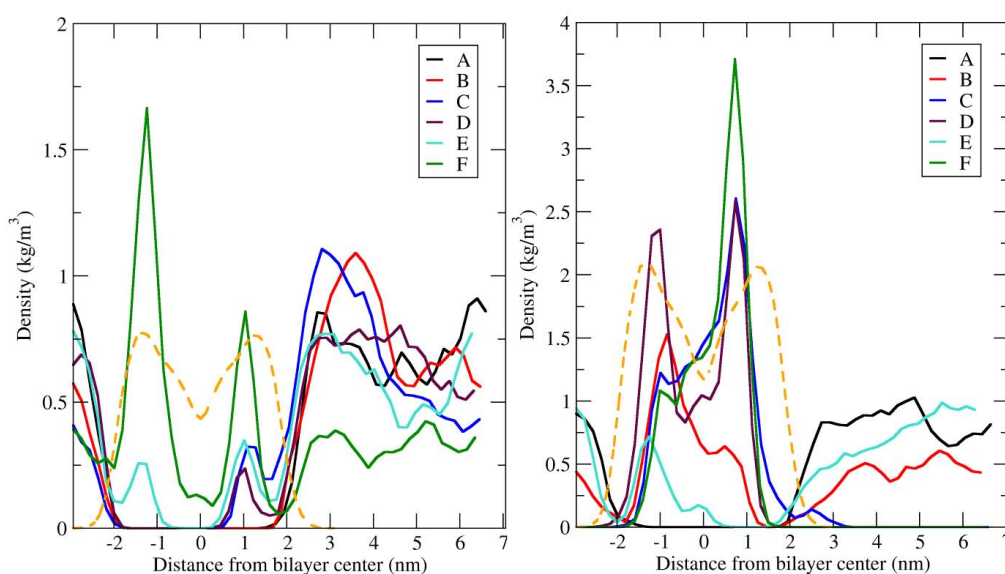


Figure 3.12: Average density distribution of DME (left) and DMP (right) during 50 ns unconstrained simulation of the selected frames (Figure 3.7). The position of the DMPC bilayer is shown as orange dashed line.

On the contrary, for DMP, all the simulations clearly show higher tendency of the molecule to reside in the aliphatic region of the bilayer (Fig. 3.12). In all of the cases, except for simulation A, spontaneous diffusion of the DMP molecule into the bilayer is observed. In the case of simulation set A, for which in the starting conformation the DMP molecule was in the water phase away from the bilayer boundary, it does not diffuse inside the bilayer and tends to stay in the water phase. From the position of the maxima in the density distribution of DMP (for B to F simulation sets) in Fig. 3.12, it is

interesting to note that once inside the bilayer, the molecules slightly prefer to distribute close to the polar headgroup region. However, for simulation A, no specific preference of the DMP molecule for the polar headgroup is observed. Three sets of simulations for both DME and DMP were considered for a further study. The starting positions of DME/DMP in these simulations are as follows:

- i) in the water phase 1 nm away from the bilayer boundary (Frame A in Fig. 3.3),
- ii) in the headgroup region of the upper layer (Frame C in Fig. 3.3) and
- iii) in the aliphatic tail region of the bilayer near to the bilayer center (Frame F in Fig. 3.3).

Simulations of DME and DMP starting from the water phase showed no spontaneous diffusion of the molecules into the bilayer for the simulation length (50 ns). The calculated diffusion coefficients from the CoM mean square displacement are equal to $0.7 \pm 0.01 \times 10^{-9} \text{ m}^2/\text{s}$ and $1.4 \pm 0.2 \times 10^{-9} \text{ m}^2/\text{s}$ for DME and DMP, respectively. From our previous work, the values of diffusion coefficients of DME and DMP models in pure water extrapolated at 310 K are $1.7 \times 10^{-9} \text{ m}^2/\text{s}$ and $1.4 \times 10^{-9} \text{ m}^2/\text{s}$, respectively.^[37] Therefore, the diffusion coefficients of DME at the DMPC interface is significantly lower than that for bulk water. It has been known that at interfaces polyethylethers are slightly hydrophobic,^[59] and their accumulation on the bilayer surface has been proven by X-ray scattering studies.^[15, 60] The free simulation indicates affinity of the DME molecules to the polar surface of lipid bilayer, resulting in very low diffusion coefficient values. DMP, having less affinity to the lipid bilayer surface (see Fig. 3.12), has higher diffusion coefficient, which is almost equivalent to that in pure water.

In the second set of simulations, the distances and the number of contacts of the respective molecules from the DMPC chains were calculated and are shown in Fig. 3.13.

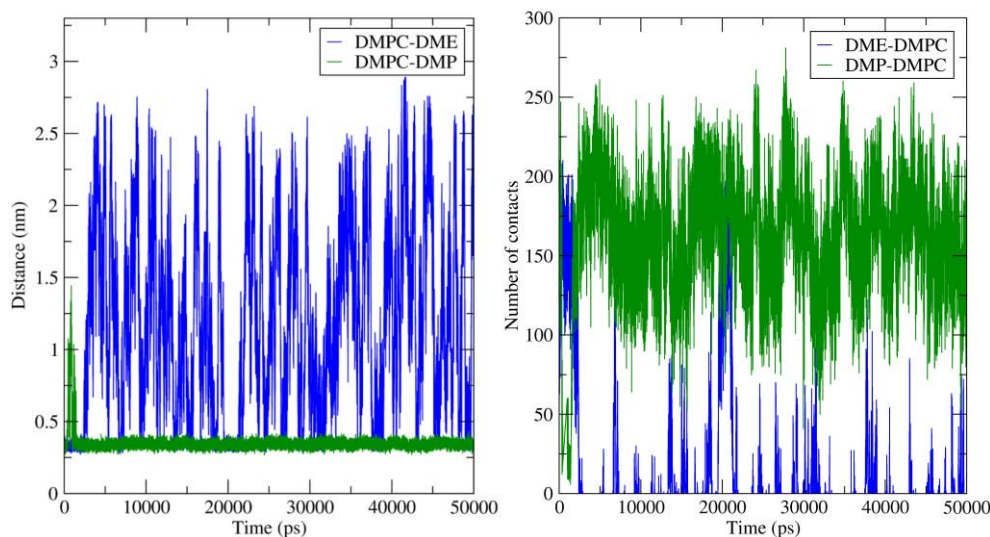


Figure 3.13: Distance of DME (blue) and DMP (green) from DMPC during 50 ns simulation are shown in the left. Numbers of contacts per ps (cutoff 0.6 nm) between DME (blue) and DMP (green) with DMPC during 50 ns simulation are shown in the right.

The values of distances clearly indicate that during the simulation, the DMP molecule tends to stay in the tail region of the bilayer phase, whereas the DME molecule tends to move out of the lipid phase and stay in the water phase close to the bilayer (Fig. 3.14). Calculating the average number of contacts for DME and DMP (within 0.6 nm of the DMPC lipid atoms) resulted in 15 and 163, respectively, which further supports this observation.

Finally, simulation (iii) shows a trend similar to that of the previous one. As expected from the calculated PMF profiles, the DMP molecule remains in the aliphatic region, whereas the DME molecule diffuses back to the water phase.

The calculated values of the diffusion coefficients for DME and DMP molecules in the lipid bilayer are $2.1 \pm 0.3 \times 10^{-9} \text{ m}^2/\text{s}$ for and $0.6 \pm 0.1 \times 10^{-9} \text{ m}^2/\text{s}$, respectively. These values are also significantly lower than those in bulk *n*-heptane, which are $3.7 \times 10^{-9} \text{ m}^2/\text{s}$ for DME and $3.6 \times 10^{-9} \text{ m}^2/\text{s}$ for DMP, respectively.^[37] The reduced diffusion coefficients with respect to the *n*-heptane is a consequence of the orderliness in the lipid tails that restricts free diffusion of the DMP molecule in the hydrophobic region. The

larger effect on the DMP is a consequence of both the larger affinity with the hydrophobic part of the lipid tail and the larger steric hindrances due to the methyl group.

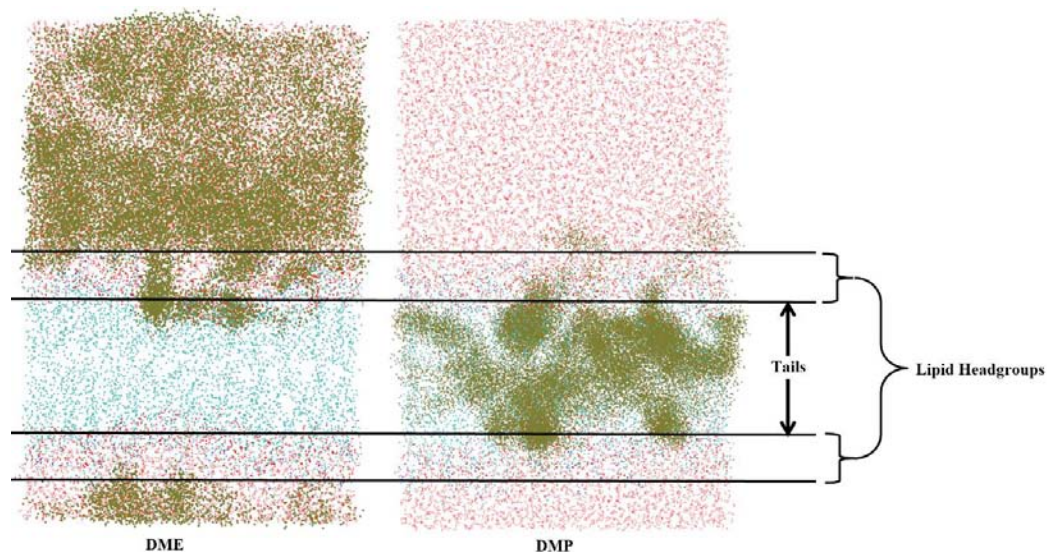


Figure 3.14: Probability distribution of DME (left) and DMP (right) in the system during a 50 ns simulation starting from a frame when the molecule is in the head group region (Frame 'C' from Figure 3.7). The position of the molecules at every 10 ps is shown as grey dot.

Simulations with Multiple DME and DMP Molecules at the water/DMPC Interface:

To understand the effect of the concentration of DME/DMP at the DMPC interface, two unconstrained simulations of 50 ns each were also run starting with nine DME and nine DMP molecules (approximate 0.6 % molar fraction with respect to water), localized in the water phase ~ 1 nm away from the bilayer. The density distributions of DME and DMP obtained from the simulations are compared in Fig. 3.15. As for the single molecules, a similar trend is observed for DME. No spontaneous diffusion of DME inside the DMPC bilayer was observed. The maximum near the polar headgroup indicates the affinity of DME and DMP toward the polar headgroup of DMPC. In the case of DMP, positive density distribution inside the bilayer region indicates a spontaneous diffusion inside the membrane. From the visual inspection of the trajectory, one molecule of DMP

was found to penetrate the lipid bilayer.

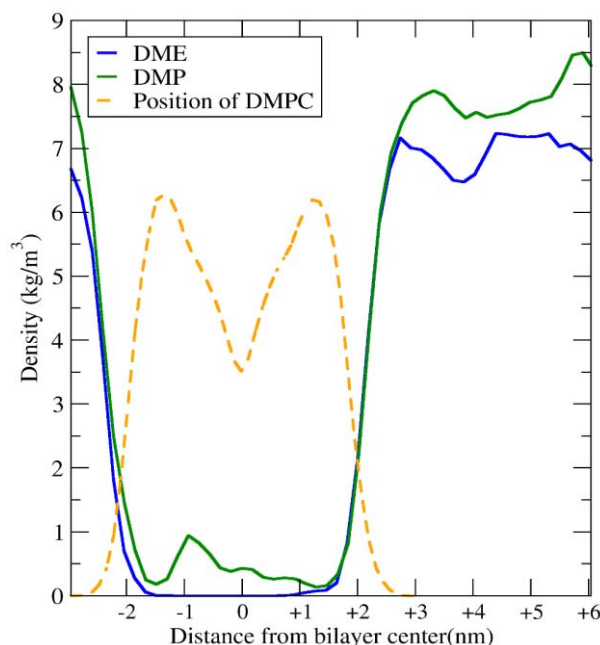


Figure 3.15: Average density distribution of 9 molecules of DME and DMP during 50 ns unconstrained simulation. The position of the DMPC bilayer is shown as orange dashed line.

CONCLUSIONS.

In this chapter, structural, dynamic, and thermodynamic properties of DME and DMP in 1-octanol, water/*n*-heptane, and water/DMPC bilayer interfaces have been investigated with molecular dynamics simulations. The Gibbs free energy of solvation of DME and DMP in 1-octanol and the partition coefficient values between water and 1-octanol show excellent agreement with available experimental data. This indicates that the models are suitable for use in complex environments such as lipid bilayer systems to study percolation behaviors.

The percolation properties of DME and DMP were first investigated at the water/*n*-heptane interface. The PMF curves for the percolation of both ethers from water to *n*-heptane to water phase were calculated. The calculated percolation barriers from water to *n*-heptane phase were calculated equal to 18.5 and 5 kJ/mol for DME, and

DMP respectively. It is shown that the better stabilization of DME in water phase (in terms of Lennard-Jones as well as Coulombic potential) and relatively better stabilization of DMP (in terms of Lennard-Jones potential) in *n*-heptane causes the large differences in the two values.

The diffusion of DME and DMP through DMPC bilayer was investigated. The PMF profile of bilayer percolation was obtained using umbrella sampling method. The energy barrier to transfer the molecules from water into the DMPC tail region was calculated to be 20 and 12 kJ/mol for DME and DMP, respectively. This height of the barrier in the tail region of DMPC is consistent and comparable to that of the water/*n*-heptane system. The details of the percolation properties have been discussed based on non-bonded energy contributions, dynamic and structural properties of the molecules. This analysis showed extra stabilization for DME in correspondence of the head group region. This explains the accumulation of polyethers at the interface of lipid bilayer as studied by Firestone et al. from X-ray scattering studies.^[15, 60] It has also been shown that electrostatic interactions play an important role in the energetics of the bilayer percolation process for the DME molecule. Finally, the results of long unconstrained DME and DMP simulations further support the behavior expected from the PMF curves. If the simulations start with the molecules located in the lipid head group region, DMP molecules tend to spontaneously diffuse to the center of the lipid bilayer whilst DME molecules prefer to remain in the lipid/water interface region. The spontaneous diffusion of DMP molecules to the interior of the lipid bilayer can be enhanced by increasing the concentration as shown by simulations starting with multiple molecules in the water phase. On the contrary, no concentration effect has been observed for DME.

In conclusion, the results of this study provide interesting insights on the mechanism of percolation of DME and DMP ether molecules into the DMPC lipid bilayer. DME and DMP are the building blocks for larger di- and triblock amphiphilic copolymers (e.g., Pluronics) which are important and widely used for designing drug carrier

micelles. Our results provide, for the first time, an accurate atomistic model on the partition behavior of hydrophilic (DME/PEO) and hydrophobic (DMP/PPO) blocks of these polymers at a membrane interface. Further computational studies are on the way to understand the effect of the polymer length and composition on the percolation process.

REFERENCES.

- [1] S. Forster, T. Plantenberg, *Angewandte Chemie-International Edition* **2002**, 41, 689.
- [2] S. Fusco, A. Borzacchiello, P. A. Netti, *Journal of Bioactive and Compatible Polymers* **2006**, 21, 149.
- [3] R. Haag, F. Kratz, *Angewandte Chemie-International Edition* **2006**, 45, 1198.
- [4] Y. Kodera, A. Matsushima, M. Hiroto, H. Nishimura, A. Ishii, T. Ueno, Y. Inada, *Progress in Polymer Science* **1998**, 23, 1233.
- [5] C. D. H. Alarcon, S. Pennadam, C. Alexander, *Chemical Society Reviews* **2005**, 34, 276.
- [6] R. K. Chowdhary, I. Sharif, N. Chansarkar, D. Dolphin, L. Ratkay, S. Delaney, H. Meadows, *Journal of Pharmacy and Pharmaceutical Sciences* **2003**, 6, 198.
- [7] I. R. Schmolka, in *Polymers for Controlled Drug Delivery* (Ed.: P. J. Tarcha), CRC Press, Boston, **1991**.
- [8] K. T. Oh, T. K. Bronich, A. V. Kabanov, *Journal of Controlled Release* **2004**, 94, 411.
- [9] A. Sahu, U. Bora, N. Kasoju, P. Goswami, *Acta Biomaterialia* **2008**, 4, 1752.
- [10] N. S. Melik-Nubarov, O. O. Pomaz, T. Y. Dorodnych, G. A. Badun, A. L. Ksenofontov, O. B. Schemchukova, S. A. Arzhakov, *FEBS Letters* **1999**, 446, 194.
- [11] F. Otis, C. Racine-Berthiaume, N. Voyer, *Journal of the American Chemical Society* **2011**, 133, 6481.
- [12] E. S. Gil, S. M. Hudson, *Progress in Polymer Science* **2004**, 29, 1173.
- [13] A. Gabizon, H. Shmeeda, Y. Barenholz, *Clinical Pharmacokinetics* **2003**, 42, 419.
- [14] A. Vonarbourg, C. Passirani, P. Saulnier, P. Simard, J. C. Leroux, J. P. Benoit, *Journal of Biomedical Materials Research Part A* **2006**, 78A, 620.
- [15] M. A. Firestone, A. C. Wolf, S. Seifert, *Biomacromolecules* **2003**, 4, 1539.
- [16] G. J. A. Sevink, J. G. E. M. Fraaije, H. P. Huinink, *Macromolecules* **2002**, 35, 1848.

-
- [17] O. N. Steve, et al., *Journal of Physics: Condensed Matter* **2004**, *16*, R481.
- [18] S. Pal, G. Milano, D. Roccatano, *Journal of Physical Chemistry B* **2006**, *110*, 26170.
- [19] G. Srinivas, M. L. Klein, *Molecular Physics* **2004**, *102*, 883.
- [20] G. Srinivas, J. C. Shelley, S. O. Nielsen, D. E. Discher, M. L. Klein, *Journal of Physical Chemistry B* **2004**, *108*, 8153.
- [21] M. Hatakeyama, R. Faller, *AIP Conference Proceedings* **2008**, *982*, 528.
- [22] L. Saiz, M. L. Klein, *Accounts of Chemical Research* **2002**, *35*, 482.
- [23] S. O. Nielsen, C. F. Lopez, G. Srinivas, M. L. Klein, *Journal of Physics-Condensed Matter* **2004**, *16*, R481.
- [24] B. Isralewitz, M. Gao, K. Schulten, *Current Opinion in Structural Biology* **2001**, *11*, 224.
- [25] S. Park, K. Schulten, *Journal of Chemical Physics* **2004**, *120*, 5946.
- [26] S. J. Marrink, O. Berger, P. Tieleman, F. Jähnig, *Biophysical Journal* **1998**, *74*, 931.
- [27] S. Stepaniants, S. Izrailev, K. Schulten, *Journal of Molecular Modeling* **1997**, *3*, 473.
- [28] C. Jarzynski, *Physical Review Letters* **1997**, *78*, 2690.
- [29] S. Park, F. Khalili-Araghi, E. Tajkhorshid, K. Schulten, *Journal of Chemical Physics* **2003**, *119*, 3559.
- [30] G. M. Torrie, J. P. Valleau, *Journal of Computational Physics* **1977**, *23*, 187.
- [31] S. Kumar, D. Bouzida, R. H. Swendsen, P. A. Kollman, J. M. Rosenberg, *Journal of Computational Chemistry* **1992**, *13*, 1011.
- [32] J. L. MacCallum, W. F. D. Bennett, D. P. Tieleman, *Biophysical Journal* **2008**, *94*, 3393.
- [33] M. Orsi, W. E. Sanderson, J. W. Essex, *The Journal of Physical Chemistry B* **2009**, *113*, 12019.
- [34] C. F. Chew, A. Guy, P. C. Biggin, *Biophysical Journal* **2008**, *95*, 5627.
- [35] M. Orsi, J. W. Essex, *Soft Matter* **2010**, *6*, 3797.
- [36] A. S. Widge, Y. Matsuoka, M. Kurnikova, *Langmuir* **2007**, *23*, 10672.
- [37] S. Hezaveh, S. Samanta, G. Milano, D. Roccatano, *Journal of Chemical Physics* **2011**, *135*, 164501.
- [38] O. Berger, O. Edholm, F. Jahnig, *Biophysical Journal* **1997**, *72*, 2002.
- [39] H. J. C. Berendsen, J. P. M. Postma, W. F. van Gunsteren, J. Hermans, (Ed.: B. Pullman), Reidel: Dordrecht, **1981**, p. 331.
- [40] W. L. Jorgensen, J. D. Madura, C. J. Swenson, *Journal of the American Chemical Society* **1984**,

- 106, 6638.
- [41] N. M. Garrido, A. J. Queimada, M. Jorge, E. A. Macedo, I. G. Economou, *Journal of Chemical Theory and Computation* **2009**, 5, 2436.
- [42] B. Hess, C. Kutzner, D. van der Spoel, E. Lindahl, *Journal of Chemical Theory and Computation* **2008**, 4, 435.
- [43] W. Humphrey, A. Dalke, K. Schulten, *Journal of Molecular Graphics* **1996**, 14, 33.
- [44] G. Bussi, D. Donadio, M. Parrinello, *Journal of Chemical Physics* **2007**, 126, 14101.
- [45] H. J. C. Berendsen, J. P. M. Postma, W. F. Vangunsteren, A. Dinola, J. R. Haak, *Journal of Chemical Physics* **1984**, 81, 3684.
- [46] B. Hess, H. Bekker, H. J. C. Berendsen, J. G. E. M. Fraaije, *Journal of Computational Chemistry* **1997**, 18, 1463.
- [47] T. Darden, D. York, L. Pedersen, *Journal of Chemical Physics* **1993**, 98, 10089.
- [48] J. Kirkwood, *Journal of Chemical Physics* **1935**, 3, 300.
- [49] A. Villa, A. E. Mark, *Journal of Computational Chemistry* **2002**, 23, 548.
- [50] E. Delgado, G. Jana, *International Journal of Molecular Sciences* **2009**, 10, 1031.
- [51] J. Wang, W. Wang, S. Huo, M. Lee, P. A. Kollman, *Journal of Physical Chemistry B* **2001**, 105, 5055.
- [52] J. Sangster, *Octanol-Water Partition Coefficients: Fundamentals and Physical Chemistry*, Wiley, Chichester ; New York, **1997**.
- [53] www.chemicaland21.com.
- [54] S. J. Marrink, H. J. C. Berendsen, *The Journal of Physical Chemistry* **1996**, 100, 16729.
- [55] B. R. Bomqvist, T. Warnheim, P. M. Claesson, *Langmuir* **2005**, 21, 6373.
- [56] B. A. Noskov, *Colloid Journal* **2006**, 68, 588.
- [57] R. Sedev, D. Exerowa, G. H. Findenegg, *Colloid and Polymer Science* **2000**, 278, 119.
- [58] R. Sedev, R. Steitz, G. H. Findenegg, *Physica B-Condensed Matter* **2002**, 315, 267.
- [59] J. Israelachvili, *Proceedings of the National Academy of Sciences of the United States of America* **1997**, 94, 8378.
- [60] M. A. Firestone, S. Seifert, *Biomacromolecules* **2005**, 6, 2678.



Chapter 4

Interaction of Polyethylene Oxide, Polypropylene Oxide and their Block Co-Polymer Pluronics with DMPC Lipid Membrane.

Interaction of Polyethylene Oxide, Polypropylene Oxide and their Block Co-Polymer Pluronics with DMPC Lipid Membrane.

ABSTRACT.

In this chapter, a theoretical study of the interaction of polyethylene oxide (PEO), polypropylene oxide (PPO) and their block co-polymer Pluronics with water/*n*-heptane and 1,2-dimyristoyl-*sn*-glycero-3-phosphatidylcholine (DMPC) lipid bilayer/water interfaces is reported. In the case of heptane/water interface the stronger preference of the PPO block for the hydrophobic heptane than water produced bottle-brush type of conformation of Pluronics molecules. It was observed that when the PPO chains have similar length as the width of the bilayer, they tend to span across the bilayer. This effect was seen for PPO20, PPO43 and Pluronic L61 & L64. The energy barriers of percolation of linear polyether were calculated and the barrier was found to be smaller for PPO than its PEO counterparts.

INTRODUCTION.

The wide ranged applications of ether based linear and block co-polymers have already been discussed in the Introduction section of this thesis.^[1-9] It is known that, the chain length and composition are important for the steric stabilization.^[10] The PEO block of these polymers has peculiar properties being hydrophilic in high and hydrophobic in low degree of hydration.^[9] This behavior influences the permeability of bio-membranes. In fact, PEO dehydrates in a hydrophobic medium and can be transported on or through bio-membranes. The percolation and accumulation of PEO-PPO-PEO block copolymers have already been proven by small and wide angle X-ray scattering studies and differential scanning calorimetric studies.^[6, 7] Though a good number of studies have already been done on the structural characteristics and interactions of Pluronics with bio-membranes and lipid bilayers ^[6, 7, 11-13], the details of permeation of polymer systems across lipid membrane itself are not known at the level of molecular interactions. Experimental techniques are restricted from being precise to probe processes on the length and time-scale of a lipid membrane. Recently we have published a study on the interaction of the shortest oligomer model of PEO, the 1,2-dimethoxyethane (DME), and PPO, the 1,2-dimethoxypropane (DMP) with water/*n*-heptane and 1,2-dimyristoyl-*sn*-glycero-3-phosphatidylcholine (DMPC) lipid bilayer/water interfaces.^[14] The percolation free energy barrier of one DME and DMP molecule from water to the DMPC lipid bilayer the barriers, estimated using umbrella sampling, provided the approximate values of 20 kJ/mol and 6 kJ/mol, respectively. The results of these simulations indicated a stronger preference of DME than DMP for the aqueous phase. In this study, we extend the previous investigations by investigating the interaction of polymers and co-polymers based on PEO and PPO units with a DMPC lipid bilayer. In particular, we have analyzed the effect of the polymer chain length and composition on interaction with hydrophobic interface (*n*-heptane/water) and with DMPC lipid bilayer. For this purpose, PEO and PPO chain of different length and three

different triblock co-polymers have been considered. The study was conducted using classical MD simulation for the study of the polymer at the interface and steered molecular dynamics simulations and umbrella sampling methods for qualitative estimation of the percolation barriers.

This chapter is organized as follows: The Methods section describes the systems simulated and details of the forcefield and methods used. The results are shown and explained in the Results and Discussion section. We have first analyzed the behavior of the polymers at the simple binary interface of water/*n*-heptane. This study is used to quantify the behavior of the polymers in the presence of pure hydrophobic surfaces and, in part, to dissect the contribution of the interior of the lipid bilayer (mimicked by the *n*-heptane interface) from the polar lipid head groups. In the second part, the interactions of the polymers with a DMPC lipid bilayer are analyzed. In this study, steered molecular dynamics simulations and umbrella sampling methods were used to make a qualitative estimation of the percolation barrier. The results are compared with our DME and DMP simulations and other published simulations on similar systems. The outcome of this study has been summarized in the Conclusions.

METHODS.

Force-field.

For the DMPC bilayer, the united atom model of Berger et al.^[15] was used. This lipid model is a combination of GROMOS and OPLS parameters, optimized to reproduce the experimental physical properties of lipid bilayer. For PEO, PPO and Pluronics, the recent models proposed by us^[16] were used. For water, the simple point charge (SPC)^[17] model and for *n*-heptane, the OPLS united atom (OPLS-UA) model^[18, 19] was used.

Simulation Setup.

All the simulations were performed using GROMACS (version 4.0.7)^[20] software package. The program VMD^[21] was used for the graphical representation of the

molecular systems. The bilayer simulations were performed at 310 K, above the crystalline fluid/liquid phase transition temperature, using the V-rescale thermostat^[22] with a coupling constant of 0.1 ps. For comparison, the water/*n*-heptane systems were simulated at the same temperature. The pressure was kept constant at 1 bar using Berendsen barostat^[23] with a coupling constant of 0.5 ps. For lipid bilayer simulations, a semi-isotropic barostat was used to take in account the difference in compressibility of the system along the x, y and z directions. The bond lengths were constrained using LINCS^[24] algorithm. An integration time-step of 2 fs was used for all the simulations. Electrostatic interactions were evaluated using particle mesh Ewald method^[25] with a cutoff of 1.0 nm, grid spacing of 0.12 nm and a fourth order spline interpolation. Lennard-Jones interactions were truncated at 1.0 nm.

In the first set of simulations, the water *n*-heptane interface was prepared using same width of solvents (5.5 nm along the z-axis) consisting of 10705 water and 1186 *n*-heptane molecules. Initially, the polymer molecules were put at the interface of water and *n*-heptane and simulated for 50 ns. The list of polymers simulated is shown in Table A2.1a in Appendix II.

For the simulations with DMPC bilayer, each layer consisted of 64 DMPC chains making a total of 128 DMPC chains. The bilayer was put in a box of dimension 6.4×6.4×9.5 nm³ along with ~8000 water molecules and equilibrated for 20 ns. The details of the simulated systems are shown in Table A2.1b in Appendix II. Two sets of simulations were run for DMPC interface. In the first set, the polymer molecule was put in the interface 1-2 nm away from the bilayer surface and simulated for 50 ns. In the second set, the simulation was started from a configuration where the polymer molecule was inside the DMPC lipid bilayer. It should be mentioned that spontaneous diffusion of polymers inside the DMPC bilayer cannot be observed within the timescale of atomistic simulations. Recently Lin et. al studied the percolation of water and dimethyl sulfoxide (DMSO) through DMPC bilayer and their study shows that the mean first passage time

for DMSO is 16.2 μs and that for water is 1.01 μs .^[26] Hence, steered molecular dynamics (SMD) simulation method was used to pull the polymer molecules inside the bilayer.

Table 4.1 List of polymers simulated for this study.

At water/ <i>n</i> -heptane interface	With DMPC bilayer	For PMF calculations
1) PEO 7	1) PEO 7	1) PEO 2
2) PEO 20	2) PEO 20	2) PEO 3
3) PEO 43	3) PEO 43	3) PEO 7 (SMD)
4) PPO 7	4) PPO 7	4) PEO 20 (SMD)
5) PPO 20	5) PPO 20	5) PEO 43 (SMD)
6) PPO 43	6) PPO 43	6) PPO 2
7) L61 (PEO ₂ -PPO ₃₀ -PEO ₂)	7) L61 (PEO ₂ -PPO ₃₀ -PEO ₂)	7) PPO 3
8) L64 (PEO ₁₃ -PPO ₃₀ -PEO ₁₃)	8) L64 (PEO ₁₃ -PPO ₃₀ -PEO ₁₃)	8) PPO 7 (SMD)
9) P85 (PEO ₂₅ -PPO ₄₀ -PEO ₂₅)	9) P85 (PEO ₂₅ -PPO ₄₀ -PEO ₂₅)	9) PPO 20 (SMD)
		10) PPO 43 (SMD)
		11) PL1 (PEO ₁ -PPO ₁ -PEO ₁)

SMD simulations. SMD method was used to speed up the diffusion of polymers through the DMPC bilayer and to calculate potential of mean force (PMF) for the percolation process and to obtain the frames for umbrella sampling simulations. Details of the method have been described in the Methods section in the Introduction (Page 10). The SMD simulations were performed using a slow pulling regime to ensure operation in near-equilibrium conditions.^[27] The pulling parameters adopted by Pal et al.^[28] to study the percolation of a PEO chain through a DMPC lipid bilayer were used. The simulation was started with the polymer molecule in the water phase 1-2 nm away from the upper boundary of the bilayer. The center of mass (CoM) of the polymer molecule was harmonically restrained to a spring of force constant $k = 200 \text{ kJ/mol}$. The spring tip was pulled with a constant velocity $v = 5 \times 10^{-4} \text{ nm/ps}$ for 10 ns.

Umbrella sampling simulations. Umbrella sampling (US) method was used to calculate

the free energy profiles for the percolation of the relatively smaller polymer molecules (PEO 2, PEO 3, PPO 2, PPO 3, and PL1 as shown in Table 4.1) through DMPC layer. This method has been described in the Methods section in the Introduction (Page 11). In the present work, we have adopted similar parameters as described in the previous chapter. A harmonic restraint with a force constant 3000 kJ/mol nm^2 was applied to the distance between the center of mass (CoM) of the polymer molecule and the head groups of the bottom DMPC layer, in the direction normal to the bilayer. Up to forty starting US configurations were taken from the path of one of the SMD trajectory. The first configurations were taken at least 3 nm away from the bilayer center and the last one in the bilayer center. The difference of distances between the CoM of the DME/DMP molecules and reference group for two consecutive conformations was always less than 0.1 nm to ensure the correct calculation of PMF profile. Each frame was simulated for 5 ns. The distance was sampled at every 100 fs. The weighted histogram analysis method (WHAM)^[29] was used to calculate the PMF profile. The free energy profiles obtained from the calculations were rescaled to assign a zero reference value to the profiles in the bulk water.

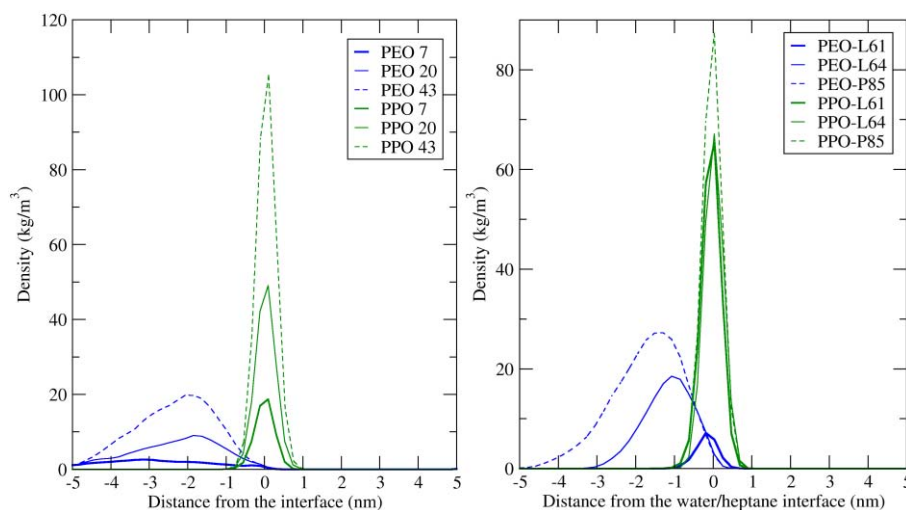


Figure 4.1: Density distributions of the PEO & PPO chains (left) and the PEO & PPO parts of the Pluronic molecules (right) during 50 ns unconstrained simulation in water/*n*-heptane interface. Water is along the negative and *n*-heptane is along the positive coordinate of the x-axis.

RESULTS AND DISCUSSION.

Polymers at water/*n*-heptane interface.

The polymer molecules were simulated at water/*n*-heptane interface with the aim to understand the behavior of the polymers at a hydrophobic interface that mimic the interior of a lipid bilayer. Though simple *n*-heptane systems lack the orderly nature of bilayer tails, they can still provide us with helpful insights on the matter.

Fig. 4.1 shows the density distributions of the polymer molecules during the courses of the simulations. Though the molecules were initially placed at the interface, PEO tends to diffuse to the water phase and stays in the water phase for throughout the course of the simulation. Quite different trend is observed for PPO chains. The PPO chains tend to stay in the interface resulting in a sharp peak in the density profile. The trend is consistent in the case of the Pluronic molecules. During the course of simulation, all the Pluronics follow similar structural and positional pattern. The PPO parts of the polymers remain in the interface while the PEO part goes in the water region forming a bottle-brush configuration. In such configuration, polymers consist of a long flexible main chain, at which flexible side chains are densely grafted resulting in an overall shape of a wormlike cylindrical brush. The final snapshots of the systems are shown in Fig. 4.2.

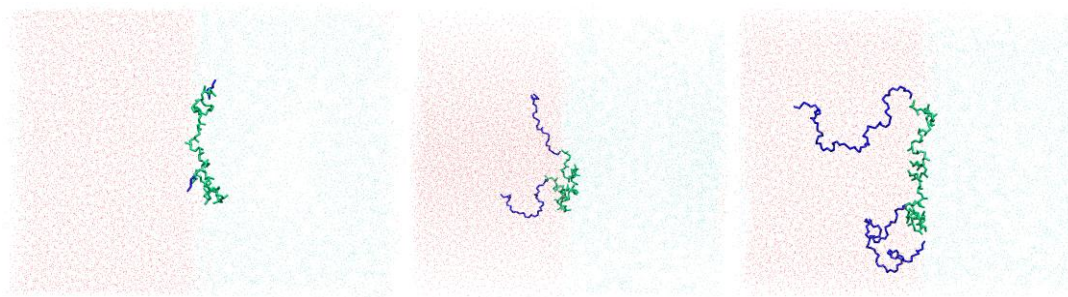


Figure 4.2: Snapshot of Pluronics L61 (left), L64 (middle) and P85 (right) at the end of 50 ns unconstrained simulation in water/*n*-heptane interface. Water is shown in red, heptane in cyan. PEO part of the polymers are shown in blue and PPO part in green.

The radius of gyration (R_g) and the end-to-end distances (R_{ee}) of the polymers were calculated for last 30 ns of the simulations and they are reported in Table 4.2. Previously, we have studied the same properties of these polymers in different solvent conditions^[16] and that provides us with an opportunity to compare them. For PEO the values of both R_g and R_{ee} are similar to their respective values in water. But for PPO, the values of R_g and R_{ee} for the longest chain, PPO43, show an elongation of the chain. The R_g value at the interface, 1.69 ± 0.22 nm, is higher than the value in bulk water (1.40 ± 0.08 nm)^[16] and much higher than the value in bulk *n*-heptane (1.10 ± 0.05 nm)^[16]. This indicates that the elongation of the PPO chain is favored by the two dimensional interface between water and heptane.

Similar observations have been reported by other groups that have experimentally studied Pluronics at similar water/oil interfaces.^[30-34] For example, recently Ramirez et al. studied three Pluronics F68, L64, and P9400 at water/hexane interface.^[30] Using ellipsometric measurements they have shown that at low polymer concentration, the Pluronics assume a two-dimensional conformation with both the PEO and PPO units at the interface. With a higher polymer concentration at the interface, PEO parts tend to protrude into the water phase forming a *coil structure*. Finally, if the concentration is further increased, a polymeric *mushroom-like* conformation is observed in which PEO units reside in the water phase and the PPO unit coils up at the interface with part of it in both the solvents.^[30] We observe exactly the same trend in our simulations. For the smallest Pluronic, L61, it assumes a linear structure and stays in the interface. With the increase of the PEO and PPO block-lengths in L64 and P85, protrusion of PEO chains in the water phase is observed.

PEO is more hydrophilic than PPO and it tends to stay in water phase rather than the hydrophobic *n*-heptane phase. Our previous study with the monomer of PEO, 1,2-dimethoxyethane (DME) and the monomer of PPO, 1,2-dimethoxypropane (DMP) shows that DMP favors the hydrophobic region more than DME does.^[14] The potential of mean

force (PMF) of percolation of DMP to *n*-heptane phase from water has a value ~ 12 kJ/mol less than that of DME.^[14] Also, we observed that the minima lie exactly at the interface. Pluronics are linear block copolymers, and hence properties of their individual blocks are supposed to be similar to that of the monomer molecules. Here, we observe similar behavior.

Table 4.2 Radius of gyration and end-to-end distances of the polymers at water/*n*-heptane interface.

Polymer	R_g (nm)	End to end distance (nm)
PEO 7	0.51 ± 0.05	1.37 ± 0.32
PEO 20	1.01 ± 0.14	2.59 ± 0.80
PEO 43	1.52 ± 0.23	3.52 ± 1.06
PPO 7	0.47 ± 0.05	1.23 ± 0.32
PPO 20	0.88 ± 0.12	2.42 ± 0.73
PPO 43	1.69 ± 0.22	3.55 ± 0.41
L61	1.32 ± 0.20	3.44 ± 0.84
L64	1.68 ± 0.21	3.29 ± 0.92
P85	2.34 ± 0.28	3.49 ± 1.07

From the simulations at water/*n*-heptane interface, it is evident that the PEO units of the Pluronics prefer being in water rather than in *n*-heptane. This tendency was also evidenced in our previous study of PEO and PPO chains in various solvent systems.^[16, 35] From these observations, we can expect that when these polymer molecules will come in contact with phospholipid bilayers (for example, DMPC in this study), the PPO part may favor the aliphatic region of the bilayer but PEO would try to be in the water phase or in the polar headgroup region of the bilayer.

PEO and PPO chains at water/DMPC bilayer interface.

To have a better insight on the effect of individual polymer chains on the behavior of the DMPC lipid bilayer, PEO and PPO chains of different length (having 7, 20, 43 monomers)

were simulated at the interface and inside the lipid bilayer. For the simulations of polymers at the interface, the polymers tend to stay in the bulk water phase and show no specific interaction with the lipid bilayer within 50 ns. For the simulation starting from a configuration where PEO was inside the bilayer, for all the three chains, PEO diffuses out of the bilayer and stays in the water phase.

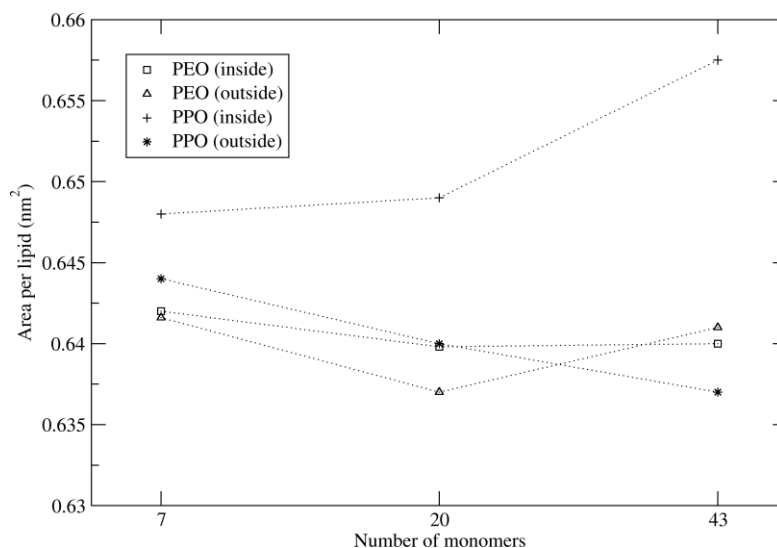


Figure 4.3: Average area per lipid for the systems starting with PEO and PPO at the a) interface, and b) inside the bilayer.

Fig. 4.3 shows the area per lipid (APL) values for the homopolymer chains. For the cases of the polymers outside the bilayer and PEO inside the bilayer, there is no major difference in the APL values. But when the simulation was started with the PPO molecules inside the bilayer, the APL values have higher values and the values increase with the increasing number of monomers in the PPO chains. The distance between the headgroup phosphorus atoms were calculated to investigate on thinning effect, if any (The figure with density distribution of the P-atoms is shown in Fig. A2.5 in Appendix II). No significant change in the membrane thickness was observed for the systems simulated.

PEO at the interface and inside the bilayer.

For the systems with PEO outside and inside the bilayer, the results are similar. When the simulations were started with the PEO inside the bilayer, the polymer promptly goes to the interface and goes out to the water phase. Hence, excluding first few nanoseconds, the behavior of the polymers and the bilayer is similar in both the cases. The R_g values were calculated in all the cases (shown in Table A2.2 in Appendix II). As the polymer chains stay mostly in the water phase, the values for each chain inside and outside the lipid bilayer have similar values and those values are comparable with the values of R_g of PEO chains in water as reported in our previous work.^[16]

PPO at the interface and inside the bilayer.

Similarly as PEO, PPO does not show any preference to interact with the DMPC lipid bilayer and stays in the water phase outside the lipid bilayer. A set of simulations were run with the PPO chains inside the lipid bilayer. For the whole time length of simulations, the PPO chains are observed to stay inside the lipid bilayer, mainly in the aliphatic tail group region of the bilayer. The density distributions of the PPO chains are shown in Figure 4.4. From the density distribution, it can be seen that the smallest PPO chain (with seven monomers) has a localized distribution near the bottom headgroup region of the lipid bilayer. In the case of PPO20, the distribution is more flat and well distributed. PPO43 stays more localized near the headgroup region but has a distribution ranging throughout the aliphatic region of the lipid bilayer.

From the APL plot shown in Figure 4.3, the APL values for PPO inside lipid bilayer are seen to be higher than all three other cases. For PPO7 and PPO20, it has comparable value with slightly higher value for PPO20. APL value is highest for PPO43 inside the lipid bilayer. Larger the number of monomers in the polymer, it takes more space to accommodate it. This results in higher APL value for larger polymers.

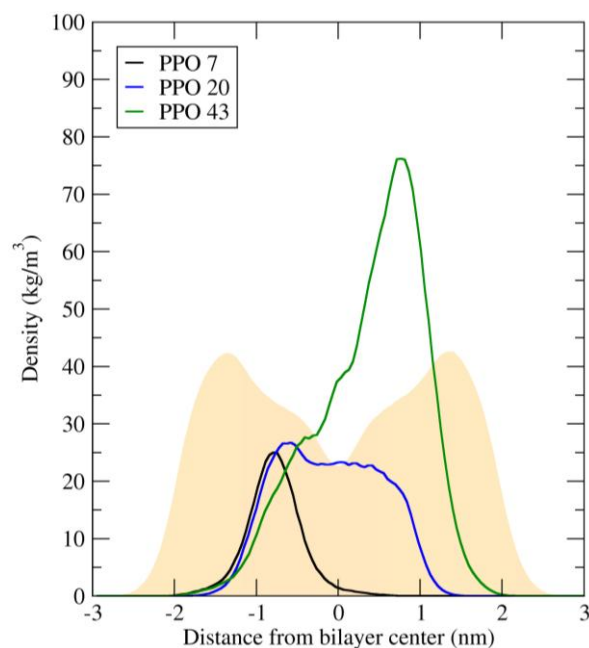


Figure 4.4: Density distributions of PPO chains inside the DMPC lipid bilayer. The position of the DMPC bilayer is shown in orange.

Also in this case R_g values of the PPO chains were calculated and they are reported in the Table A2.2 in the Appendix II. For PPO chains outside lipid bilayer the R_g values are similar to that of in bulk water.^[16] But for PPO chains inside the lipid bilayer, the R_g have smaller values for respective chains. The R_g values inside the bilayer has comparable values as for that in bulk *n*-heptane as reported in our previous study.^[16]

Pluronics at water/DMPC bilayer interface and inside DMPC bilayer.

In this part, the results of simulations of polymers at water/DMPC interface and inside the lipid bilayer are reported. The polymer molecules were put in the water phase ~1 nm away from the boundary of the bilayer and simulated for 50 ns. In the previous chapter we have shown that spontaneous diffusion of the DME and DMP molecule inside the bilayer does not occur within 50 ns.^[36] Hence, to study at a qualitative level the permeation process and the conformational behavior of the polymer inside the bilayer, steered molecular dynamics simulations were used for this purpose.

To see the effect of Pluronics on the structure of the bilayer, the average area-per-lipid (APL) and the distance between the phosphorus atoms in the top and bottom bilayer were calculated for L61, L64 and P85 when outside and inside the bilayer (Average area per lipid values are shown in Fig. 4.5).

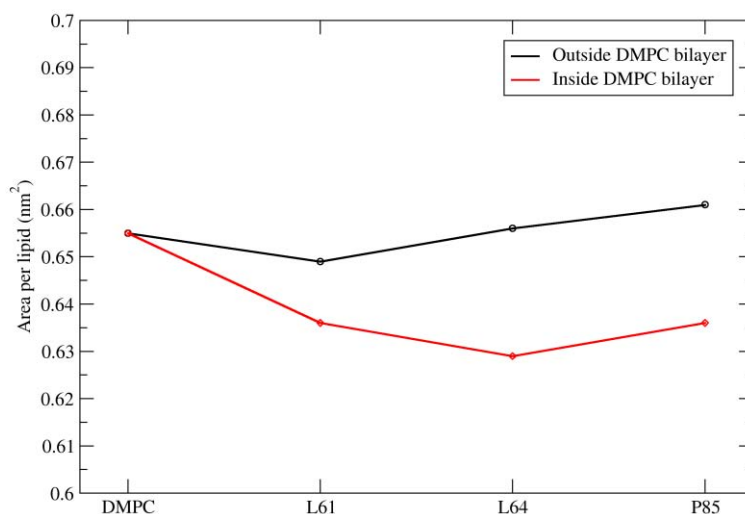


Figure 4.5: Average area per lipid for the polymers simulated.

With the polymers at the interface of the bilayer, the range of variation is quite small. When the simulations were started with the polymers inside the bilayer, the APL value drops slightly below the normal value for pure DMPC bilayer and they have more or less similar value for all the Pluronics molecules. The distance between the phosphorus atoms of the top and bottom layer of DMPC bilayer was calculated to investigate change in the width of the bilayer, if any. Fig. 4.6 shows the density distribution of the P atoms in both the layers. The dotted lines represent the density profile of the P-atoms when the polymers were outside the bilayer at the water phase. No significant change in the width of the membrane is observed in this scenario. But when the simulation was started with the polymer molecules inside the bilayer, we don't see much difference in the case of P85, but there are significant increase in the distance between the P-atoms for L61 and L64. This means, though P85 does not have any effect on the width of the bilayer within this timescale but L61 and L64 elongate the

bilayer to some extent.

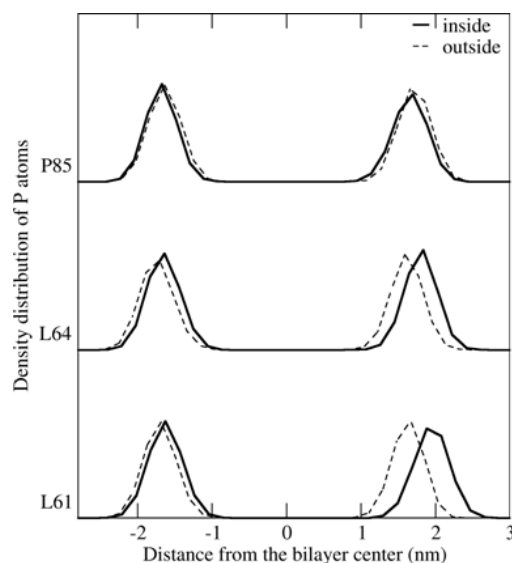


Figure 4.6: P-P density profiles for systems B during the last 25 ns of simulation.

Fig. 4.7 shows the final conformation of the systems for the systems when the simulation was started with the polymers inside the lipid bilayer. For L61 and L64, PPO part extends along the width of the bilayer and the PEO part resides in the lipid headgroup region. For P85, the PPO part remains coiled and the PEO part in the headgroup region of the upper layer and the water just outside. The density distribution of the polymers along with its components are shown in Fig. 4.8 and that also shows that in the case of L61 and L64, the PPO chain remains extended to form a bridge and the PEO part stays in the headgroup region of the bilayer or in the water phase. The length of the PPO chain of L61 and L64 is shorter than P85 and the length is comparable to the width of the bilayer. Hence for L61, the hydrophobic PPO chain can extend throughout the width of the aliphatic region of bilayer keeping the PEO parts in the polar and more favorable headgroup region. On the contrary, the PEO chains of the L64, being longer, extend into the water phase as well. In both these cases, the PPO block adopts a flat orientation with respect to the interface. This might help to increase the structural stability of the membrane by sealing defects. In the case of P85, the length of the PPO

chain is longer than the width of the bilayer and cannot extend along the width of the bilayer.

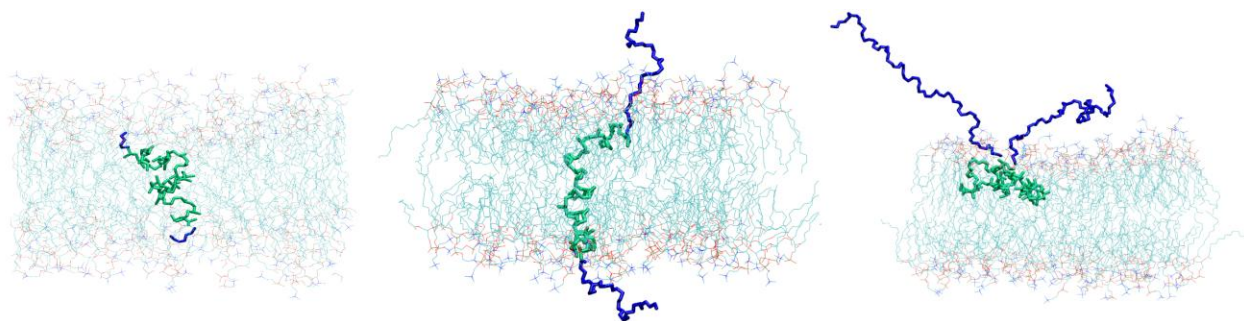


Figure 4.7: Final conformation of Pluronic a) L61, b) L64 and c) P85 at the end of 50 ns unconstrained simulations inside the DMPC lipid bilayer. PEO part of the polymers are shown in blue and PPO part is shown in green. For the sake of clarity water is not shown.

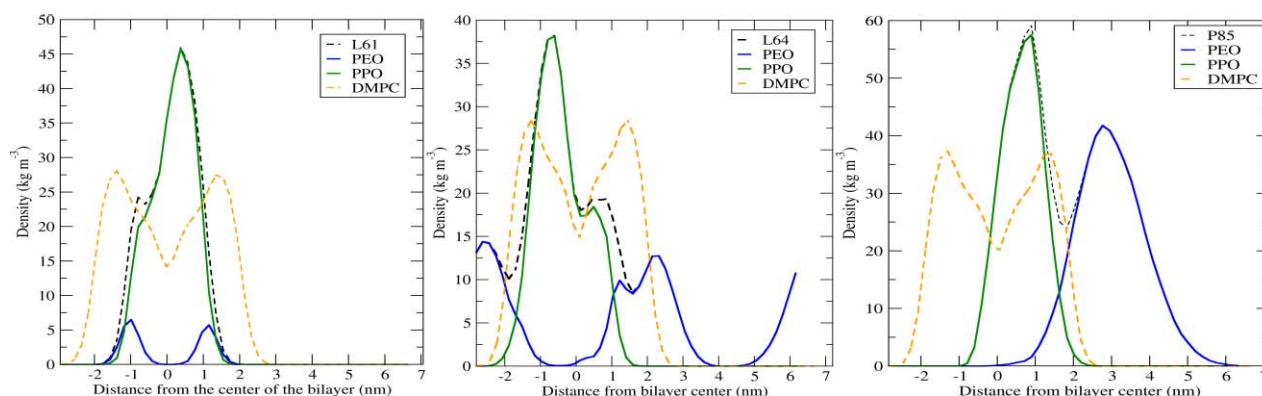


Figure 4.8: Density distribution of Pluronic a) L61, b) L64 and c) P85 during 50 ns unconstrained simulations inside the DMPC lipid bilayer. Density distribution of the PEO part of the polymers are shown in blue and PPO part is shown in green. The density of the polymer in whole is shown in dashed black and the position of the DMPC bilayer is shown in dashed orange.

Fig. 4.9 shows the evolution of the radius of gyration (R_g) and end-to-end distance ($\langle h \rangle$) of the polymers during the course of the simulation. In comparison, L61 has the lowest R_g value and the other two polymers have similar R_g values post 10 ns of the simulation. The trend of $\langle h \rangle$ values is order of the length of the polymer for L61 and L64 but P85, although being the longest of them all, has relatively small $\langle h \rangle$ value.

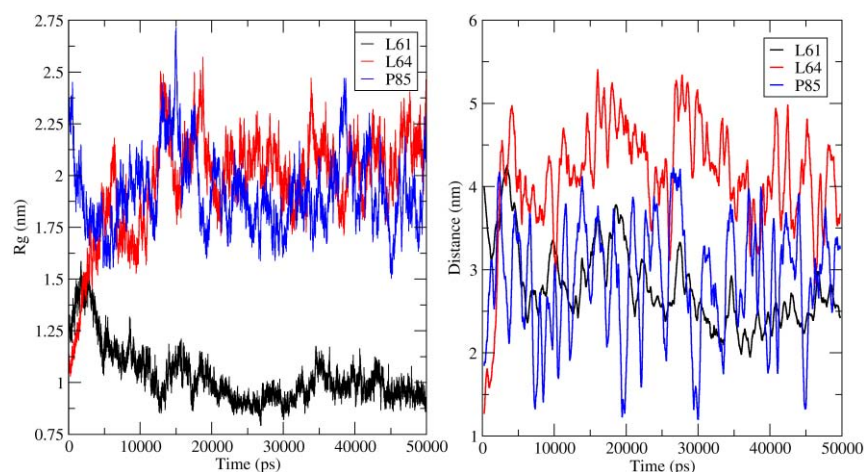


Figure 4.9: Distribution of radius of gyration (left) and end-to-end distance (right) of the Pluronics a) L61, b) L64 and c) P85 during 50 ns unconstrained simulation inside a DMPC bilayer.

Percolations of polymers in lipid bilayer.

In the previous chapter, we have reported the properties of percolation of DME and DMP through DMPC lipid bilayer. To check the effect of the length of the polymers, the potential of mean force for the percolation of small polymers through DMPC lipid bilayer was calculated using umbrella sampling method. The frames for umbrella sampling simulations were generated from a single SMD simulation (details in the Methods section). The simulated polymers were the di- and trimers of PEO and PPO (i.e., PE02, PE03, PP02, and PP03) and the smallest Pluronic molecule PEO-PPO-PEO (denoted as PLU1). The differences in heights of the PMF barriers for percolation from the reference water phase to the aliphatic tail region of the bilayer for these polymers are shown in Fig. 4.10.

From the plot, we see a gradual increase of the height of the energy barrier for percolation with the increase of the chain length of the polymers of same type. Though bulkier, the PPO chains have less high-energy barriers than their corresponding PEO counterparts. For PLU1, the height of PMF of percolation is quite low. The relative difference between PEO and PPO can be attributed to the non-bonded and electrostatic

energy contributions as explained in the previous chapter. Also, the loss of stability due to the loss of hydrogen bonds is much more extensive for DME/PEO. These effects result in a higher PMF barrier for PEO chains compared to their PPO counterparts. But for PLU1, the low barrier is a result of the hydrophilic-lipophilic balance of the polymer. This indicates that the Pluronic molecules have better permeability in lipid bilayer than a PEO or PPO chain of similar length.

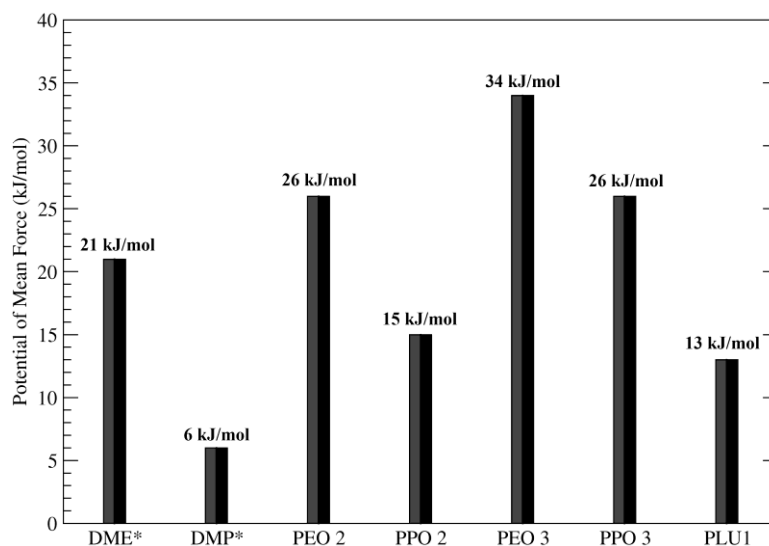


Figure 4.10: The height of PMF profiles for percolation of small polymer chains inside DMPC lipid bilayer. The data for DME and DMP is put for comparison.^[14] Individual plots are shown in Appendix III.

Steered molecular dynamics simulations: Percolation of PEO and PPO inside lipid bilayer.

In the previous chapter, it was shown that umbrella-sampling method is more accurate than SMD simulation method to calculate PMF profile for the percolation of small molecules through lipid bilayer. However, it was also shown that if multiple PMF profiles (obtained by starting the simulations from different starting configurations) are averaged, the barrier for percolation could be quantitatively reproduced. The PMF of percolation of PEO and PPO polymers of chain length 7, 20 and 43, thorough DMPC were calculated using multiple SMD simulations. Fig. 4.11 shows the average PMF plots of ten

SMD simulations for each polymer.

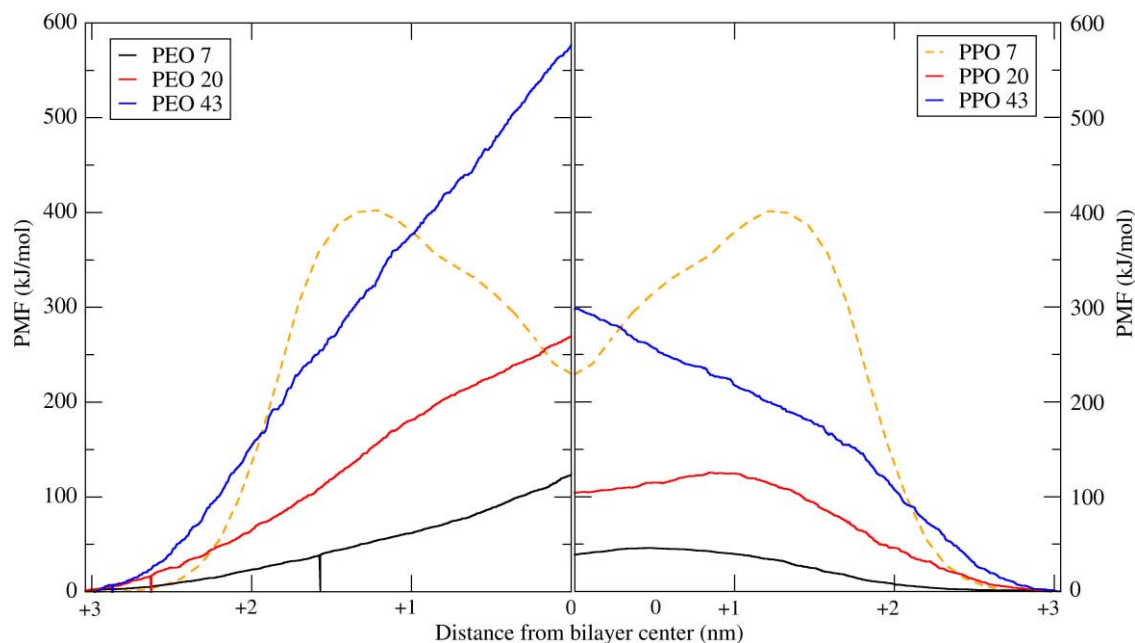


Figure 4.11: PMF profiles for percolation of PEO and PPO chains inside DMPC lipid bilayer. Each individual plot is average of ten SMD simulations. The position of the DMPC bilayer is shown in orange.

In agreement with the results for small polymers, the height of the PMF barrier is lower for PPO in comparison to their PEO counterparts. This must be noted that being a non-equilibrium process, the PMF profiles from SMD simulations are often overestimated. So, the profiles do not quantitatively represent the height of the barrier. But from the point of view of qualitative behavior, we can expect easier percolation of PPO inside the lipid bilayer.

CONCLUSIONS.

In this chapter, structural properties of ether based linear and block polymers in water/*n*-heptane, and water/DMPC bilayer interfaces have been investigated with molecular dynamics simulation. The properties of PEO, PPO and Pluronics were first investigated at the water/*n*-heptane interface. Our study shows that while PPO prefers to stay in the water/*n*-heptane interface, PEO tends to diffuse to the water phase. This

produces the bottle-brush type of structure for Pluronics molecules at water/*n*-heptane interface. This observation is in agreement with available experimental results.

The polymers at the water/DMPC interface did not render significant effects within 50 ns. Spontaneous diffusion of polymers inside lipid membrane is out of reach of atomistic simulations as the time-scale for that may extend to microseconds.^[36, 37] Hence the properties of polymers inside lipid bilayer were studied by pulling them inside the bilayer using SMD simulations. PEO chains did not show any preference for the interior of the bilayer and diffused out of the bilayer. The PPO chains preferred to stay inside the bilayer. Relatively longer PPO20 and PPO43 tend to span across the width of the bilayer while short PP07 chain stayed in the tail region of the bilayer near the polar headgroups. Pluronic L61 and L64 have PPO blocks with a length comparable to the width of the tail region of the bilayer. They spanned across the bilayer with the hydrophilic PEO blocks in the polar headgroup region and water in both sides. The PPO block length of P85 is longer than the width of the bilayer and it assumed a conformation where the PPO block stays in the aliphatic tailgroup region of the bilayer and the PEO blocks stayed in the headgroup region and water phase in the same side of the bilayer.

The PMF profile of bilayer percolation was obtained using umbrella sampling method for small polymers. For the larger linear polyethers the percolation barriers were evaluated using SMD simulations. The energy barrier to transfer the polymers from water into the DMPC tail region was found to be smaller for PPO chains of all lengths (2, 3, 7, 20 and 43 monomer long) than their PEO counterparts. This explains the accumulation of PEO blocks of a Pluronic at the interface, and extension of PPO block of a Pluronic along the width of the lipid bilayer as studied by Firestone et al. from X-ray scattering studies.^[6, 7]

In conclusion, the results of this study provide interesting insights on the mechanism of percolation of polyethers (PEO, PPO and Pluronics) into the DMPC lipid

bilayer. Pluronics are important and widely used for designing drug carrier micelles. Our results provide an accurate atomistic model on the partition behavior of hydrophilic PEO and hydrophobic PPO blocks of these polymers at a membrane interface.

REFERENCES.

- [1] S. Fusco, A. Borzacchiello, P. A. Netti, *Journal of Bioactive and Compatible Polymers* **2006**, *21*, 149.
- [2] R. Haag, F. Kratz, *Angewandte Chemie International Edition* **2006**, *45*, 1198.
- [3] Y. Kodera, A. Matsushima, M. Hiroto, H. Nishimura, A. Ishii, T. Ueno, Y. Inada, *Progress in Polymer Science* **1998**, *23*, 1233.
- [4] C. D. H. Alarcon, S. Pennadam, C. Alexander, *Chemical Society Reviews* **2005**, *34*, 276.
- [5] R. K. Chowdhary, I. Sharif, N. Chansarkar, D. Dolphin, L. Ratkay, S. Delaney, H. Meadows, *Journal of Pharmacy and Pharmaceutical Sciences* **2003**, *6*, 198.
- [6] M. A. Firestone, A. C. Wolf, S. Seifert, *Biomacromolecules* **2003**, *4*, 1539.
- [7] M. A. Firestone, S. Seifert, *Biomacromolecules* **2005**, *6*, 2678.
- [8] A. Sahu, U. Bora, N. Kasoju, P. Goswami, *Acta Biomaterialia* **2008**, *4*, 1752.
- [9] N. S. Melik-Nubarov, O. O. Pomaz, T. Y. Dorodnych, G. A. Badun, A. L. Ksenofontov, O. B. Schemchukova, S. A. Arzhakov, *FEBS Letters* **1999**, *446*, 194.
- [10] X. Liang, G. Mao, K. Y. S. Ng, *Journal of Colloid and Interface Science* **2005**, *285*, 360.
- [11] G. J. A. Sevink, J. G. E. M. Fraaije, H. P. Huinink, *Macromolecules* **2002**, *35*, 1848.
- [12] O. N. Steve, et al., *Journal of Physics: Condensed Matter* **2004**, *16*, R481.
- [13] L. Saiz, M. L. Klein, *Accounts of Chemical Research* **2002**, *35*, 482.
- [14] S. Samanta, S. Hezaveh, G. Milano, D. Roccatano, *Journal of Physical Chemistry B* **2012**, *116*, 5141.
- [15] O. Berger, O. Edholm, F. Jahnig, *Biophysical Journal* **1997**, *72*, 2002.
- [16] S. Hezaveh, S. Samanta, G. Milano, D. Roccatano, *Journal of Chemical Physics* **2012**, *136*, 124901.
- [17] H. J. C. Berendsen, J. P. M. Postma, W. F. van Gunsteren, J. Hermans, (Ed.: B. Pullman), Reidel: Dordrecht, **1981**, p. 331.
- [18] W. L. Jorgensen, J. D. Madura, C. J. Swenson, *Journal of the American Chemical Society* **1984**,

- 106, 6638.
- [19] N. M. Garrido, A. J. Queimada, M. Jorge, E. A. Macedo, I. G. Economou, *Journal of Chemical Theory and Computation* **2009**, 5, 2436.
- [20] B. Hess, C. Kutzner, D. van der Spoel, E. Lindahl, *Journal of Chemical Theory and Computation* **2008**, 4, 435.
- [21] W. Humphrey, A. Dalke, K. Schulten, *Journal of Molecular Graphics* **1996**, 14, 33.
- [22] G. Bussi, D. Donadio, M. Parrinello, *Journal of Chemical Physics* **2007**, 126, 14101.
- [23] H. J. C. Berendsen, J. P. M. Postma, W. F. Vangunsteren, A. Dinola, J. R. Haak, *Journal of Chemical Physics* **1984**, 81, 3684.
- [24] B. Hess, H. Bekker, H. J. C. Berendsen, J. G. E. M. Fraaije, *Journal of Computational Chemistry* **1997**, 18, 1463.
- [25] T. Darden, D. York, L. Pedersen, *Journal of Chemical Physics* **1993**, 98, 10089.
- [26] J. Lin, B. Novak, D. Moldovan, *Journal of Physical Chemistry B* **2012**, 116, 1299.
- [27] S. Park, F. Khalili-Araghi, E. Tajkhorshid, K. Schulten, *Journal of Chemical Physics* **2003**, 119, 3559.
- [28] S. Pal, G. Milano, D. Roccatano, *Journal of Physical Chemistry B* **2006**, 110, 26170.
- [29] S. Kumar, D. Bouzida, R. H. Swendsen, P. A. Kollman, J. M. Rosenberg, *Journal of Computational Chemistry* **1992**, 13, 1011.
- [30] P. Ramirez, A. Stocco, J. Munoz, R. Miller, *Journal of Colloid and Interface Science* **2012**, 378, 135.
- [31] P. Holmqvist, P. Alexandridis, B. Lindman, *Journal of Physical Chemistry B* **1998**, 102, 1149.
- [32] P. Alexandridis, U. Olsson, B. Lindman, *Journal of Physical Chemistry* **1996**, 100, 280.
- [33] P. Alexandridis, *Current Opinion in Colloid and Interface Science* **1996**, 1, 490.
- [34] G. Gotchev, T. Kolarov, K. Khristov, D. Exerowa, *Colloids and Surfaces A: Physicochemical and Engineering Aspects*, 354, 56.
- [35] S. Hezaveh, S. Samanta, G. Milano, D. Roccatano, *Journal of Chemical Physics* **2011**, 135, 164501.
- [36] S. Hezaveh, S. Samanta, A. De Nicola, G. Milano, D. Roccatano, *Journal of Physical Chemistry B* **2012**, in press.
- [37] S. Hezaveh, Jacobs University Bremen (Bremen), **2012**.



Chapter 5

Interaction of Curcumin with PEO-PPO-PEO Block Copolymers

Interaction of Curcumin with PEO-PPO-PEO Block Copolymers.

ABSTRACT.

Curcumin, a naturally occurring drug molecule, has been extensively investigated for its various potential usages in medicine. Its water insolubility and high metabolism rate require the use of drug delivery systems to make it effective in the human body. Among various types of nanocarriers, block copolymers based ones are the most effective. These polymers are broadly used as drug-delivery systems but the nature of this process is poorly understood. In this paper, we propose a molecular dynamics simulation study of the interaction of Curcumin with block copolymer based on polyethylene oxide (PEO) and polypropylene oxide (PPO). The study has been conducted considering the smallest PEO and PPO oligomers and multiple chains of the block copolymer Pluronic P85. Our study shows that the more hydrophobic PPO molecules and PPO block preferentially coat the Curcumin molecule. In the case of the Pluronic P85, simulation shows formation of a drug-polymer aggregate within 50 ns. This process leaves exposed the PEO part of the polymers resulting in better solvation and stability of the drug in water.

INTRODUCTION.

Curcumin, a polyphenol derived from the root of turmeric (*Curcuma longa*) is widely used as a dietary spice and natural food coloring agent throughout the world.^[1, 2] It also finds its place in traditional Indian medicine system, Ayurveda for its wide ranged therapeutic applications as an anti-biotic, anti-inflammatory, anti-rheumatic, anti-arthritic, antioxidant agent and as a cure for several other diseases.^{[3] [4]} Recent studies reveal that Curcumin has potent anticancer effects both alone or with other anticancer drugs.^[5, 6] This has been tested *in vivo* and *in vitro* with melanoma, mantle cell lymphoma, hepatic, prostatic, ovarian and pancreatic carcinomas.^[7] Curcumin has been reported to have diverse effects on signaling molecules down-regulation of the expression of angiogenesis-associated genes, activation of the apoptotic mechanisms and induction of the cell cycle arrest.^[8] It also enhances chemotherapeutic responses of cancer cells to several anticancer drugs.^[5, 9] Curcumin is a potential inhibitor of nuclear factor kappaB (NF- κ B) signaling pathway.^[10] NF- κ B promotes carcinogens in liver, colon, lung and leukemia and prostate cancer and NF- κ B excess is a main reason for the failure of chemotherapy with many drugs as well.^[11] Curcumin also prevents accumulation of amyloid- β (A β) aggregates as soluble oligomers, and hence preventing Alzheimer's disease.^[12-14]

In spite of aforementioned therapeutic potentials, low solubility in water and high degradation rate hinders the clinical development of Curcumin. It is not soluble in water at neutral or acidic pH and dissociates in alkaline condition.^[15, 16] Clinical study on rats revealed disappearance of Curcumin from blood in 1 hour after a dose of 40mg/kg scale and confirms only 10 ng/mL serum concentration upon 2g of oral dose.^[17, 18] For these reasons, there is a need to associate the drug with a delivering carrier to prevent these problems.

Amphiphilic block co-polymers that can assemble to form a micelle can be used as a carrier of poorly soluble drug molecules to cells.^[19-21] Different studies of Curcumin

with different amphiphilic block copolymers based carrier have been reported in the literature.^[22-27] They increase solubility, improve stability and control release profile. In particular, polyethylene oxide (PEO) and polypropylene oxide (PPO) based triblock copolymers, Pluronics are among the most effective carriers for Curcumin.^[27] Pluronics are non-toxic, inexpensive, and easily customizable, polymers.^[21] Moreover, Pluronics having tendency to accumulate in tumor cells, enhance the efficiency of chemotherapeutics and decrease chances of side effects on the immune system.^[28, 29] However, the molecular mechanics of interaction of the polymers with drugs and their delivery at molecular level are not yet clearly understood. So far, experimental studies on these topics for Curcumin are very limited and there are no theoretical investigations present in literature.

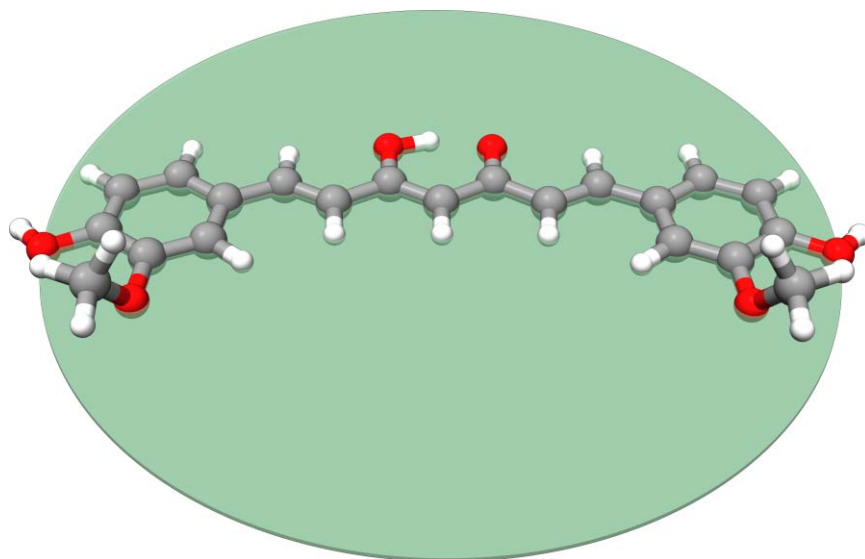


Figure 5.1: Optimized structure of Curcumin. The carbon atoms are shown in dark grey, oxygen atoms in red and hydrogen atoms in white. The green plane helps to understand the planarity of the molecules.

In this work, using molecular dynamics simulations, we aim to understand the interaction of Curcumin with polymer surfactants based on PEO/PPO units. In particular, we have studied the interaction of the drug molecule with the Pluronic P85 (PEO₂₅-PPO₄₀-PEO₂₅). P85 is a variant of Pluronic with good hydrophilic-lipophilic

balance and has a molar ratio of 1.03 for PEO/PPO units. The 'hydrophilic lipophilic balance' (HLB) ratio for P85 is 17. This value is comparable to the Pluronic F68 (HLB ratio = 17.8) and F127 (HLB ratio = 24) which were used by Sahu et. al to experimentally study the encapsulation of Curcumin in Pluronic.^[27] Furthermore, this model has previously been extensively tested in different solvent conditions and performed satisfactorily.^[30]

In addition, interactions of the drug molecule with 1,2-dimethoxyethane (DME) and 1,2-dimethoxypropane (DMP), which are the smallest oligomers of PEO and PPO, have been studied. The Curcumin model has been tested by conducting simulations in water, methanol and 1-octanol.

In this chapter, the details of the force fields and methodologies used are described in the 'Methods' section. The results of the simulations of Curcumin in water, methanol, 1-octanol, DME/DMP/water mixture, and in the presence of Pluronic P85 are explained in the 'Results and Discussions' section. Finally in the 'Conclusions' section, the findings of this work have been summarized.

METHODS.

Force Field.

Fig. 5.1 shows the chemical structure of Curcumin ((1E,6E)-1,7-bis (4-hydroxy-3-methoxyphenyl) -1,6-heptadiene-3,5-dione). It exhibits keto-enol tautomerisation and, depending upon the solvent, the enol form can constitute up to 95% of the conformations.^[31] Quantum mechanical calculations were performed on the enol form of the molecule to obtain the optimized structure and the partial charges of the atoms. Geometry optimization was done using the restricted B3LYP method with the 6-31G** basis set, and the atomic charges were calculated using the ChelpG procedure.^[32] The optimized structure of Curcumin is shown in Fig. 5.1. The coordinates of the atoms of the optimized structure and their corresponding partial charges are reported in Table

A3.1 and A3.2 of the Appendix III. For the Curcumin model, parameters for partial charges, bond lengths, bond angles, and dihedral angles were based upon the QM calculations (Table A3.3, A3.4 and A3.5 in the Appendix III). The force constants for the bond angles and the torsional interactions and the Lennard-Jones parameters were adapted from the GROMOS96 parameters. The quality of the model was tested by calculating its partition coefficient in water/1-octanol system ($\log P_{\text{octanol/water}}$) following the method explained in our previous publication.^[33] For DME, DMP and P85 polymer, the recent models by Hezaveh et al.^[30, 34] were used. The simple point charge (SPC)^[35] model for water and OPLS united atom (OPLS-UA) model for methanol^[36] and 1-octanol^[37] was used.

Table 5.1: Description of the systems simulated.

System	Components (number of molecules in parenthesis)	Box size (x × y × z)/ nm ³	Number of atoms
A	(1) Curcumin + (4124) water	5×5×5	12408
B	(1) Curcumin + (1866) methanol	5×5×5	5634
C	(1) Curcumin + (413) 1-octanol	5×5×5	4166
D	(1) Curcumin + (23) DME + (24) DMP + (2695) water	4.5×4.5×4.5	8427
E	(1) Curcumin + (1) P85 + (6917) water	6×6×6	21106
F	(1) Curcumin + (8) P85 + (22393) water	9×9×9	69767
G	(8) P85 + (22393) water	9×9×9	69731
Systems A-E were simulated for 50 ns; systems F and G were simulated for 100 ns.			

Simulation Setup:

The quantum mechanical calculations were performed using Gaussian 03 program.^[38] All the molecular dynamics simulations were performed using GROMACS (version 4.5.5)^[39] software package and VMD^[40] was used for visualization purpose. Details of the simulated systems are shown in Table 5.1. For all the simulations, the temperature was kept constant at 298 K using the V-rescale thermostat^[41] with a coupling constant of 0.1 ps. The pressure was maintained constant at 1 bar using Berendsen barostat^[42] with a coupling constant of 0.5 ps. The bond-lengths were constrained using LINCS^[43] algorithm. An integration time step of 2 fs was used for all the simulations. Electrostatic interactions were evaluated using particle mesh Ewald method^[44] with a cutoff of 1.0 nm, grid spacing of 0.12 nm and a fourth order spline interpolation. Lennard-Jones interactions were truncated at 1.0 nm.

Calculation of the spatial density distribution:

The spatial density distribution of the solvent molecules around the Curcumin molecule was calculated using *g_spatial* program of the GROMACS package. A cubic grid with 0.1 nm grid spacing was used for all the calculations. The solvent molecules were centered around the Curcumin molecule in each trajectory frame using a translational-rotational fit to the first configuration of the MD trajectory and removing the periodic boundary conditions. Finally, the atomic positions of the selected atoms of solvent molecules were mapped on a cubic grid centered on the geometric center of the Curcumin molecule and averaged with respect to the number of frames analyzed. The averaged volumetric density data obtained was analyzed using the program VMD.

Calculation of free energy of solvation (ΔG) and partition coefficient ($\log P_{\text{octanol/water}}$):

The final frames of the simulation of Curcumin in water, methanol, and 1-octanol (for 50 ns) were taken as the starting structures for the calculation of free energy of solvation.

Gibbs free energy of solvation in water (ΔG_{hyd}), in methanol (ΔG_{met}), and in 1-octanol (ΔG_{oct}) at 298 K was calculated using the thermodynamic integration (TI) method.^[45] The TI integration was performed on 21 λ points: 0, 0.05, 0.1, 0.15, 0.2, 0.25, 0.3, 0.35, 0.4, 0.45, 0.5, 0.55, 0.6, 0.65, 0.7, 0.75, 0.8, 0.85, 0.9, 0.95, and 1.00. The soft-core parameters α and σ were assigned the values of 1.5 and 0.30 respectively. For each λ -point, the equilibrated system was run for 2 ns. From ΔG_{hyd} and ΔG_{oct} at the temperature T , the corresponding partition coefficient is calculated according to the following formula^[37],

$$\log P_{\text{octanol/water}} = \frac{\Delta G_{\text{hyd}} - \Delta G_{\text{oct}}}{2.303RT} \quad (\text{Eqn. 5.1})$$

where R is the universal gas constant.

RESULTS AND DISCUSSIONS.

Simulation of Curcumin in water, methanol and 1-octanol.

The values of free energies resulted in $\Delta G_{\text{hyd}} = 4.6 \pm 1.1$ kJ/mol, $\Delta G_{\text{met}} = -5.3 \pm 0.9$ kJ/mol, and $\Delta G_{\text{oct}} = -2.1 \pm 0.6$ kJ/mol. The free energy of solvation value indicates insolubility of Curcumin in water and better solubility in methanol than in 1-octanol. This is in agreement with the available chemical information.

The value of $\log P_{\text{octanol/water}}$ resulted in 1.17. Unfortunately, there are no experimental chemical data that can be used to verify the results of our MD simulations. However, theoretically calculated values of $\log P_{\text{octanol/water}}$ result in 3.07 ± 0.4 ^[46] or 2.517 (using CONFLEX/PM3 method)^[47]. Qualitatively, the values are in agreement and indicate Curcumin's higher affinity towards 1-octanol than water.

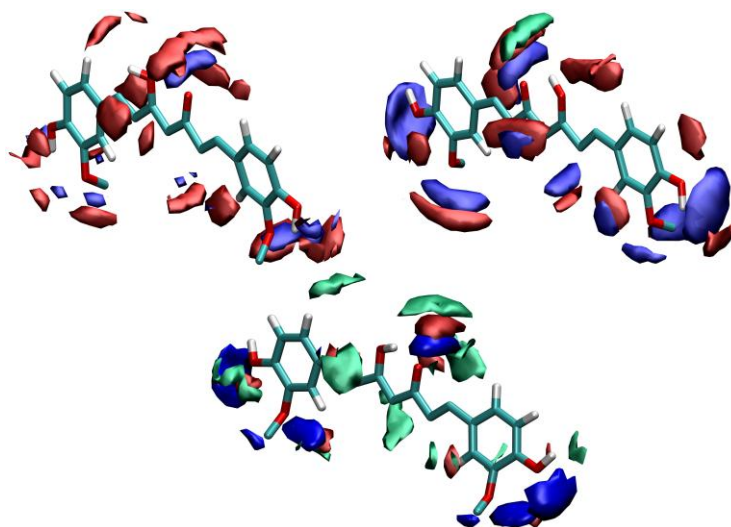


Figure 5.2: Spatial distribution of solvent atoms around Curcumin molecule in water (top-left), methanol (top-right) and 1-octanol (bottom). Hydrogen atoms are shown in blue, oxygen atoms in red and carbon atoms in green. Contour values of the iso-surfaces are 20 for both hydrogen and oxygen of water and 35 for all three types of atoms in methanol. Isovalue for 1-octanol carbon is 20 and that for 1-octanol oxygen and hydrogen are 200.

To understand the behavior of Curcumin in simple solutions, it was simulated in water, in methanol and in 1-octanol. Fig. 5.2 shows the spatial distribution of solvent atoms around the Curcumin molecule during a 50 ns free simulation. As expected, the solvent molecules tend to gather around the hydrophilic and polar region of Curcumin. High density of solvent hydrogen atoms around the oxygen atoms of Curcumin indicates a good extent of hydrogen bonding with the solvent molecules.

Fig. 5.3 shows the root mean square fluctuation (RMSF) per atom plot of the Curcumin molecule during a 50 ns free simulation in different solvent conditions – in water, in methanol, in 1-octanol, and in water with DME and DMP. As expected, five major fluctuations are seen in the molecule and they correspond to the three –OH groups and two –OCH₃ groups. In the case of methanol and 1-octanol, only four major fluctuations are seen – all in the –OH and –OCH₃ groups attached to the phenyl rings. The enol hydroxyl group remains stable resulting in low RMSF per residue. This implies that the rotation along the O-H bond is restricted in methanol and 1-octanol.

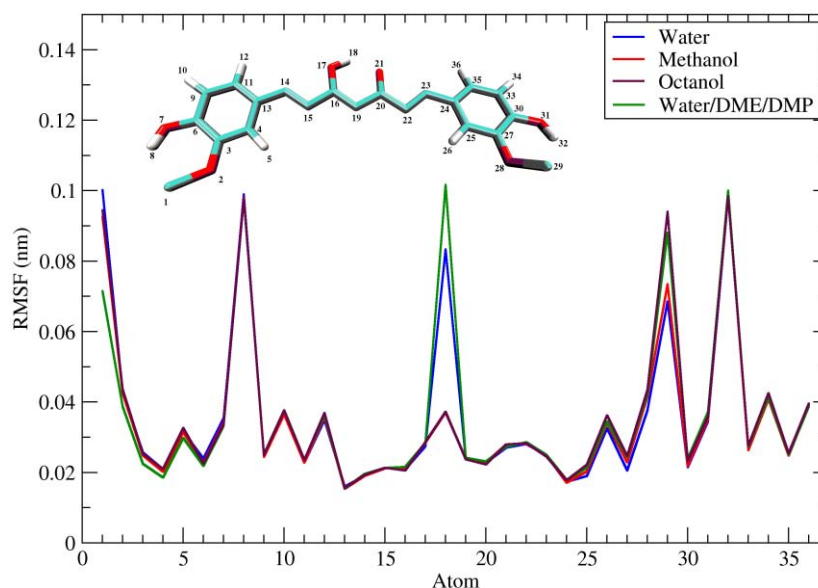


Figure 5.3: Root mean square fluctuation (RMSF) of the atoms of Curcumin in water (blue), methanol (red), 1-octanol (maroon) and in presence of DME and DMP in water (green). The atom numbers are shown in inset.

To further evaluate the scenario, average distance between the enol hydrogen and keto oxygen was calculated. Fig. 5.4 shows the distribution of average distance of the enol hydrogen and the keto oxygen of Curcumin during a 50 ns free simulation in water, methanol and 1-octanol. In methanol and 1-octanol, we observe a single peak at 0.16 nm but in water, we observe a bimodal distribution having a large peak at the same position as of methanol and a shorter second peak at 0.35 nm. In methanol and 1-octanol, the enol hydrogen tends to point towards the keto oxygen (as seen in Fig. 5.2) but in water, though mostly its conformation is the same, but there is a significant contribution of the conformer where the hydrogen points away from the keto oxygen atom (as seen in Fig. 5.2).

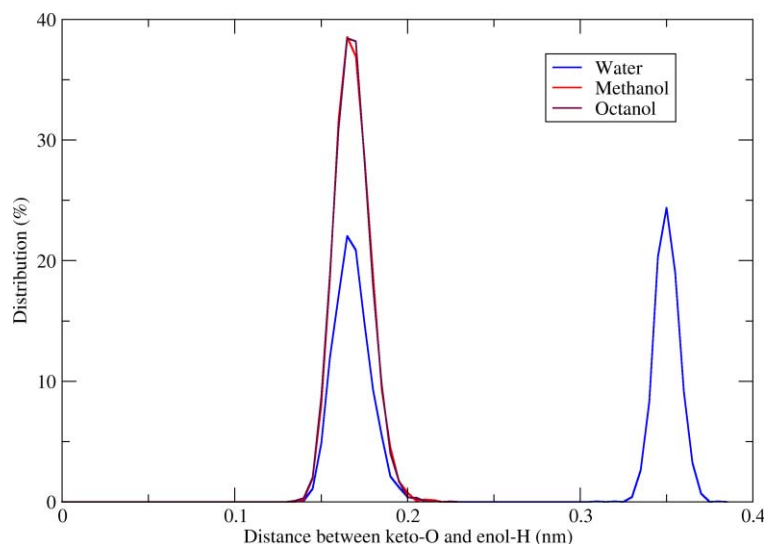


Figure 5.4: Distribution of average distance between the enol hydrogen (atom number 18) and the keto oxygen (atom number 21) in water, methanol and 1-octanol.

Fig. 5.5 shows the hydrogen bonding between Curcumin and solvent molecules. From the figure, we can observe that the oxygen of water tends to form a hydrogen bond with the enolic hydrogen of Curcumin. As a result, the O–C bond is rotated and the hydrogen atom faces away from the keto oxygen atom. Methanol and 1-octanol oxygen being less electronegative cannot form this type of hydrogen bond and hence, the enolic hydrogen always keeps facing the keto oxygen of the Curcumin molecule.

The radial distribution function (RDF) of the oxygen atoms of the solvent molecules with respect to the two types of rings present in the Curcumin molecule is shown in Fig. 5.6. RDF was calculated with respect to the ring formed by six central atoms (as shown in Fig. 5.6) and one of the phenyl rings. The positions of the first peaks in all the cases have lower value for methanol and 1-octanol than that of water indicating the hydrophobic nature of the molecule. High value of RDF for 1-octanol indicates high attractive interaction between 1-octanol and Curcumin. From the RDF curves, it's clear that water has the least attractive interaction with Curcumin between the three solvents used for simulation.

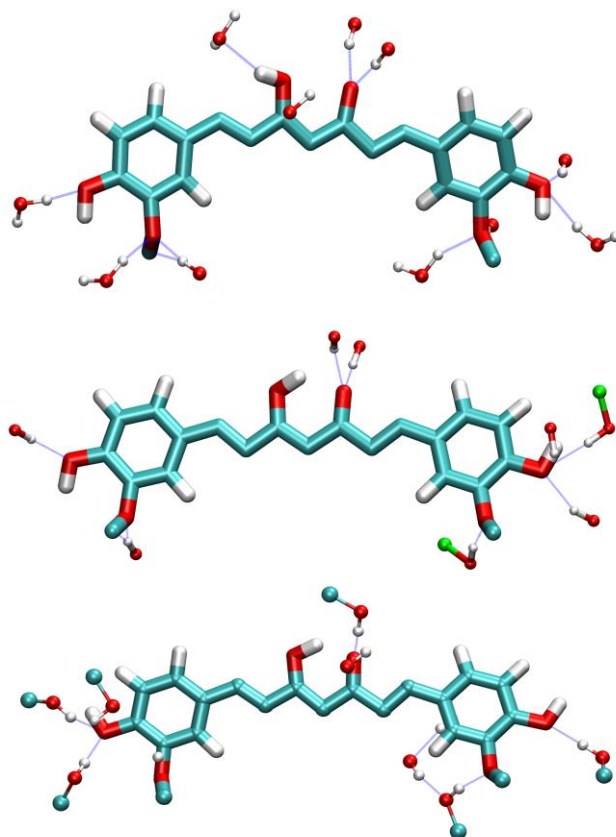


Figure 5.5: Hydrogen bonding of Curcumin in water (top), in methanol (middle) and in 1-octanol (bottom).

For all the solvents, the first peak for the nonpolar phenyl rings is shifted to longer distance than that of the polar middle ring indicating more interaction with the middle ring. The same was observed from the spatial distribution of solvent atoms around the drug molecule (Fig. 5.2). The average number of contacts (N_{cont}) between the Curcumin molecule and the solvent molecules was found to be 82 (± 3) for water, 40 (± 2) for methanol and 26 (± 3) for 1-octanol.

Diffusion coefficient value in water, methanol and 1-octanol was found to be $2.61 (\pm 0.24) \times 10^{-9} \text{ m}^2/\text{s}$, $1.17 (\pm 0.07) \times 10^{-9} \text{ m}^2/\text{s}$, and $0.53 (\pm 0.01) \times 10^{-9} \text{ m}^2/\text{s}$, respectively. Restricted mobility of the Curcumin molecule indicates stronger interactions with methanol and 1-octanol. Low diffusion coefficient value for 1-octanol

is in agreement with the RDF data. Diffusion coefficient of the solvents are $4.19 (\pm 0.01) \times 10^{-9} \text{ m}^2/\text{s}$, $2.820 (\pm 0.002) \times 10^{-9} \text{ m}^2/\text{s}$ and $0.12 (\pm 0.01) \times 10^{-9} \text{ m}^2/\text{s}$ for water, methanol and 1-octanol, respectively. These values are similar to the diffusion coefficient values for pure solvents at 298 K.[34, 48, 49] This indicates that Curcumin has no significant effect on the bulk properties of the solvents at infinite dilution condition.

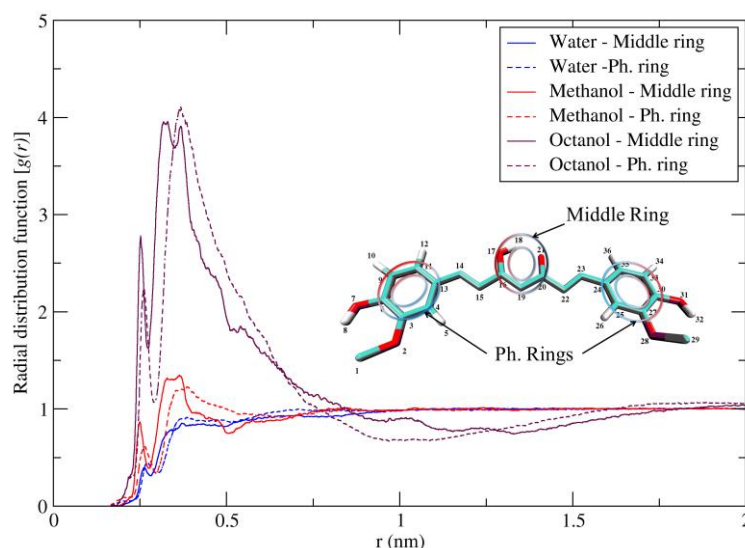


Figure 5.6: Radial distribution function of the oxygen atoms of the solvent molecules with respect to the two different types of rings in the Curcumin molecule.

Simulation of Curcumin in DME/DMP mixture in water.

50 ns simulation of Curcumin in a box of water with 23 of DME and 24 DMP molecules was performed. Fig. 5.7 shows the spatial distribution of DME and DMP molecules throughout the simulation. The distribution indicates preference of DMP towards the hydrophobic part of the Curcumin molecule. DME does not contribute much to the spatial distribution apart from the keto-enol part in the molecule.

During the same simulation, the minimum distance of the center of mass (CoM) of the Curcumin molecule from the CoM of the DME and DMP molecules are shown in the Fig. 5.8. As seen in the spatial distribution, the distance distribution also shows that the

DMP molecules always tend to stay closer to the Curcumin molecule.

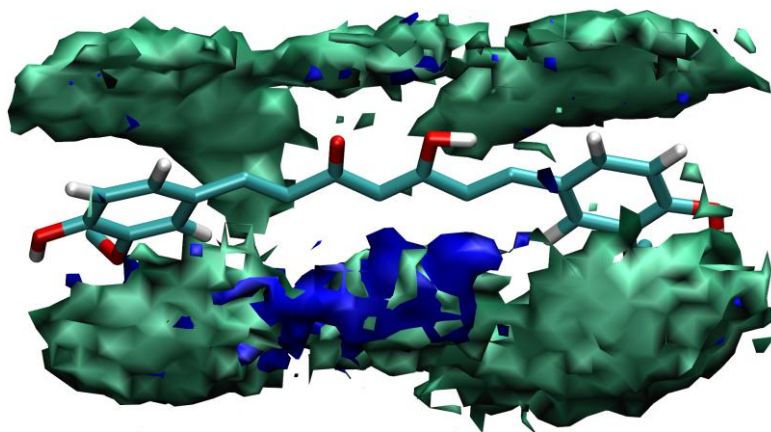


Figure 5.7: Spatial distribution of DME and DMP molecules around Curcumin molecule. DME is shown in blue, DMP in green. The density surfaces have isovalue of 45 for both DME and DMP. For the sake of clarity, water is not shown.

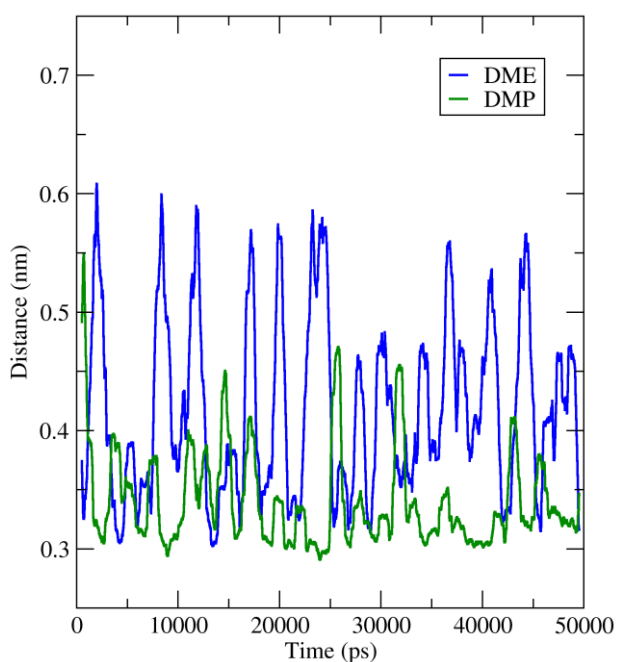


Figure 5.8: Minimum distance of the DME and DMP molecules from the center of mass of the Curcumin molecule during a 50 ns simulation. A distance cutoff of 0.6 nm was used.

The average number of contacts (N_{cont}) between the Curcumin molecule and the solvent molecules was found to be 2 (± 1) for DME, 3 (± 2) for DMP and 70 (± 6) for water. As DMP stays closer to Curcumin, the N_{cont} value is significantly high for DMP than that of DME. Also, the N_{cont} value for Curcumin with water is lower than that of N_{cont} value in bulk water. This indicates Curcumin's favor towards relatively more hydrophobic molecules when put in a hydrophilic environment. To further support the observation, the RDF for the oxygen atoms of the DME, DMP and water molecules with respect to the rings of the Curcumin molecule (as shown in Fig. 5.6) was calculated and it is shown in the Fig. A3.2 in the Appendix III. The interactions with the solvents are significantly different at chemically dissimilar parts of the Curcumin molecule. The peak position for the RDF value of DME has the lowest value for the more polar keto-enol ring of the molecule, followed by water and DMP. The trend is quite different for the phenyl rings where the peak position for RDF has lowest value for DMP, followed by DME and water. The phenyl rings being more hydrophobic than the middle part of the Curcumin molecule, favors less hydrophilic DMP molecules than DME or water. The keto-enol part is more polar and favors DME and water over DMP.

Diffusion coefficient value of the Curcumin molecule in DME/DMP/water mixture was found to be $0.32 (\pm 0.07) \times 10^{-9} \text{ m}^2/\text{s}$ and this value is significantly lower than the values of diffusion coefficient in water and in methanol. This significant depression in diffusion coefficient value supports formation of an aggregation with the ether molecules resulting in better solubility and stability in water. Fig. 5.9 shows the trend of diffusion coefficient values of the Curcumin molecule in all the systems simulated.

Simulation of Curcumin in the presence single Pluronic (P85) chain.

Fig. 5.10 shows the initial and final conformations of Curcumin and one P85 chain from a 50 ns simulation in water. In the initial conformation of the P85 chain, the polymer

was taken as a coiled structure and after 50 ns simulation, the PPO part is seen to be still in the coiled conformation close to the Curcumin molecule, whereas the PEO parts stretch in the water.

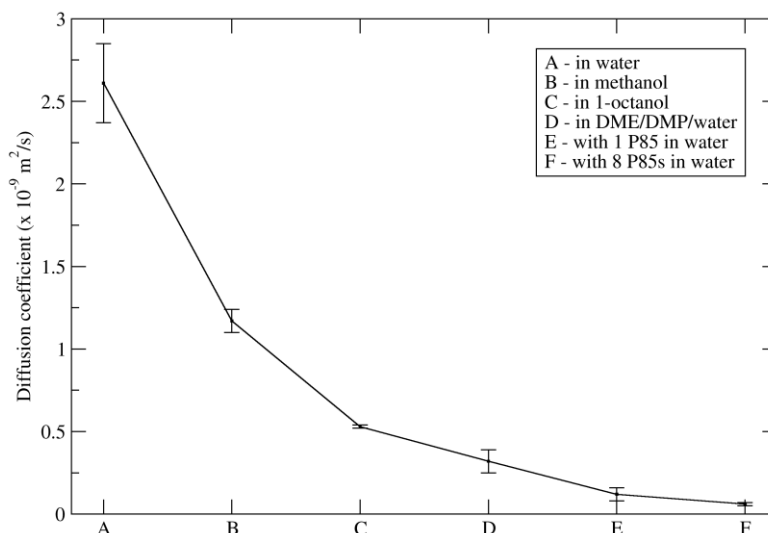


Figure 5.9: Diffusion coefficient of the Curcumin molecule in different systems simulated. The line is put to help as a visual guide.

The radius of gyration (R_g) value of the P85 chain was 2.13 ± 0.40 nm, which is very close to 2.25 ± 0.04 nm, the R_g value for single P85 chain in water at 298 K.^[30] The hydrophobic PPO part of the P85 chain, when put in water, is supposed to form a core and the hydrophilic PEO parts remain extended in the solvent. In this scenario, we observe a similar behavior. The Curcumin molecule being hydrophobic prefers to stay close to the hydrophobic core of the P85 chain and as a result, the mobility of the drug molecule is suppressed to a great extent. The diffusion coefficient of the Curcumin molecule was calculated to be $0.12 (\pm 0.04) \times 10^{-9} \text{ m}^2/\text{s}$, which is much less than that of free Curcumin in water (Fig. 5.9).

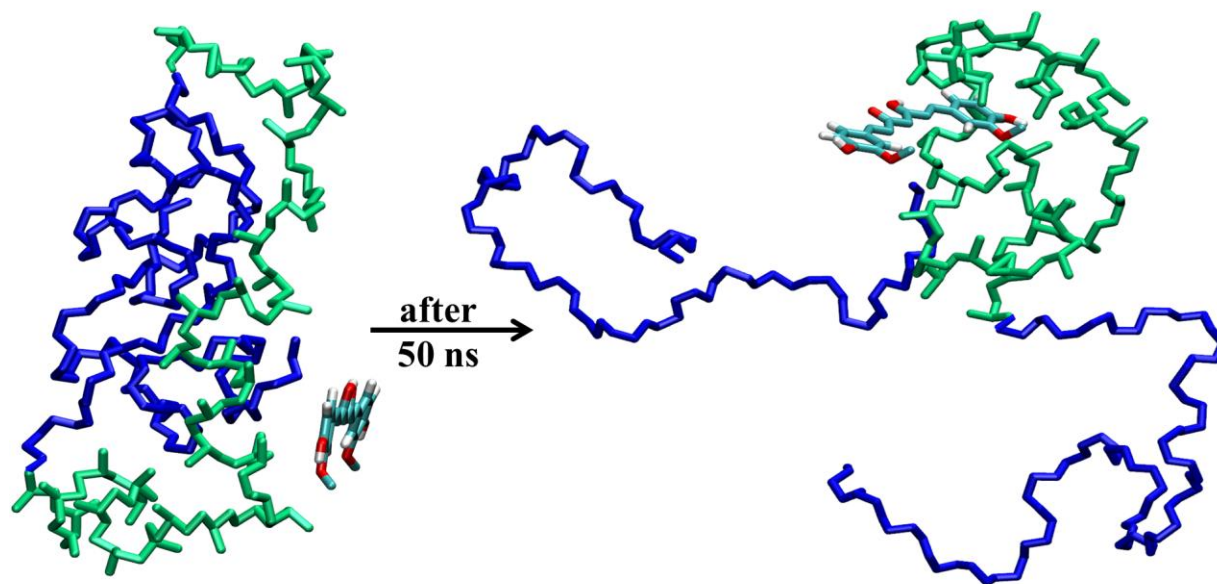


Figure 5.10: Snapshot of the P85 and the Curcumin molecule at the beginning and at the end of a 50 ns simulation. The PEO part of P85 is shown in blue and the PPO part is shown in green.

Fig. 5.11 shows the number of contacts (within 0.6 nm) between the Curcumin molecule with PEO (blue) and PPO (green). The plot shows significantly higher number of contacts for PPO than that for PEO. In the same figure, distribution of minimum distance of the PEO and PPO parts of P85 from the center of mass of Curcumin during the simulation of a Curcumin molecule in the presence of one P85 chain in water is shown. Throughout the simulation, the PPO part is seen to be closer to Curcumin molecule than the PEO parts. This observation goes hand in hand with the findings from the simulation of Curcumin in the presence of DME and DMP. In that case as well, we have observed that the hydrophobic DMP molecules tend to stay close to the Curcumin molecule.

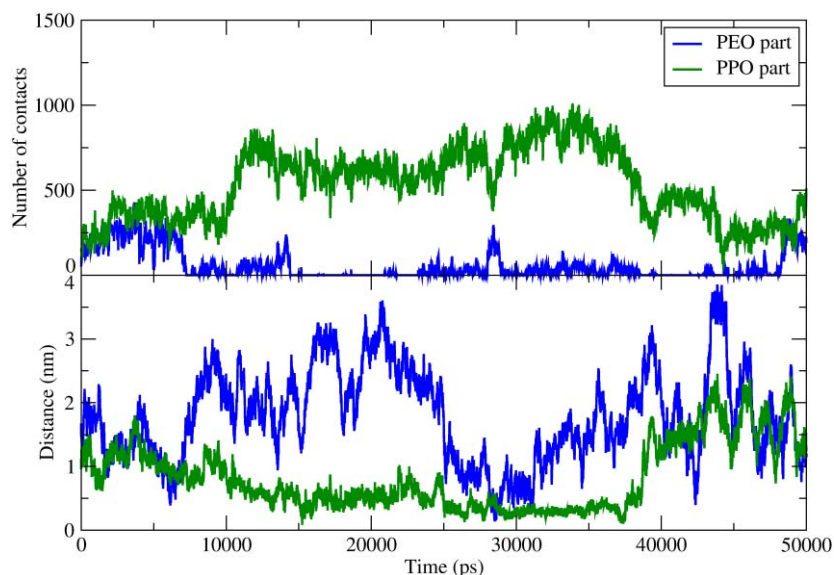


Figure 5.11: Average number of contacts between the PEO and PPO with P85 chain is shown in the top. A distance cutoff of 0.6 nm was used. Minimum distance of the PEO part and PPO part of the Pluronic P85 molecule from the center of mass of the Curcumin molecule during a 50 ns simulation is shown in the bottom panel.

Simulation of Curcumin in the presence multiple Pluronics (P85) chains.

Simulation of a single P85 chain with Curcumin shows potential to form a drug-polymer aggregate. Sahu et al.^[27] have experimentally studied encapsulation of Curcumin in Pluronics micelles. They have found that in the presence of Curcumin, spherical micelles with sizes in a range of 20-80 nm are formed. Also, fluorescence emission spectra indicated that Curcumin molecules are encapsulated in the hydrophobic core of the micelle and form a stable aggregate. But no specific information about the composition and formation of the aggregate/micelle is available. To investigate the properties of the aggregation, one Curcumin molecule was simulated in a box of water with eight P85 chains. Fig. 5.12 shows the final conformation of the system. The snapshot shows hydrophobic core formed with the hydrophobic PPO part of four P85 chains that wrap the Curcumin molecule while the hydrophilic PEO parts flank in water. Moreover, it is seen that only four P85 chains take part in formation of an aggregation with the Curcumin molecule. The radius of gyration of the drug-polymer aggregation was found

to be 5.0 ± 1.2 nm. Using these results, we can roughly estimate that the aggregation numbers for micelles of the same size observed by Sahu et al.^[27] for F68 and F127 are in the range from 30 to 2000. As seen for the simulations of Curcumin in DME/DMP/water mixture and with one P85 chain in water, hydrophobic interaction between Curcumin and PPO is the main driving force for the formation of the aggregate.

Eight P85 chains were also simulated in water in the absence of the Curcumin molecule to check if Curcumin affects the aggregation tendency of the Pluronic chains. Within the same simulation time, aggregation of the polymer chains, monitored as number of contacts along the simulation time, was observed with no major changes in the aggregation tendency.

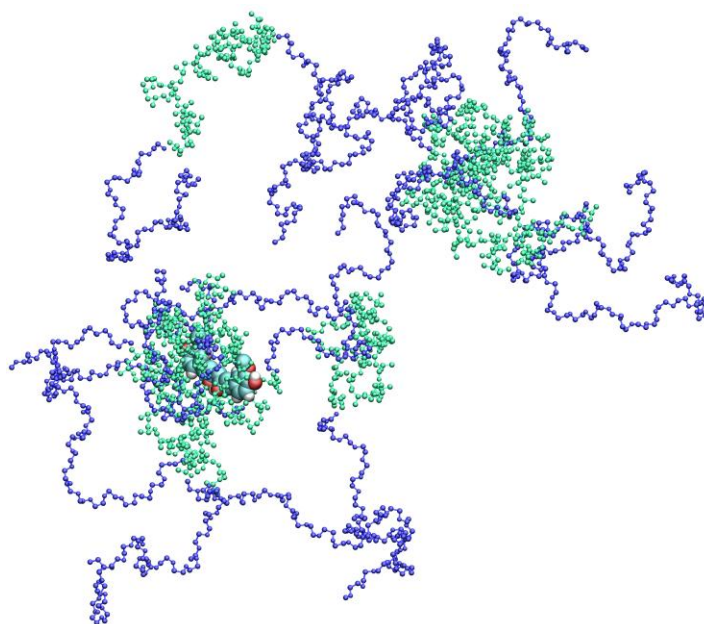


Figure 5.12: Snapshot of the final conformation of P85 chains around the Curcumin molecule after a 50 ns simulation. The hydrophilic PEO chains are shown in blue and the hydrophobic PPO chains are shown in green.

The spatial distribution of PEO and PPO chains around the drug molecule is shown in Fig. 5.13. At the level of the same isovalue, the hydrophobic PPO is seen to form a pocket on one side of the Curcumin molecule and the PEO chains have a

relatively smaller contribution towards the spatial distribution. Similar distribution is seen for the spatial distribution of DME and DMP around Curcumin in aqueous solution. The number of hydrogen bonds and the number of pairs within 0.35 nm between water and Curcumin decreases in the presence of P85 chains in comparison to that of in bulk water (Figure A3.3 in Appendix III). The number of contacts (within 0.6 nm) between water and Curcumin is 2442 in bulk water but it reduces to 1108 in the presence of P85 chains. These indicate that the stability of the Curcumin molecule in the aggregate is enhanced by reducing its interaction with water in the presence of Pluronic P85.

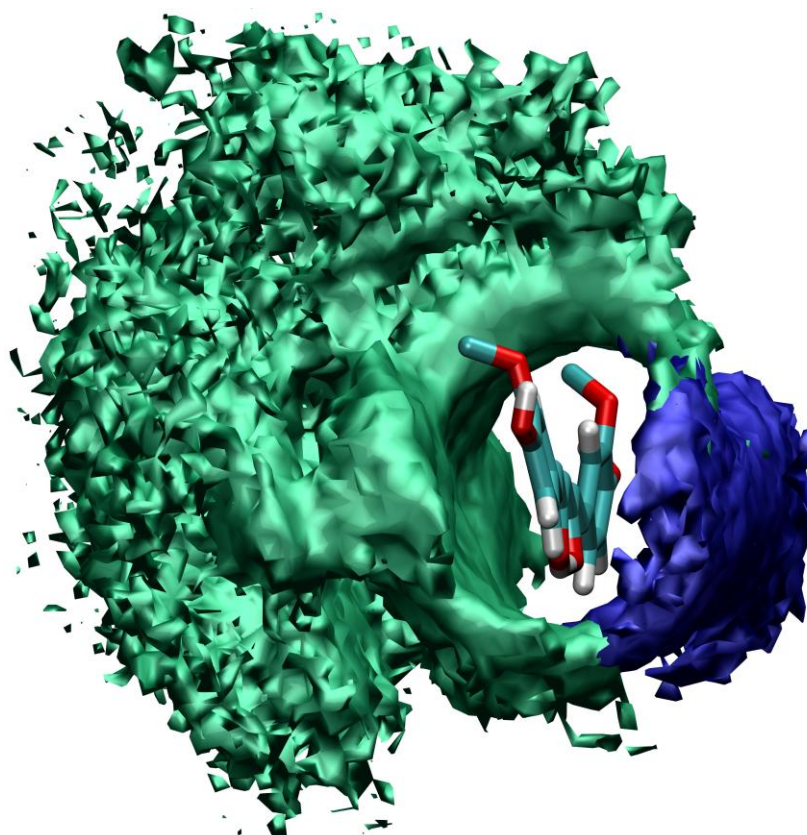


Figure 5.13: Spatial distribution of PEO and PPO chains around Curcumin molecule. PEO is shown in blue, PPO in red. The density surfaces have isovalue of 250 for both PEO and PPO.

Also, the diffusion coefficient of Curcumin molecule in this system is the lowest of all the systems simulated (Figure 9). It has a value of only $0.06 (\pm 0.01) \times 10^{-9} \text{ m}^2/\text{s}$. The aggregation of multiple Pluronic chains around the drug molecule makes mobilization

even harder. Strong interaction with hydrophobic PPO part of the Pluronic P85 and reduced mobility result in slow and sustained release of the drug in physiological condition. This is particularly advantageous as chemotherapy requires a controlled concentration of drug in blood for a relatively longer period.

CONCLUSIONS.

The aim of the present work was the better understanding of interaction of Curcumin with one of its potential carriers, i.e., PEO-PPO-PEO block copolymers (Pluronic). Molecular dynamics simulations have been used to analyze these interactions at the molecular level. A novel model of Curcumin based on GROMOS96 force field has been proposed. Firstly, the model was used to study the properties of the molecule in water, methanol and 1-octanol. Subsequently, on DME and DMP in water solution and in the presence of the Pluronic P85 chains was analyzed.

The Curcumin model reproduces in fair agreement the trend of theoretical data of water/1-octanol partition coefficient. It shows relatively better solvation tendency in methanol than that of in 1-octanol, and indicates insolubility in water. The trend of free energy of solvation was observed to be $\Delta G_{\text{hyd}} > \Delta G_{\text{oct}} > \Delta G_{\text{met}}$ and it is consistent with the existing knowledge of the chemical nature of Curcumin.


In the presence of DME and DMP molecules, the more hydrophobic DMP molecules preferentially coat the Curcumin. The same behavior was observed in the presence of single and multiple P85 chains in water. In the case of P85, the hydrophobic PPO chains wrap around the Curcumin molecule leaving the PEO parts exposed and thus resulting in better solvation and stability of the drug molecule in water. This also affects the mobility of the drug molecule by decreasing its diffusion coefficient. The formation of drug-polymer aggregation is observed within 50 ns of simulation. This observed condensing nuclei could be the first step to form the larger micelle observed in the experimental study reported in literature. Further study at coarse-grained level will provide a complete picture of the process.

REFERENCES.

- [1] in *WHO Food Additives Series 6*, World Health Organization, Geneva, **1975**.
- [2] V. S. Govindarajan, W. H. Stahl, *C R C Critical Reviews in Food Science and Nutrition* **1980**, *12*, 199.
- [3] T. V. Padma, *Nature* **2005**, *436*, 486.
- [4] S. Shishodia, G. Sethi, B. B. Aggarwal, *Annals of the New York Academy of Sciences* **2005**, *1056*, 206.
- [5] M. Notarbartolo, P. Poma, D. Perri, L. Dusonchet, M. Cervello, N. D'Alessandro, *Cancer Letters* **2005**, *224*, 53.
- [6] M. L. Kuo, T. S. Huang, J. K. Lin, *Biochimica et Biophysica Acta (BBA)* **1996**, *1317*, 95.
- [7] R. A. Sharma, A. J. Gescher, W. P. Steward, *European Journal of Cancer* **2005**, *41*, 1955.
- [8] B. B. Aggarwal, A. Kumar, A. C. Bharti, *Anticancer Research* **2003**, *23*, 363.
- [9] A. B. Kunnumakkara, S. Guha, S. Krishnan, P. Diagaradjane, J. Gelovani, B. B. Aggarwal, *Cancer Research* **2007**, *67*, 3853.
- [10] S. Singh, B. B. Aggarwal, *Journal of Biological Chemistry* **1995**, *270*, 24995.
- [11] A. C. Bharti, B. B. Aggarwal, *Biochemical Pharmacology* **2002**, *64*, 883.
- [12] J. M. Ringman, S. A. Frautschy, G. M. Cole, D. L. Masterman, J. L. Cummings, *Current Alzheimer Research* **2005**, *2*, 131.
- [13] G. M. Cole, T. Morihara, G. P. Lim, F. Yang, A. Begum, S. A. Frautschy, *Annals of the New York Academy of Sciences* **2004**, *1035*, 68.
- [14] L. N. Zhao, S.-W. Chiu, J. Benoit, L. Y. Chew, Y. Mu, *Journal of Physical Chemistry B* **2012**, *116*, 7428.
- [15] H. H. Tønnesen, M. Másson, T. Loftsson, *International Journal of Pharmaceutics* **2002**, *244*, 127.
- [16] H. H. Tønnesen, J. Karlsen, *Zeitschrift für Lebensmitteluntersuchung und -Forschung A* **1985**, *180*, 402.
- [17] G. Shoba, D. Joy, T. Joseph, M. Majeed, R. Rajendran, P. S. S. R. Srinivas, *Planta Med* **1998**, *64*, 353.
- [18] C. Ireson, S. Orr, D. J. L. Jones, R. Verschoyle, C.-K. Lim, J.-L. Luo, L. Howells, S. Plummer, R. Jukes, M. Williams, W. P. Steward, A. Gescher, *Cancer Research* **2001**, *61*, 1058.

-
- [19] A. V. Kabanov, E. V. Batrakova, V. Y. Alakhov, *Journal of Controlled Release* **2002**, 82, 189.
- [20] I. R. Schmolka, in *Polymers for Controlled Drug Delivery* (Ed.: P. J. Tarcha), CRC Press, Boston, **1991**.
- [21] K. T. Oh, T. K. Bronich, A. V. Kabanov, *Journal of Controlled Release* **2004**, 94, 411.
- [22] Z. Ma, A. Haddadi, O. Molavi, A. Lavasanifar, R. Lai, J. Samuel, *Journal of Biomedical Materials Research Part A* **2008**, 86A, 300.
- [23] A. Sahu, U. Bora, N. Kasoju, P. Goswami, *Acta Biomaterialia* **2008**, 4, 1752.
- [24] R. Vakil, G. S. Kwon, *Langmuir* **2006**, 22, 9723.
- [25] A. S. Zahr, M. de Villiers, M. V. Pishko, *Langmuir* **2004**, 21, 403.
- [26] R. K. Das, N. Kasoju, U. Bora, *Nanomedicine: Nanotechnology, Biology and Medicine* **2009**, 6, 153.
- [27] A. Sahu, N. Kasoju, P. Goswami, U. Bora, *Journal of Biomaterials Applications* **2011**, 25, 619.
- [28] N. S. Melik-Nubarov, O. O. Pomaz, T. Y. Dorodnych, G. A. Badun, A. L. Ksenofontov, O. B. Schemchukova, S. A. Arzhakov, *FEBS Letters* **1999**, 446, 194.
- [29] E. V. Batrakova, T. Y. Dorodnych, E. Y. Klinskii, E. N. Kliushnenkova, O. B. Shemchukova, O. N. Goncharova, S. A. Arjakov, V. Y. Alakhov, A. V. Kabanov, *British Journal of Cancer* **1996**, 74, 1545.
- [30] S. Hezaveh, S. Samanta, G. Milano, D. Roccatano, *Journal of Chemical Physics* **2012**, 136, 124901.
- [31] S. M. Khopde, K. Indira Priyadarsini, D. K. Palit*, T. Mukherjee, *Photochemistry and Photobiology* **2000**, 72, 625.
- [32] C. M. Breneman, K. B. Wiberg, *Journal of Computational Chemistry* **1990**, 11, 361.
- [33] S. Samanta, S. Hezaveh, G. Milano, D. Roccatano, *Journal of Physical Chemistry B* **2012**, 116, 5141.
- [34] S. Hezaveh, S. Samanta, G. Milano, D. Roccatano, *Journal of Chemical Physics* **2011**, 135, 164501.
- [35] H. J. C. Berendsen, J. P. M. Postma, W. F. van Gunsteren, J. Hermans, (Ed.: B. Pullman), Reidel: Dordrecht, **1981**, p. 331.
- [36] W. L. Jorgensen, D. S. Maxwell, J. TiradoRives, *Journal of the American Chemical Society* **1996**, 118, 11225.

- [37] N. M. Garrido, A. n. J. Queimada, M. Jorge, E. n. A. Macedo, I. G. Economou, *Journal of Chemical Theory and Computation* **2009**, 5, 2436.
- [38] M. J. Frisch, G. W. Trucks, H. B. Schlegel, G. E. Scuseria, M. A. Robb, J. R. Cheeseman, J. A. Montgomery, T. Vreven, K. N. Kudin, J. C. Burant, J. M. Millam, S. S. Iyengar, J. Tomasi, V. Barone, B. Mennucci, M. Cossi, G. Scalmani, N. Rega, G. A. Petersson, H. Nakatsuji, M. Hada, M. Ehara, K. Toyota, R. Fukuda, J. Hasegawa, M. Ishida, T. Nakajima, Y. Honda, O. Kitao, H. Nakai, M. Klene, X. Li, J. E. Knox, H. P. Hratchian, J. B. Cross, V. Bakken, C. Adamo, J. Jaramillo, R. Gomperts, R. E. Stratmann, O. Yazyev, A. J. Austin, R. Cammi, C. Pomelli, J. W. Ochterski, P. Y. Ayala, K. Morokuma, G. A. Voth, P. Salvador, J. J. Dannenberg, V. G. Zakrzewski, S. Dapprich, A. D. Daniels, M. C. Strain, O. Farkas, D. K. Malick, A. D. Rabuck, K. Raghavachari, J. B. Foresman, J. V. Ortiz, Q. Cui, A. G. Baboul, S. Clifford, J. Cioslowski, B. B. Stefanov, G. Liu, A. Liashenko, P. Piskorz, I. Komaromi, R. L. Martin, D. J. Fox, T. Keith, A. Laham, C. Y. Peng, A. Nanayakkara, M. Challacombe, P. M. W. Gill, B. Johnson, W. Chen, M. W. Wong, C. Gonzalez, J. A. Pople, **2003**.
- [39] B. Hess, C. Kutzner, D. van der Spoel, E. Lindahl, *Journal of Chemical Theory and Computation* **2008**, 4, 435.
- [40] W. Humphrey, A. Dalke, K. Schulten, *Journal of Molecular Graphics* **1996**, 14, 33.
- [41] G. Bussi, D. Donadio, M. Parrinello, *Journal of Chemical Physics* **2007**, 126, 14101.
- [42] H. J. C. Berendsen, J. P. M. Postma, W. F. Vangunsteren, A. Dinola, J. R. Haak, *Journal of Chemical Physics* **1984**, 81, 3684.
- [43] B. Hess, H. Bekker, H. J. C. Berendsen, J. G. E. M. Fraaije, *Journal of Computational Chemistry* **1997**, 18, 1463.
- [44] T. Darden, D. York, L. Pedersen, *Journal of Chemical Physics* **1993**, 98, 10089.
- [45] J. Kirkwood, *Journal of Chemical Physics* **1935**, 3, 300.
- [46] ACD/Labs, V11.02 ed., Advanced Chemistry Development, Inc. , Toronto, On, Canada, **1994-2012**.
- [47] S. Fujisawa, M. Ishihara, Y. Murakami, T. Atsumi, Y. Kadoma, I. Yokoe, *In Vivo* **2007**, 21, 181.
- [48] P. Mark, L. Nilsson, *Journal of Physical Chemistry A* **2001**, 105, 9954.
- [49] Y. Marcus, *The properties of solvents*, Wiley, Chichester ; New York, **1998**.



Summary and Outlook

Summary.

The aim of this thesis was to model the interactions of amphiphilic block co-polymers with biological interfaces and small molecules using computer simulation based on Molecular Dynamics techniques.

For this purpose, a novel force field for MD simulations of PEO, PPO and Pluronics® polymers was developed. The force field models for DME and DMP was tested in methanol, carbon tetrachloride, and *n*-heptane solutions. The models reproduced the behavior of both of the oligomers in non-aqueous solvents consistently with their expected physical and thermodynamic properties. The results of the study showed that the ΔG_{sol} of DME shows a decreasing trend going from methanol, carbon tetrachloride, and *n*-heptane, which is in agreement with the dielectric constant of the solvents. In contrary DMP was found to be more soluble in non-polar solvents as *n*-heptane.

The optimization was further extended to investigate the effect of non-aqueous solvents (methanol, chloroform, carbon tetrachloride and *n*-heptane) on the conformation and dynamics of PEO and PPO chains and Pluronic P85. The dihedral distributions in methanol and chloroform were found in very good agreement with NMR data. The C-C bond dihedrals in both PEO and PPO showed preference for gauche conformation. The solvents enhanced the contents of gauche conformations of both PEO and PPO polymers in the following order: methanol>chloroform>carbon tetrachloride~*n*-heptane. On contrary, the population of trans conformations increased in the order: carbon tetrachloride~*n*-heptane>chloroform >methanol. In addition, the hydrogen bonding with polar solvent molecules was studied and, in the case of PEO, different types of hydrogen bonding were observed. In particular, the simulations in chloroform showed the occurrence of bifurcated hydrogen bonds between the hydrogen of a chloroform molecule and two oxygen atoms of a polymer chain in agreement with experimental observations. In the case of PPO, no strong

hydrogen bonding was observed. The calculated radius of gyration and end-to-end distances with their relaxation time also showed good agreement with the available experimental data. In case of non-polar solvents, PEO polymer chains became more compact than in polar solvent. PPO chains showed a less compact structure than PEO ones in carbon tetrachloride and *n*-heptane, and more compact in water, methanol and chloroform, for chains longer than 18 units due to its more hydrophobicity.

Structural, dynamic, and thermodynamic properties of DME and DMP in water/*n*-heptane, and water/DMPC bilayer interfaces were also investigated. The models of DME and DMP were further tested in 1-octanol and the partition coefficient values between water and 1-octanol showed excellent agreement with available experimental data. The calculated percolation barrier from water to *n*-heptane phase was found to be higher for DME than that of DMP. Solvation free energy calculations of the DME and DMP in water and heptane phase clearly indicate the preference of DMP for more hydrophobic environment than DME. The calculated PMF profiles resulted in a higher percolation barrier for DME than DMP as well. This height of the barrier in the tail region of DMPC was found to be consistent and comparable to that of the water/*n*-heptane system. In this case as well, analysis showed extra stabilization for DME in correspondence of the head group region. It was proved that electrostatic interactions play an important role in the energetics of the bilayer percolation process for the DME molecule. The results of long unconstrained simulations of DME and DMP further supported the behavior expected from the PMF curves. For the simulations with the molecules located in the lipid head group region, DMP molecules spontaneously diffused to the center of the lipid bilayer whilst DME molecules remained in the lipid/water interface region. The spontaneous diffusion of DMP molecules to the interior of the lipid bilayer can be enhanced by increasing the concentration but no concentration effect was observed for DME.

The investigation was then extended to study structural properties of ether

based linear and block polymers in water/*n*-heptane and water/DMPC bilayer interfaces. Our study with the polymers at water/*n*-heptane interface showed that PPO chains stay at the water/*n*-heptane interface but PEO diffuse to the water phase. In agreement with available experimental results, simulations produced the bottle brush chain configurations at water/*n*-heptane interface. The polymers at the water/DMPC interface did not showed a significant percolation within 50 ns. Therefore, properties of polymers into lipid bilayer were studied by pulling them inside the bilayer using SMD simulations. PEO chains did not show any preference for the interior of the bilayer and quickly diffused out in the water phase. On the contrary, the PPO chains remained inside the bilayer for all the simulation. Relatively longer PPO20 and PPO43 span across the width of the bilayer while short PPO7 chain stayed in the tail region of the bilayer near the polar head-groups. Pluronic L61 and L64 spanned across the bilayer with the hydrophilic PEO blocks in the polar headgroup region and water in both sides. Pluronic P85 assumed a conformation where the PPO block stays in the aliphatic tail-group region of the bilayer and the PEO blocks stayed in the headgroup region and water phase in the same side of the bilayer. The PMF profiles of bilayer percolation were obtained for the polymers and the energy barrier to transfer the polymers from water into the DMPC tail region was found to be smaller for PPO chains of all lengths (2, 3, 7, 20 and 43 monomer long) than their PEO counterparts.

Finally, the focus was directed towards better understanding of interaction of hydrophobic drug Curcumin with one of its potential carriers, i.e., PEO-PPO-PEO block co-polymer Pluronic. A novel model of Curcumin (based on GROMOS96 force field) was proposed and tested in water, methanol and 1-octanol. The Curcumin model reproduces in fair agreement the trend of theoretical data of water/1-octanol partition coefficient. It showed relatively better solvation tendency in methanol than in 1-octanol, and indicated insolubility in water. The trend of free energy of solvation was observed to be $\Delta G_{\text{hyd}} > \Delta G_{\text{oct}} > \Delta G_{\text{met}}$ and it is consistent with the existing knowledge of the chemical nature of Curcumin. In the presence of DME and DMP molecules, the more hydrophobic

DMP molecules preferentially coated the Curcumin molecule. The same behavior was observed in the presence of single and multiple P85 chains in water. In the case of P85, the hydrophobic PPO chains wrapped around the Curcumin molecule leaving the PEO parts exposed and thus resulting in better solvation and stability of the drug molecule in water. The formation of drug-polymer aggregation was observed within 50 ns of simulation.

Outlook.

This thesis addresses the interaction of ether based polymers with interfaces and with hydrophobic drug molecules. Having accomplished the goal of understanding the nature of the interactions at molecular level, this study opens several possibilities for future investigations.

The understanding of the interaction of Pluronics with lipid bilayer interfaces are somehow restricted by high computational cost of long atomistic simulations. A set of coarse-grained model for these polymers has already been proposed and validated by our group (Hezaveh et. al *J. Phys. Chem. B* 2012 doi: 10.1021/jp306565e). These simulations at coarse-grained level range to microseconds in timescale against the cost of loss in details of interactions. There is a possibility to utilize the advantages of both the methods by reverse mapping of atomistic configurations from different timescales from the long coarse-grained simulations and simulate them to obtain the details of interactions at atomic level.

In the case of Curcumin, the possibilities of further research are numerous. The atomistic simulations of Curcumin can be extended to other polymers with different PEO/PPO chain-length to study the effect of composition of the polymer on the formation of drug-polymer aggregation. As the formation of polymer micelles is out of reach of the atomistic simulations, simulations at coarse-grained level will definitely help to shade lights

on the procedure of encapsulation of Curcumin in Pluronic micelles.

From atomistic point of view, molecular details of the anti-disease properties of Curcumin are not yet understood. For example, very little work has been done to understand how Curcumin prevents the aggregation of Amyloid- β to prevent Alzheimer's disease or how Curcumin inhibits nuclear factor kappaB (NF- κ B) signaling pathway. This study can be extended to address these problems in details.

One possible line of future investigations is to address the interaction of ether based linear and block polymers with peptide and protein molecules. It is experimentally known that Pluronics have the potential to thermally stabilize several protein molecules (e.g., Lysozyme). A possible line of work may address how these polymers affect the conformation and structure of simple helical or beta-sheet peptides and then use the information to understand the interaction of large protein molecules with polymers.

|Appendix

Table A1.1: Dipole moment values of DME/DMP in different solvents at 318 K and 298 K.

Dipole moment values (in Debye) at 318K and 298K (in parenthesis) for DME in different solvents.				
Solvents	TGT	TGG'	TGG	
Methanol	2.6 (2.7)	1.9 (2.3)	3.3 (3.2)	
Carbon tetrachloride	1.8 (1.7)	1.5 (1.4)	3.2 (2.7)	
<i>n</i> -heptane	1.8 (1.7)	1.5 (1.4)	3.2 (2.8)	
Dipole moment values at 318K and 298K (in parenthesis) for DMP in different solvents.				
Solvents	TGT (1.3)*	TG'T (1.8)*	GGT (2.8)*	GTT (2.1)*
Methanol	2.1 (3.0)	2.3 (5.0)	3.0 (3.1)	2.5 (3.3)
Carbon tetrachloride	1.6 (2.0)	1.9 (2.0)	2.8 (2.7)	2.3 (2.4)
<i>n</i> -heptane	1.6 (2.0)	1.9 (1.5)	2.8 (2.7)	2.3 (2.4)

* Values are the ones from ab-initio molecular orbital calculation in water as solvent at 318 K.^[1]

Table A1.2: The solvent coordination numbers of DME in the different solvents and for the first two solvation shells are reported.

Solvent coordination number for one DME in different solvents at 318K and 298K (in parenthesis) for the first two minima (distances in nm).		
Methanol	1 st min=0.30	0.94(0.86)
	2 nd min=0.60	11.26(11.00)
Carbon tetrachloride	1 st min=0.80	11.75(11.94)
	2 nd min=1.32	55.40(56.20)
<i>n</i>-heptane	1 st min=0.83	9.17(9.29)
	2 nd min=1.15	25.49(25.77)

Table A1.3: Solvent coordination number of DMP is reported for different solvents. First and second minima are almost in the same points but the solvent coordination number reduces going from DME to DMP as the effect of methyl group.

Solvent coordination number for one DMP in different solvents at 318K and 298K (in parenthesis) for the first two minima (distances in nm).		
Methanol	1 st min=0.32	0.56(0.41)
	2 nd min=0.58	8.52(6.26)
Carbon tetrachloride	1 st min=0.84	13.50(13.72)
	2 nd min=1.33	56.59(57.42)
<i>n</i>-heptane	1 st min=0.83	9.10(9.20)
	2 nd min=1.15	25.38(25.68)

Table A1.4: Summary of the simulations with sizes and compositions (number of molecules) of cubic simulation boxes.

PEOn	Box size (nm/side)	Water #	Methanol #	CHCl ₃ #	CCl ₄ #	<i>n</i> -heptane #
2	3	882	1719	767	664	427
3	3	882	1719	767	664	427
4	3	878	1719	767	664	427
5	3	874	1719	767	664	427
6	3	870	1719	767	664	427
7	4	871	1719	767	664	427
9	5	4116	1715	765	658	423
18	6	7110	3037	1371	1173	737
27	6	7093	3030	1365	1164	734
36	7	11328	4815	2211	1901	1235
43	7	11307	4799	2203	1893	1229
PPOn						
2	3	882	999	768	600	429
3	3	882	999	768	600	429
4	3	878	999	768	600	429
5	3	874	999	768	600	429
6	3	870	999	768	600	429
7	4	871	999	768	600	429
9	5	4104	1677	764	608	432
18	6	7098	2709	1371	1080	757
27	6	7072	2702	1599	1075	750
36	7	11305	4826	2199	1826	1198

Reference.

- [1] Y. Sasanuma, *Macromolecules* **1995**, 28, 8629.

Figure A2.1: Comparison of the potential of mean force profile for percolation of DME in DMPC layer obtained by averaging large number of SMD simulation (black) and the umbrella sampling simulation (green). Average of ten SMD simulations quantitatively reproduces the PMF profile but the details are missing.

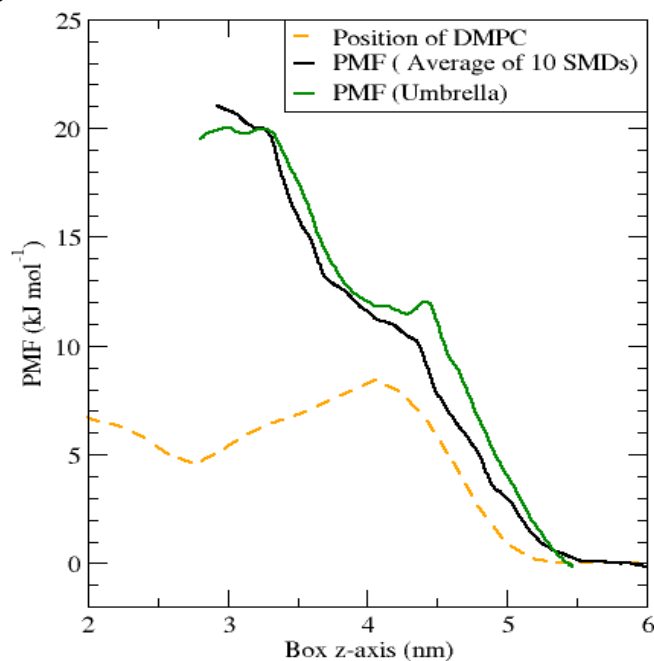


Figure A2.2: PMF profiles obtained by SMD runs with different starting positions for DME. The average is shown in the previous figure.

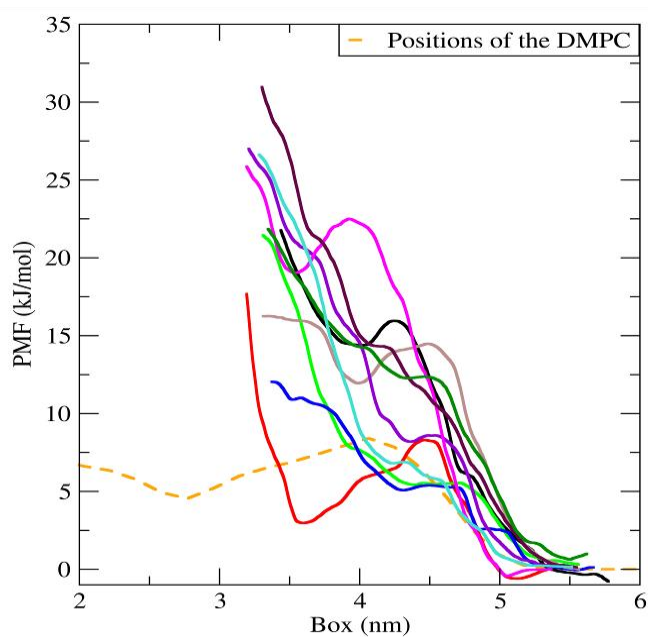


Figure A2.2: Comparison of PMF profiles obtained for percolation of DME in DMPC layer obtained by umbrella sampling simulation where each frame was simulated for varied timescale. The similarity of PMF profiles for time scale 5 ns and 7 ns indicates that for the systems in concern, 5 ns simulation per US window is enough.

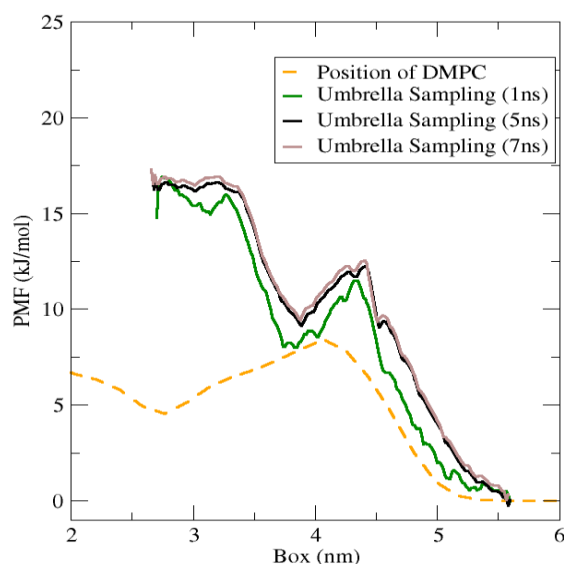


Figure A2.4: Comparison of PMF profiles DME and DMP (both atomistic and coarse-grained models) calculated using umbrella sampling method. The adopted coarse-grained model did not reproduce the atomistic PMF. If the parameters are changed to improve the agreement, the interaction with the membrane show destabilization effects and the results lose the qualitative agreement with the experimental data. The trend for the DME is similar to the atomistic one but for the DMP the difference is larger. We thought that this problem is due to the lack of stereochemistry in the DMP coarse-grained model. This affects the entropy part of the permeation free energy. The adjustment of the enthalpy term does not help to recover the profile atomistic behavior. However, the difference between the coarse-grained PMF energy and atomistic are of the same order observed between the coarse-grained lipid and atomistic model of the lipids bilayer.

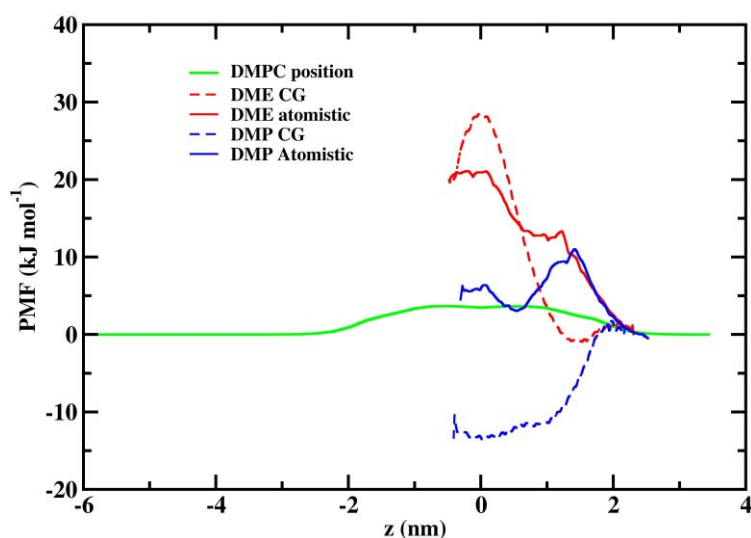


Table A2.1a: Description of all the systems simulated for water/*n*-heptane interface. In all the cases, the polymers were put at the interface and then simulated for 50 ns.

System	Polymer used	Number of water molecules	Number of <i>n</i> -heptane molecules	Total number of atoms	Dimension of the box (nm×nm×nm)
A1	L61	10705	1186	40550	8 × 8 × 11
A2	L64	10705	1186	40616	8 × 8 × 11
A3	P85	10705	1186	40736	8 × 8 × 11
A4	PEO 7	10705	1186	40441	8 × 8 × 11
A5	PEO 20	10705	1186	40480	8 × 8 × 11
A6	PEO 43	10705	1186	40549	8 × 8 × 11
A7	PPO 7	10705	1186	40448	8 × 8 × 11
A8	PPO 20	10705	1186	40500	8 × 8 × 11
A9	PPO 43	10705	1186	40592	8 × 8 × 11

Table A2.1b: Description of all the systems simulated for water/DMPC interface. In all the cases, the systems were simulated for 50 ns.

System	Polymer used	Number of DMPC molecules	Number of water molecules	Total number of atoms
B1 (a,b)	L61	128	7856	29589
B2 (a,b)	L64	128	7821	29550
B3 (a,b)	P85	128	8167	30708
C1 (a-e)	PEO 7	128	8002	29918
C2 (a-e)	PEO 20	128	7967	29852
C3 (a-e)	PEO 43	128	7941	29843
D1 (a-e)	PPO 7	128	7992	29859
D2 (a-e)	PPO 20	128	8141	30394
D3 (a-e)	PPO 43	128	8141	30486

- i. Simulation system details: a) polymer at the interface of DMPC/water, b) polymer inside the aliphatic region of DMPC, c-e) SMD simulations starting from a configuration where the polymer was in water region outside the DMPC bilayer.
- ii. All the boxes have initial dimension of ~ 6.4 nm × 6.4 nm × 9.5 nm.
- iii. All the free simulations (a, b) were run for 50ns.
- iv. All the SMD simulations (c, d, e) were run for 10 ns.

Figure A2.5: P-P density profiles for PEO and PPO polymers of different chain-lengths during

the last 25 ns of simulation.

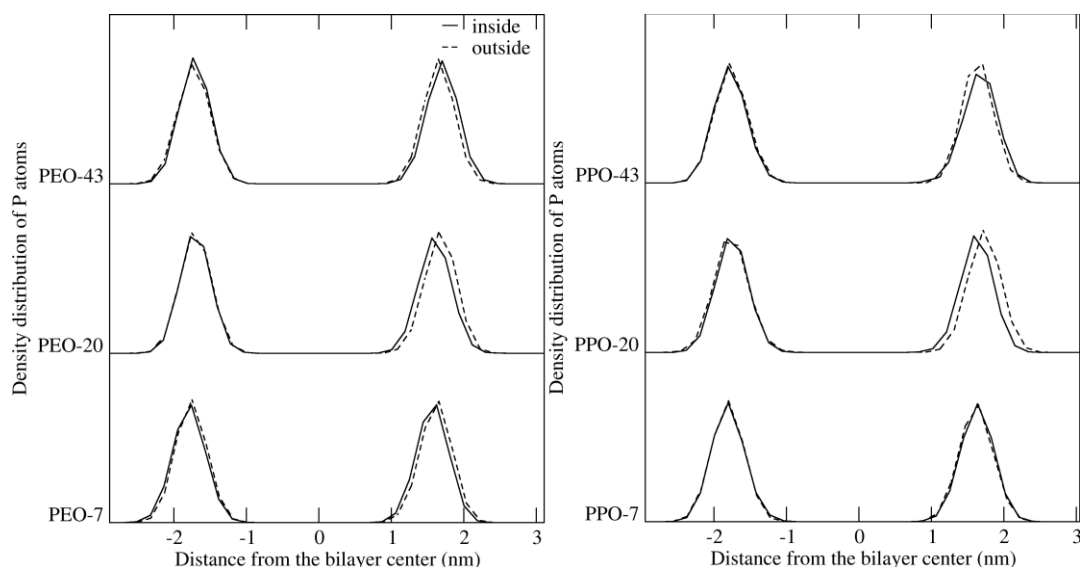


Table A2.2: Radius of gyration values of PEO and PPO chains inside and outside DMPC lipid bilayer.

	PEO			PPO		
	PEO7	PEO20	PEO43	PPO7	PPO20	PPO43
inside	0.512 (± 0.05)	0.992 (± 0.14)	1.609 (± 0.25)	0.449 (± 0.04)	0.773 (± 0.07)	1.00 (± 0.08)
outside	0.514 (± 0.05)	0.998 (± 0.14)	1.596 (± 0.44)	0.477 (± 0.04)	0.899 (± 0.12)	1.619 (± 0.23)

Figure A2.6: Density distribution of Pluronics a) L61, b) L64 and c) P85 (left to right) during 50 ns unconstrained simulation on the top of a DMPC lipid bilayer. The position of the DMPC bilayer is shown in orange dashed line.

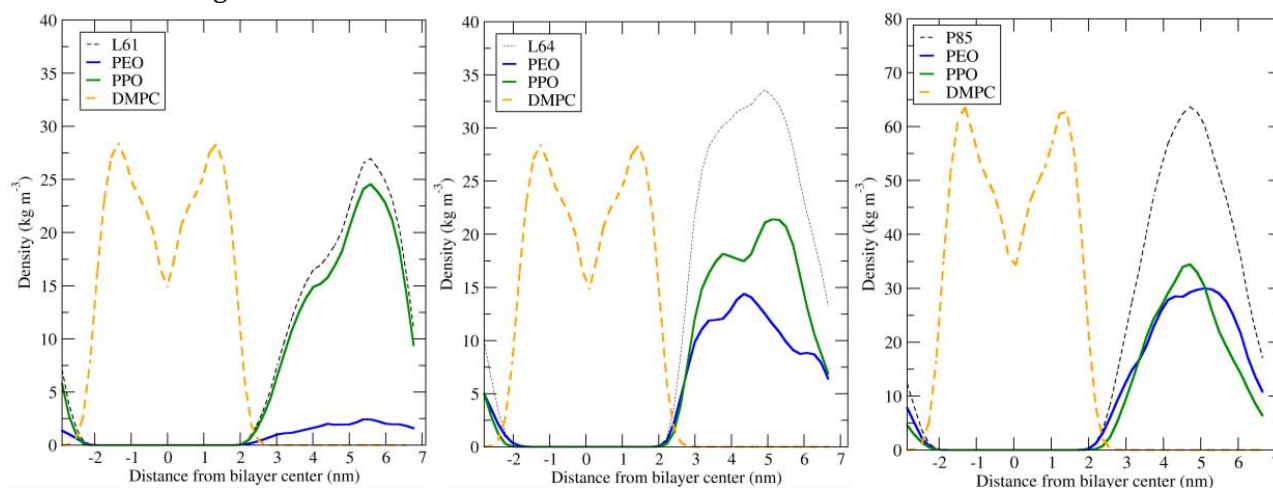


Figure A2.7: Distribution of radius of gyration (left) and end-to-end distance (right) of the Pluronic a) L61, b) L64 and c) P85 during 50 ns unconstrained simulation inside a DMPC bilayer.

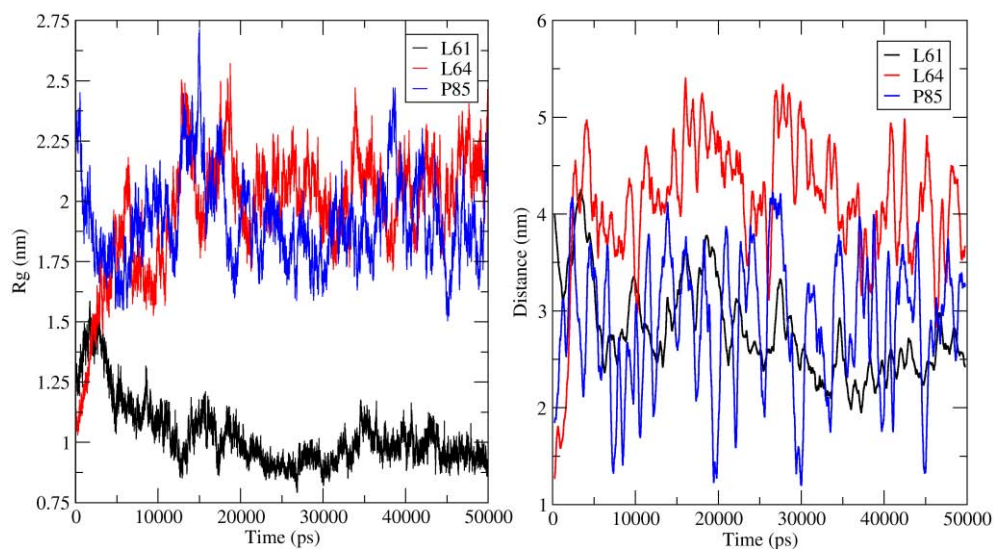


Figure A2.8: Comparison of PMF profiles of percolation of small polymers using umbrella sampling method. The position of the DMPC bilayer is shown in orange dashed line.

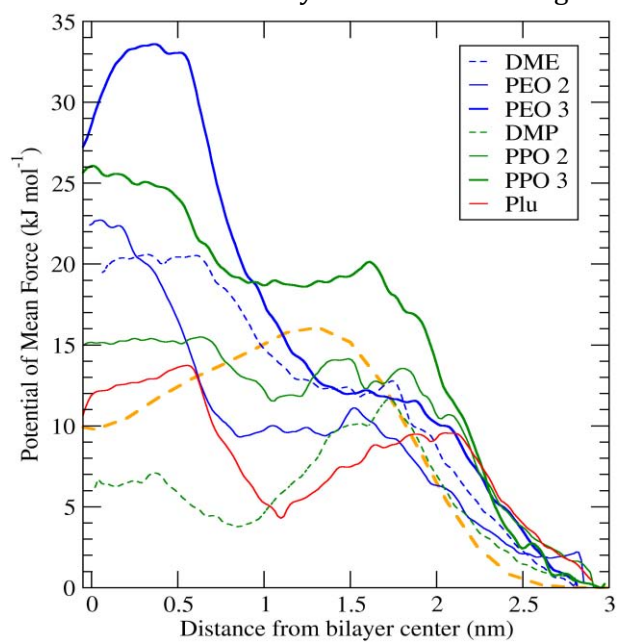
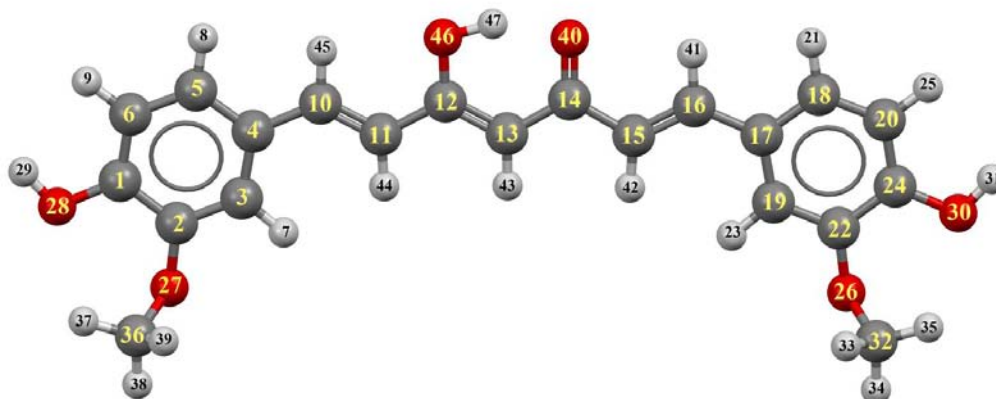


Table A3.1: Co-ordinates of the atoms in the optimized structure of Curcumin. The figure shows the optimized structure and numbering of the atoms in the Curcumin molecule.



Atom	X	Y	Z
1 C	14.286619	0.709999	-0.440229
2 C	12.167077	2.291662	-0.458722
3 C	9.790827	1.262130	-0.271393
4 C	9.421750	-1.347906	-0.059033
5 C	11.545652	-2.882102	-0.023011
6 C	13.954282	-1.868006	-0.214125
7 H	8.222728	2.549432	-0.308774
8 H	11.333065	-4.896543	0.145619
9 H	15.578088	-3.095223	-0.194479
10 C	6.912265	-2.525743	0.130943
11 C	4.678589	-1.387849	-0.033790
12 C	2.288115	-2.760694	0.187684
13 C	0.029686	-1.566088	0.002559
14 C	-2.342972	-2.924686	0.220365
15 C	-4.694289	-1.423087	-0.014065
16 C	-6.939418	-2.536329	0.147828
17 C	-9.447987	-1.359522	-0.037883
18 C	-11.574513	-2.886425	0.070999
19 C	-9.811597	1.245041	-0.318249
20 C	-13.983038	-1.870236	-0.109394
21 H	-11.363021	-4.895932	0.290842
22 C	-12.187068	2.276937	-0.495993
23 H	-8.237868	2.521831	-0.421044
24 C	-14.310293	0.702234	-0.399828

25 H	-15.610354	-3.090414	-0.031288
26 O	-12.452273	4.802464	-0.853130
27 O	12.432536	4.825551	-0.747857
28 O	16.578625	1.802336	-0.639200
29 H	17.865646	0.570688	-0.680164
30 O	-16.601506	1.796017	-0.592435
31 H	-17.892595	0.567989	-0.578145
32 C	-13.210527	6.212854	1.274464
33 H	-13.279841	8.166949	0.683879
34 H	-15.061817	5.634439	1.926467
35 H	-11.852352	6.012868	2.800669
36 C	13.236564	6.173038	1.403867
37 H	15.099080	5.572885	2.001661
38 H	13.298413	8.143061	0.868050
39 H	11.908492	5.931689	2.950426
40 O	-2.419538	-5.204768	0.581448
41 H	-6.930599	-4.548905	0.446986
42 H	-4.492944	0.574210	-0.324697
43 H	0.005121	0.434594	-0.317914
44 H	4.510587	0.610180	-0.349305
45 H	6.918490	-4.536672	0.427738
46 O	2.498687	-5.211365	0.575881
47 H	0.831113	-5.920310	0.687834

Figure A3.1: Numbering of the atoms as used in the topology of the Curcumin molecule.

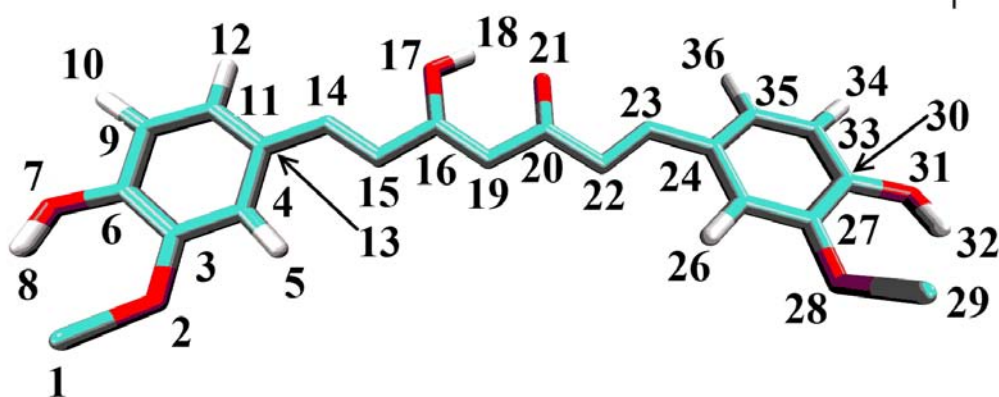


Table A3.2: Atomtype, mass and charges on the atoms of Curcumin. Numbers indicate atoms as shown in Figure A4.1.

#	Atomtype	Mass	Charge	#	Atomtype	Mass	Charge
1	CH3	15.035	0.477834	19	CH1	13.019	-1.297194
2	OS	15.999	-0.853475	20	C	12.011	1.759552
3	CR6	12.011	0.312169	21	O	15.999	-0.956858
4	CR6	12.011	0.040850	22	CH1	13.019	-0.728733
5	HCR	1.008	0.000000	23	CH1	13.019	0.632797
6	CR6	12.011	0.709119	24	CR6	12.011	-0.263750
7	OA	15.999	-0.650377	25	CR6	12.011	0.047839
8	HO	1.008	0.000000	26	HCR	1.008	0.000000
9	CR6	12.011	-0.151799	27	CR6	12.011	0.313782
10	HCR	1.008	0.000000	28	OS	15.999	-0.852854
11	CR6	12.011	0.124751	29	CH3	15.035	0.475933
12	HCR	1.008	0.000000	30	CR6	12.011	0.703991
13	CR6	12.011	-0.238451	31	OA	15.999	-0.639671
14	CH1	13.019	0.569946	32	HO	1.008	0.000000
15	CH1	13.019	-0.546862	33	CR6	12.011	-0.158053
16	C	12.011	1.429210	34	HCR	1.008	0.000000
17	OA	15.999	-0.390917	35	CR6	12.011	0.131222
18	HO	1.008	0.000000	36	HCR	1.008	0.000000

Table A3.3: Parameters for bonds. The bonds were constrained using LINCS algorithm. Numbers indicate atoms as shown in Figure A4.1.

Bond between atoms	Bondlength	Bond between atoms	Bondlength
1-2	0.143	19-20	0.144
2-3	0.137	20-21	0.127
3-4	0.139	20-22	0.147
3-6	0.141	22-23	0.135
4-5	0.108	23-24	0.146
4-13	0.141	24-25	0.141
6-7	0.136	24-35	0.140
6-9	0.139	25-26	0.108
7-8	0.097	25-27	0.138
9-10	0.109	27-28	0.137
9-11	0.139	27-30	0.141
11-12	0.108	28-29	0.143
11-13	0.140	30-31	0.136
13-14	0.146	30-33	0.139
14-15	0.135	31-32	0.097
15-16	0.145	33-34	0.109
16-17	0.132	33-35	0.139
16-19	0.138	35-36	0.108
17-18	0.102		

Table A3.4: Parameters for angles. Numbers indicate atoms as shown in Figure A4.1.

Atoms involved	Angle (deg.)	Atoms involved	Angle (deg.)
1-2-3	116.1	16-19-20	120.0
2-3-4	118.8	19-20-21	121.1
2-3-6	121.6	19-20-22	118.3
4-3-6	119.5	21-20-22	120.6
3-4-5	116.9	20-22-23	120.0
3-4-13	121.9	22-23-24	120.0
5-4-13	121.2	23-24-25	123.3
3-6-7	117.7	23-24-35	119.0
3-6-9	119.3	25-24-35	117.7
7-6-9	123.0	24-25-26	121.1
6-7-8	108.9	24-25-27	121.8
6-9-10	119.4	26-25-27	117.0
6-9-11	120.5	25-27-28	118.9
10-9-11	120.1	25-27-30	119.5
9-11-12	119.5	28-27-30	121.6
9-11-13	121.1	27-28-29	116.5
12-11-13	119.4	27-30-31	117.7
4-13-11	117.6	27-30-33	119.3
4-13-14	120.0	31-30-33	123.0
11-13-14	120.0	30-31-32	109.0
13-14-15	120.0	30-33-34	119.3
14-15-16	120.0	30-33-35	120.5
15-16-17	117.0	34-33-35	120.1
15-16-19	122.1	24-35-33	121.1
17-16-19	120.1	34-35-36	119.4
16-17-18	107.7	33-35-36	119.5

Table A3.5: List of proper dihedrals with values. Numbers indicate atoms as shown in Figure A4.1.

Atoms involved	Value (deg.)	Atoms involved	Value (deg.)
6-3-2-1	-60	16-19-20-22	180
3-6-7-8	-180	19-20-22-23	180
11-13-14-15	180	20-22-23-24	180
13-14-15-16	180	35-24-23-22	180
14-15-16-19	-180	25-27-28-29	-120
15-16-17-18	180	27-30-31-32	180
15-16-19-20	180		

Figure A3.2: RDF plots of the oxygen atoms of DME, DMP and water with respect to the two types of rings in the Curcumin molecule.

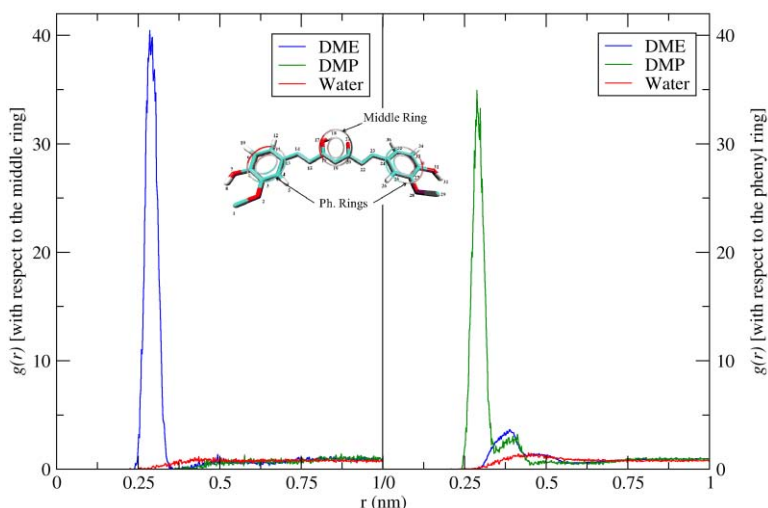
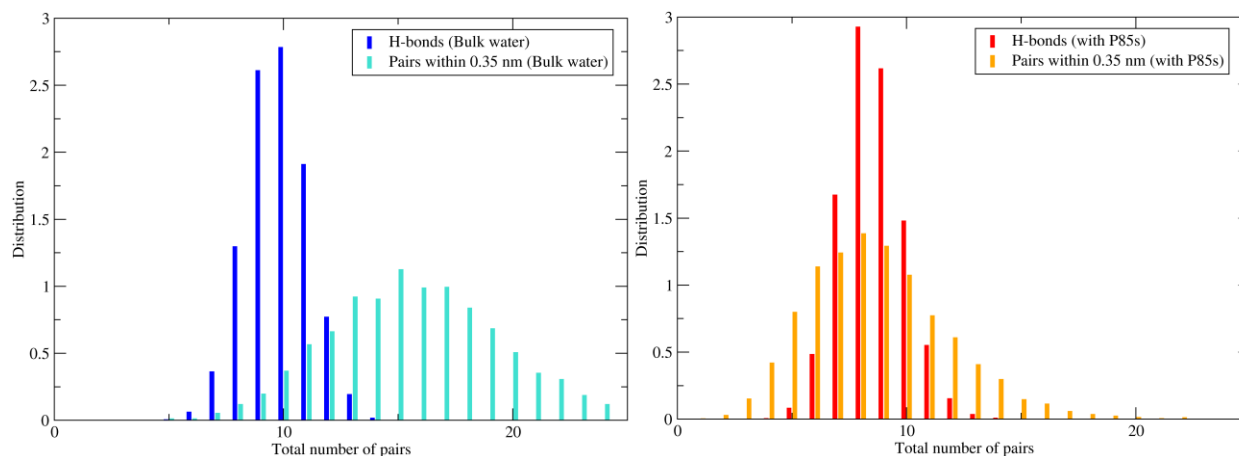


Figure A3.3: Distribution of the number of hydrogen bonds and pairs within 0.35 nm within Curcumin and the water molecules in bulk water (left) and in water with 8 P85 chains (right).



List of abbreviations.

B3LYP :	Becke 3-parameter Lee Yang Parr
CCl ₄ :	Carbon tetrachloride
CHELPG:	Charges from Electrostatic Potentials using a grid based method
CoM:	Center of Mass
DME:	1,2-dimethoxyethane
DMP:	1,2-dimethoxypropane
DMPC:	1,2-dimyristoyl- <i>sn</i> -glycero-3-phosphatidylcholine
LINCS:	Linear Constraint Solver
LJ:	Lennard-Jones
MD:	Molecular Dynamics
OPLS:	Optimized Parameters for Liquid Simulations
PBC:	Periodic Boundary Condition
PEO:	Polyethylene oxide
PME:	Particle Mesh Ewald
PMF:	Potential of Mean Force
PPO:	Polypropylene oxide
RDF:	Radial Distribution Function
SDF:	Spatial Distribution Function
SMD:	Steered Molecular Dynamics
TI:	Thermodynamic Integration
US:	Umbrella Sampling
WHAM:	Weighted Histogram Analysis Method

List of tables.

Description	Page
Table 1: Description of the Pluronics molecules used in this study.	5
Table 1.1: Free energy of solvation values of DME and DMP in solvents at 298 K.	26
Table 1.2: Diffusion coefficient values of DME and the solvents at 318 K and 298 K.	27
Table 1.3: Dihedral distributions (in percentage) of DME in the solvents at 318 K and 298 K.	30
Table 1.4: Diffusion coefficient values of DMP and the solvents at 318 K and 298 K.	31
Table 1.5: Percentage of conformational population of DMP in the solvents at 318 K and 298 K.	33
Table 2.1: Dihedral distribution of O-C-C-O bond (above) and C-O-C-C bond (below) for PEO in different solvents. Carbon tetrachloride and <i>n</i> -heptane are having the same distribution.	47
Table 2.2: The calculated end-to-end distance relaxation times (in ps) for the PEO chains.	53
Table 2.3: Dihedral angle population distribution (in percentage) of PPO with different chain tacticity.	54
Table 2.4: Radius of gyration (in nm) and end-to-end average distances (in nm) for PPO9 with different tacticities.	57
Table 2.5: End-to-end relaxation times (in ps) for each PPO length.	58
Table 2.6: Radius of gyration (in nm) for P85 at different temperature.	59
Table 3.1: The distance form bottom heads of the bilayer and fluctuation in end-to-end distances (right) of DME for the six selected frames as shown in Figure 3.7.	83
Table 3.2: The distance form bottom heads of the bilayer and fluctuation in end-to-end distances (right) of DMP for the six selected frames as shown in Figure 3.7.	83
Table 4.1 List of polymers simulated for this study.	100
Table 4.2 Radius of gyration and end to end distances of the polymers at water/ <i>n</i> -heptane interface.	104
Table 5.1: Description of the systems simulated.	122

List of figures.

Description	Page
Figure 1: Chemical structure of polyethylene oxide/PEO (left) and polypropylene oxide/PPO (right) polymers.	3
Figure 2: Chemical structure of PEO and PPO based triblock co-polymer Pluronics.	4
Figure 3: Schematic diagram of the setup used for SMD simulations.	11
Figure 4: A schematic diagram showing the workflow of umbrella sampling method:	12
Figure 1.1: Molecular structures of DME and DMP with their partial charge on the heavy-atoms.	22
Figure 1.2: RDF plots of $O_{DME}-O_{MeOH}$, $O_{DME}-C(4)_{hep}$, and $O_{DME}-C_{CCl4}$ and in comparison with $O_{DME}-O_W^{[41, 42]}$ at 318 K for one DME molecule in different solvents.	28
Figure 1.3: Spatial density distributions of the solvent atoms in the first solvation shell of DME and DMP at 318 K.	29
Figure 1.4: Dipole moment distribution of DME in methanol, carbon tetrachloride, and <i>n</i> -heptane in comparison to water at 318 K.	31
Figure 1.5: RDF plots of $O_{DMP}-O_{MeOH}$, $O_{DMP}-C(4)_{hep}$, and $O_{DMP}-C_{CCl4}$ in comparison with $O_{DMP}-O_W$ at 318 K for one DMP molecule in different solvents.	32
Figure 1.6: Dipole moment distribution of DMP in methanol, carbon tetrachloride, and <i>n</i> -heptane in comparison to water at 318 K.	34
Figure 2.1: Dihedral distribution of O-C-C-O bond and C-O-C-C bond for PEO in different solvents.	46
Figure 2.2: Hydrogen bonds between PEO2 and methanol molecules.	47
Figure 2.3: Hydrogen bonds between PEO2, PEO7 and chloroform molecules.	48
Figure 2.4: Radius of gyration for PEO18-43 plotted against molecular weight for all solvents at 298 K.	49
Figure 2.5: End-to-end distance of PEO chains in all solvents.	50
Figure 2.6: End-to-end distribution of PEO2-43 chains in all solvents.	52
Figure 2.7: Radius of gyration and end-to-end distances of PPO in the different solvents plotted against molecular weight.	55
Figure 3.1: Molecular structures of DME, DMP and one chain of DMPC.	67
Figure 3.2: Schematic diagram of the density profile of the DMPC bilayer along z-axis.	71
Figure 3.3: The selected six frames from the umbrella sampling simulations for detailed investigations.	74

Figure 3.4: PMF profiles for percolation of DME and DMP molecules from water to water layer through <i>n</i> -heptane layer.	76
Figure 3.5: Non-bonded energy contribution in terms of Lennard-Jones (LJ) and Coulombic (CL) potential for percolation of DME (left) and DMP (right) through <i>n</i> -heptane.	77
Figure 3.6: Average density distribution of DME and DMP during 50 ns unconstrained simulation at water/ <i>n</i> -heptane interface.	78
Figure 3.7: The comparison of PMF profiles of percolation of DME and DMP molecule using umbrella sampling.	80
Figure 3.8: Nonbonded energy contributions calculated from all the frames of the umbrella sampling simulations: Lennard-Jones (LJ) and Coulombic (CL) energies for percolation of DME and DMP through DMPC.	81
Figure 3.9: Comparison of population distribution of the three dihedrals of the DME molecule for the six selected sets of simulations.	82
Figure 3.10: Plot for average number of hydrogen bonds for DME and DMP throughout the path of percolation through DMPC bilayer.	84
Figure 3.11: Comparison of the PMF profile for percolation of charged and non-charged DME and DMP in DMPC layer obtained by umbrella sampling method.	85
Figure 3.12: Average density distribution of DME and DMP during 50 ns unconstrained simulation of the selected frames.	86
Figure 3.13: Distance of DME and DMP from DMPC during 50 ns simulation are shown in the left.	88
Figure 3.14: Probability distribution of DME and DMP in the system during a 50 ns simulation starting from a frame when the molecule is in the head group.	89
Figure 3.15: Average density distribution of 9 molecules of DME and DMP during 50 ns unconstrained simulation.	90
Figure 4.1: Density distributions of the PEO & PPO chains and the PEO & PPO parts of the Pluronic molecules during 50 ns unconstrained simulation in water/ <i>n</i> -heptane interface.	101
Figure 4.2: Snapshot of Pluronics L61, L64 and P85 at the end of 50 ns unconstrained simulation in water/ <i>n</i> -heptane interface.	102
Figure 4.3: Average area per lipid for the systems starting with PEO and PPO at the a) interface, and b) inside the bilayer.	105
Figure 4.4: Density distributions of PPO chains inside the DMPC lipid bilayer.	107
Figure 4.5: Average area per lipid for the polymers simulated.	108
Figure 4.6: P-P density profiles for systems B during the last 25 ns of simulation.	109
Figure 4.7: Final conformation of Pluronics L61, L64 and P85 at the end of 50 ns unconstrained simulations inside the DMPC lipid bilayer.	110

Figure 4.8: Density distribution of Pluronics L61, L64 and P85 during 50 ns unconstrained simulations inside the DMPC lipid bilayer.	110
Figure 4.9: Distribution of radius of gyration and end-to-end distance of the Pluronics L61, L64 and P85 during 50 ns unconstrained simulation inside a DMPC bilayer.	111
Figure 4.10: The height of PMF profiles for percolation of small polymer chains inside DMPC lipid bilayer.	112
Figure 4.11: PMF profiles for percolation of PEO and PPO chains inside DMPC lipid bilayer.	113
Figure 5.1: Optimized structure of Curcumin.	120
Figure 5.2: Spatial distribution of solvent atoms around Curcumin molecule in water, methanol and 1-octanol.	125
Figure 5.3: Root mean square fluctuation (RMSF) of the atoms of Curcumin in water, methanol, 1-octanol and in presence of DME and DMP in water.	126
Figure 5.4: Distribution of average distance between the enol hydrogen and the keto oxygen in water, methanol and 1-octanol.	127
Figure 5.5: Hydrogen bonding of Curcumin in water, in methanol and in 1-octanol.	128
Figure 5.6: Radial distribution function of the oxygen atoms of the solvent molecules with respect to the two different types of rings in the Curcumin molecule.	129
Figure 5.7: Spatial distribution of DME and DMP molecules around Curcumin molecule.	130
Figure 5.8: Minimum distance of the DME and DMP molecules from the center of mass of the Curcumin molecule during a 50 ns simulation.	130
Figure 5.9: Diffusion coefficient of the Curcumin molecule in different systems simulated.	132
Figure 5.10: Snapshot of the P85 and the Curcumin molecule at the beginning and at the end of a 50 ns simulation.	133
Figure 5.11: Average number of contacts between the PEO and PPO with P85 chain is shown in the top. Minimum distance of the PEO part and PPO part of the Pluronic P85 molecule from the center of mass of the Curcumin molecule during a 50 ns simulation is shown in the bottom panel.	134
Figure 5.12: Snapshot of the final conformation of P85 chains around the Curcumin molecule after a 50 ns simulation.	135
Figure 5.13: Spatial distribution of PEO and PPO chains around Curcumin molecule.	136

Name: Susruta Samanta

Personal Details: Date of Birth: 17th April, 1983
Nationality: Indian

Education: **M.Sc. (Chemistry) 2005-2007**
Sikkim Manipal University, India.

B.Sc. (Chemistry) 2001-2005
University of Calcutta, India.



- List of Publications:**
- 1)** "Structure and Dynamics of 1,2-dimethoxyethane and 1,2-dimethoxypropane in Aqueous and Non-aqueous Solutions: A Molecular Dynamics Study"
S. Hezaveh, **S. Samanta**, G. Milano & D. Roccatano*
The Journal of Chemical Physics, **2011**, 135, 164501.
 - 2)** "Diffusion of 1,2-dimethoxyethane and 1,2-dimethoxypropane Through Phosphatidycholine Bilayers: A Molecular Dynamics Study"
S. Samanta, S. Hezaveh, G. Milano & D. Roccatano*
The Journal of Physical Chemistry B, **2012**, 116, 5141.
 - 3)** "Molecular Dynamics Simulation Study of Solvent Effects on Conformation and Dynamics of Polyethylene Oxide and Polypropylene Oxide Chains in Water and in Common Organic Solvents"
S. Hezaveh, **S. Samanta**, G. Milano & D. Roccatano*
The Journal of Chemical Physics, **2012**, 136, 124901.
 - 4)** "Understanding the Interaction of Block Copolymers with DMPC Lipid Bilayer using Coarse-Grained Molecular Dynamics Simulations"
S. Hezaveh, **S. Samanta**, A. De Nicola, G. Milano* & D. Roccatano*
The Journal of Physical Chemistry B, **2012**, in press.
 - 5)** "Interaction of Curcumin with PEO-PPO-PEO Triblock Copolymers: A Molecular Dynamics Study."
S. Samanta, D. Roccatano*
Submitted (2012).